

Founded 1925

Incorporated
by Royal Charter 1961

*"To promote the advancement
of radio, electronics and kindred
subjects by the exchange of
information in these branches
of engineering."*

VOLUME 41 No. 11

NOVEMBER 1971

THE RADIO AND ELECTRONIC ENGINEER

The Journal of the Institution of Electronic and Radio Engineers

The Engineer in Europe

COLLABORATION between engineers has been firmly advocated on numerous occasions in this *Journal*. Radio and electronic engineering is a good example of a discipline which depends upon international cooperation, but while we would not underrate the American achievement, it is undoubtedly true that the European community of radio engineers has always collaborated on all levels, on the biggest as well as on some of the smallest schemes. The earliest days of wireless communication called for this international outlook. Later we saw the growth of ambitious international link-ups, the culmination of which came in 1951 with the building of the Cassel station, thus paving the way for interchanges between European television services. Today, under the convenient name of Eurovision, such interchanges are commonplace.

European engineers have also made outstanding contributions to colour television and the PAL system is now widely in use throughout Europe. With regard to space research in Europe, this cannot yet match the achievements of the U.S.A. or the U.S.S.R., but under the guidance of the European Space Research Organization (ESRO), it represents a commendable example of international collaboration and holds great promise for the future. In other disciplines engineers of many nations are working together in joint ventures, for example, in the field of aircraft construction, for EURATOM, for CERN, or for the International Atomic Energy Agency.

From a trading point of view, the radio and electronics industry needs international markets for its products, if the advantages of quantity production are to be realized. Each home market of the many individual nations within the Community is relatively small but the sum total forms a vast and economically rewarding market for the industry. Europe compares in size with the United States—which has prospered through inter-state trading—or with South America, the continent of Africa, the great expanse of China, or the complicated land masses of South-East Asia. Europe, however, has the great advantage of being compact, of possessing good facilities for transport and, overall, high standards of living.

In Great Britain the arguments still go on but public opinion is broadly in favour of *some* form of European market, and Parliament has voted for it—provided that controversial details, such as the systems of law, finance and distribution (agriculture and fisheries, for example), are arranged to our satisfaction. With a general acceptance of the principle and validity of the Community—and no doubt individual engineers will continue to hold their own views about this—the fact is that in terms of professional activity, the next decade will see great opportunities for engineers from all the countries within the Community to work even more closely together.

The success of such close cooperation depends on many factors, most important of which is goodwill between the engineers themselves; prejudices will rock the boat. In the conventional alliances between commercial organizations there must be the highest standards of integrity, honesty and diplomacy on the part of management and a readiness on the part of workers to deliver the goods.

The engineer who chooses to work in another country will need additional help; he will find this through the Council of Engineering Institutions which has already laid valuable guidelines on his behalf through its membership of FEANI. The European Register of Engineers will ensure that the qualifications and experience of a Chartered Engineer from Britain can readily be equated to those in other countries.

Such interchanges of craftsmanship and professional skills must surely lead towards greater understanding at personal levels as well as at national level, and thus the attainment of a real European Community.

Contributors to this issue



Mr. Storeton-West was promoted to assistant experimental officer.

Mr. T. J. Storeton-West joined the Fisheries Laboratory at Lowestoft in 1966 as a scientific assistant and since then has worked on the development of instruments for use in fisheries research. During this time he studied at the Lowestoft College of Further Education, obtaining an H.N.C. in electrical and electronic engineering and in the past year he has been working for H.N.C. endorsements. In May 1970



Dr. Branko D. Popovic received the B.Sc., M.Sc. and D.Sc. degrees of the University of Belgrade in 1958, 1963 and 1967 respectively. From 1959 to 1966 he was employed as an 'Assistant', and in 1966 he was appointed a 'Docent' with the Department of Electrical Engineering of the University of Belgrade. He is at present an Associate Professor in the same Department.

From January 1968 to September 1969, Dr. Popovic conducted graduate and undergraduate courses at the Electrical Engineering Department of Virginia Polytechnic Institute, Blacksburg, Virginia, as an exchange visitor. He has been a consultant to the Institute 'Nikola Tesla' in Belgrade, doing research on submarine power cables, and to the Radio Industry Zagreb, participating in the design of medium-wave antenna arrays.

Dr. Popovic has twice been awarded the Distinguished Teachers' Award by his Belgrade students, and he was a co-recipient of the Belgrade October Prize for technical sciences in 1967. He is the author or co-author of numerous technical papers and has written two textbooks.



Mr. Zoran D. Popovic received the B.Sc. degree in technical physics in 1965 and the M.Sc. degree in physics of materials in 1969, both from the University of Belgrade. From 1965 to 1971 he was employed as an 'Assistant' with the Department of Electrical Engineering of the University of Belgrade, simultaneously doing part-time research with the Institute for Physics of the University. Mr. Popovic is working at present

at McMaster University, Hamilton, Ontario, towards a Ph.D. degree in the field of materials science.

Biographical notes on Dr. D. R. Wilson and Mr. R. B. Mitson were given in the issues of *The Radio and Electronic Engineer* for September 1969 and August 1971 respectively.



Dr. R. W. Williams is a graduate of the University College of North Wales, Bangor, and obtained his doctorate from the University of Wales in 1941 for research in the field of X-ray crystallography. During the war years, he worked on the development of anti-aircraft predictors with the Ministry of Supply and the Admiralty. In 1946 he went to the Physics Department of Liverpool University to work on cyclotron development and experiments, with the aid of a Fellowship from the University of Wales. He joined the Guided Weapons Division of the English Electric Co. Ltd., now part of the British Aircraft Corporation, in 1949 and up to 1962 was concerned with various aspects of guided missile systems. In 1962 he was transferred to the Industrial Products Group of the company and, among other projects, was responsible for the design and development of the B.A.C. Fluid Network Analyser. Since 1969 he has been local head of research at the Stevenage Works of B.A.C. Dr. Williams is the author of several papers and a book on analogue computers and simulation topics, and he has written a book entitled 'Analogue Computation'.



Mr. R. M. Barker (Member 1966) was educated at Manchester Grammar School and Manchester College of Technology, where he obtained a B.Sc. (Tech.) degree in electrical engineering. After war-time service as an R.A.F. signals officer, he taught in several technical colleges in Lancashire and Cheshire. Ten years ago he came to Llanelli Technical College, Carmarthenshire, where he is a senior lecturer in electrical engineering. His particular interest is the history of electrical engineering and, in 1970 he was awarded an M.Sc. in the history of science and technology by the University of Manchester Institute of Science and Technology.



Dr. L. T. Bruton obtained the B.Sc. degree from the University of London in 1964, the M.Eng. degree from Carleton University, Ottawa, in 1967 and the Ph.D. degree from the University of Newcastle upon Tyne in 1970. In 1964 he joined the Northern Electric Company of Montreal, where he first worked as a communications development engineer in the Transmission Systems Department. From 1965 to 1967 he was with the Research and Development Laboratories of Northern Electric in Ottawa and was involved, as a project leader, in the development of a high capacity frequency division multiplex system. In 1967 Dr. Bruton returned to England and was appointed to a lectureship in electrical engineering at the University of Newcastle upon Tyne. During this period he acted as a consultant to the Royal Radar Establishment, Malvern, on active filter design. Last year he was appointed to an assistant professorship in electrical engineering at the University of Calgary.

A Transponding Acoustic Fish Tag

By

R. B. MITSON†

and

T. J. STORETON-WEST†

A description is given of the design, construction and trials of an acoustic fish tag. The tag contains receiver and transmitter sections used in a transponding mode. The size of the unit is 5 cm long by 1 cm diameter, and it weighs 4.0 g in sea water of salinity 35‰. Further development is discussed. Battery life is dependent on the rate of interrogation. Applications include the study of fish behaviour, migration and reaction to gear, and the tracking of seabed drifters.

1. Introduction

Acoustic tags were reported as being used successfully on fish in the mid-1950s, and records of fish tracking by such means are given by various authors.¹⁻¹² Continuous wave or pulsed transmitting tags were used in the experiments described in these publications, the bearing of a fish target relative to the ship being obtained within the limits of the bearing resolution of the ship's sonar equipment. Range information was not available but this was of little consequence when general patterns of movement only were required. This form of tracking has been carried out both in rivers and in the open sea, yielding useful information which would have been difficult or impossible to obtain by other means. However, when more detailed information of fish movements is required there is considerable advantage in using a transponding acoustic tag.

When the transponding principle is used, the pulse transmitted from the ship's sonar is received by the tag and used to trigger its transmitter, thus sending a return pulse to the ship. This gives an accurate range measurement between the ship and the fish. The other measurements needed are bearing and depth: these cannot be obtained with any degree of accuracy by commercially available sonars because of the necessarily wide beams used in such equipments. A sonar equipment fitted to the Fisheries Research Vessel *Clione* has, however, adequate characteristics. This is an electronic sector scanning sonar known as the A.R.L. (Admiralty Research Laboratory) scanner.^{13, 14} It has a unique facility whereby either azimuth or elevation scanning may be selected at will, the changeover from one to the other being accomplished in 3 seconds. Thus the position of a target in the water column may be determined, relative to the ship, within the accuracy of the receiving beam, which has an angular resolution of 0.33° in the scanning plane. The beam in this plane scans a sector of 30° (Figs. 1 and 2).

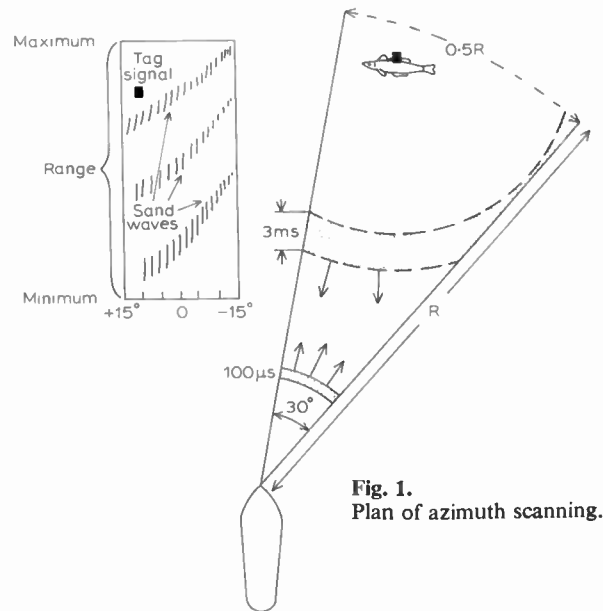


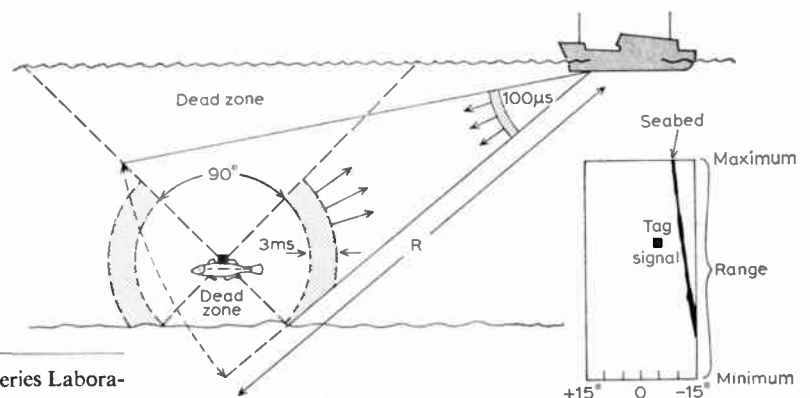
Fig. 1. Plan of azimuth scanning.

2. The Mitson-West Acoustic Tag

Although single fish can be detected and followed by sonar equipment without the use of acoustic tags, individuals cannot be identified. A transponding acoustic tag has therefore been designed to assist in the study of fish behaviour, migration, reaction to fishing gear and movements relative to bottom features.

To obtain the high angular resolution of the A.R.L. sonar with a transducer of practical dimensions, the operating frequency is high, i.e. 300 kHz. The use of such a frequency for fish tags, whilst permitting a suitably small transducer, does create a number of difficulties, the most important being the propagation losses in sea water. In this application the sum of the spreading loss and the absorption loss make up the total propagation loss for all practical purposes, since because there is a transmitter and receiver at each point, i.e. the ship and

Fig. 2. Plan of elevation scanning.



† Ministry of Agriculture, Fisheries and Food, Fisheries Laboratory, Lowestoft, Suffolk.

the fish, one-way loss only has to be considered. The spreading loss for a maximum range of 370 m is 52 dB. At 300 kHz, attenuation due to absorption varies with temperature from approximately 30 dB at 5°C to 48 dB at 25°C. For 8°C, which is a typical North Sea winter temperature, the attenuation is 36 dB, giving a total propagation loss of 88 dB.

The acoustic properties of the tag must be such that the sensitivity of the receiving section is adequate for detection of the pulse from the A.R.L. scanner out to maximum range. Measurements of the tag transducers when used as a hydrophone show that a typical response is -93 dB/volt/ μ bar. The receiver provides sufficient amplification to increase the signals to the required level to trigger the transmitter. The acoustic pulse then transmitted by the tag must be powerful enough to be detected, with a good signal/noise ratio, by the ship's scanning sonar. For the first trials a pulse length of 400 μ s was transmitted, but although the signal showed up as a bright spot on the c.r.t. display, difficulty was found in distinguishing it from other high-intensity signals, particularly when the bottom reverberation was high. To make identification quite positive the pulse length was increased to 3 ms so that the signal appears as a rectangle and extends over approximately 30 lines of the display raster. Because the pattern of this signal is entirely different from that of other signals being received, the operator can without ambiguity observe and track the fish. The transmitter source level was measured as $+57$ dB/ μ bar/m.

The ship's sonar needs high resolution within its scanned sector to locate the tag signal accurately, but the tag itself must have the widest possible coverage and, preferably, omnidirectional characteristics. This would need a spherical transducer with rather careful mounting to avoid masking the signals. However, in the transponding tag a lead zirconate titanate cylinder 3.2 mm high by 3.1 mm outside diameter has been used; it operates at a hoop mode resonant frequency of 305 kHz \pm 5 kHz. If this is fitted to the fish in such a way that the axis of the cylinder is vertical under normal swimming conditions (as shown in Fig. 2) dead zones for reception or transmission will appear immediately above and below the fish. These are not important for it is impossible to track the fish from a position directly overhead.

Examination of the acoustic radiation pattern shows that it is very much as expected in the vertical plane, i.e. as in Fig. 2. In the horizontal plane it is cardioid-shaped, the dip in response occurring at the rear of the tag casing due to the electronic assembly masking the transducer. No precise measurements have yet been possible, but it appears that the masking reduces the signal over an angle of 45°. However, this is unlikely to cause any difficulty unless the tag is being interrogated at long ranges from the direction in which the fish is facing; normally the fish is being followed. In practice, ranges between 225 and 320 m were found to be most satisfactory for ship manoeuvre. Tests showed that a range of approximately 550 m could be achieved. Although this is beyond the normal maximum range gate of the sonar a divider circuit can be switched in to

reduce the interrogation rate to 1 per second, thus providing a range gate of 365 to 730 m.

3. Recent Developments

When the design of a transponding fish tag was first considered, approaches were made to companies concerned with the manufacture of integrated and thick film circuits. Very little encouragement was received on the feasibility of producing such a circuit in an integrated form if economy of power was to be achieved together with a realistic price for the small quantities required.

To date (June 1971) 35 tags have been made in the form described in this paper, the first 10 at the Fisheries Laboratory and the others by Marconi Space and Defence Systems Ltd of Camberley, Surrey. The total cost of the components when bought in quantities of between 100 and 200 pieces is about £10 per tag. It is not possible to give an estimate of the production cost of this form of construction; as it is obviously unsuited to mass production techniques Marconi Space and Defence Systems Ltd have designed and made a printed circuit board. This consists of a very flexible fibreglass board, to whose copper conductors the standard tag components are soldered. The board can then be folded tightly around the capacitor C10, or used in flat form with the batteries at one end and the transducer at the other, C10 fitting alongside. The flat form of construction has not yet been used in practice.

Some recent work has resulted in the overall length of the tag being reduced to 4 cm and the weight in air made less by 0.5 g. These improvements are due to some circuit rearrangement in the receiver, whereby L1 is replaced by a resistor and suitable adjustments are made to the working conditions of TR2. Although some increase in receiver bandwidth occurs, the effect has not been detrimental to normal performance except that on one occasion in water about 15 m deep the tag was triggered by noise from a ship when it passed directly over the fish. It was assumed that the tag transducer had acted as a low frequency hydrophone and produced voltages of such a level that the selectivity of T1 circuit was insufficient to reject the signals.

4. Future Development

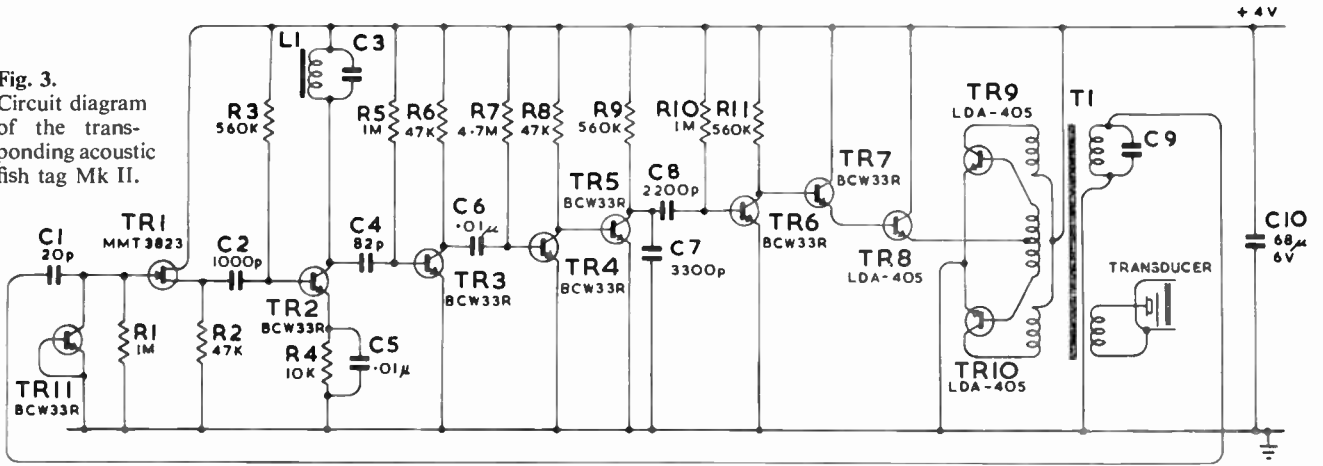
An acoustic tag of this type lends itself to the telemetering of physiological data from the fish and it is this aspect of development which is receiving attention at present. If the remote monitoring of physiological data can be achieved whilst the fish is observed and tracked in its natural habitat by a sonar equipment with the acuity of the A.R.L. Scanner, a great deal will be learned about normal fish behaviour and reaction to trawl gear, etc.

The present design could be further reduced in size and weight at the expense of some loss of detection range. However, a great deal of work can be carried out with the existing design, so modifications of this nature are not regarded as being of high priority at present.

5. Circuit Description

A circuit diagram is given in Fig. 3. It shows a common transducer used for both receiver and transmitter.

Fig. 3. Circuit diagram of the transponding acoustic fish tag Mk II.



The transducer is coupled into the receiver via a tuned winding on transformer T1, the step-up ratio at this transformer being 3 : 5. From this tuned winding the signal is coupled via a 20 pF capacitor to the gate of the source follower TR1. When the transmitter is fired the gate source voltage rises to about 100 V pk-pk, and a clipping diode TR11 was therefore incorporated at this point in order to keep the gate source voltage below its breakdown level. A pair of diodes are connected back-to-back from the gate of TR1 to ground, the gate source junction forming one of these diodes. A field effect transistor MMT 3823 in micro-T form was used at the input of the receiver and connected as a source follower so that the input impedance could be kept

reasonably high; thus C1 could be small in capacitance and in physical size. It was also important to keep C1 (20 pF) low in value, because when the back-to-back diodes conduct it is effectively connected in parallel with C9. This condition occurs on transmit. As C9 has a value of 680 pF, C1 placed in parallel has only a small effect and the transmit frequency differs only slightly.

C2 couples the source of TR1 to the base of the tuned amplifier TR2, the inductance in the collector of this stage being tuned to 305 kHz by C3. Three untuned amplifiers TR3, 4 and 5 follow, each stage being biased so that it is close to saturation. The time-constant in the base of TR4 was chosen to give a blocking effect to the receiver during transmission and so prevent oscillation,

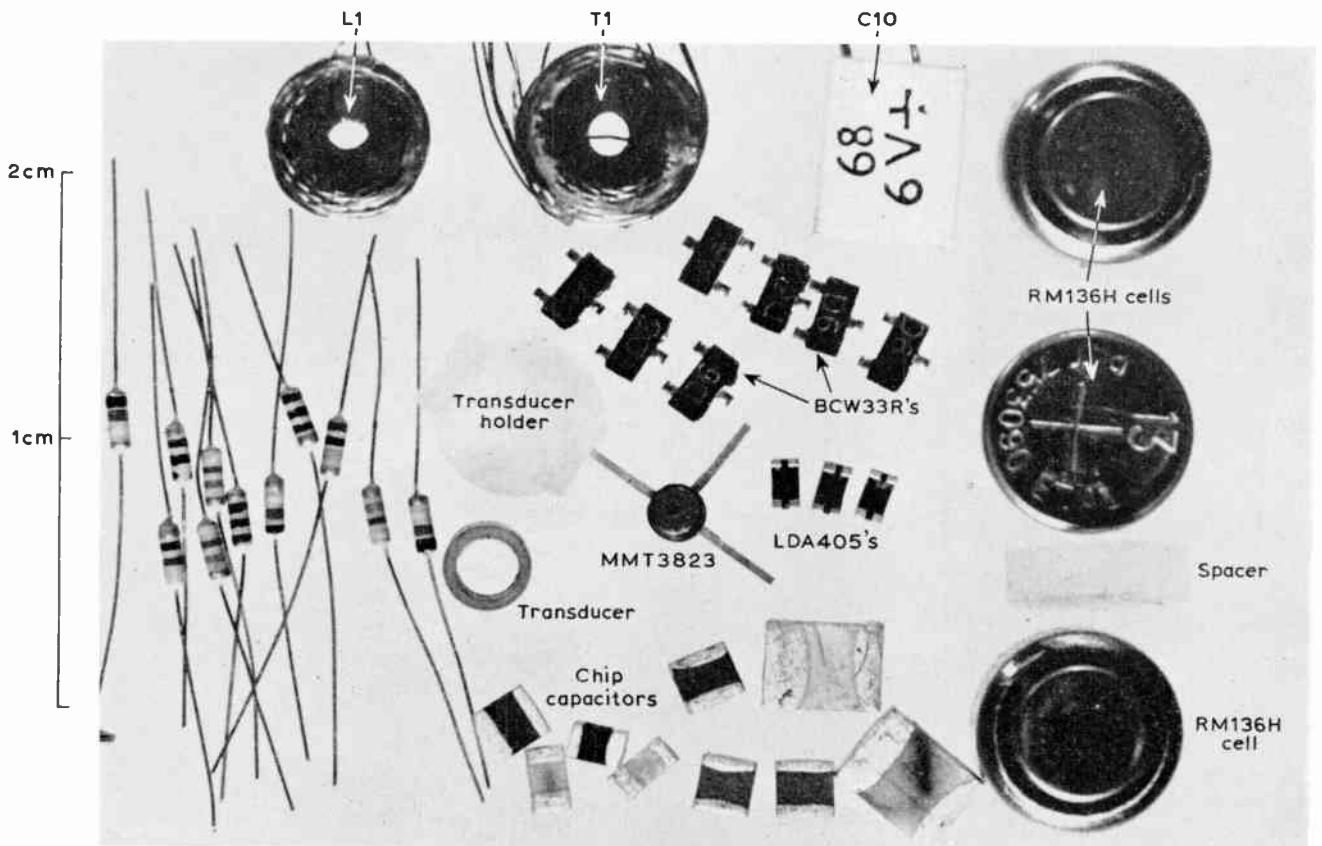


Fig. 4. Tag components before assembly.

the blocking time being a nominal 25 ms from the beginning of the 3 ms transmission pulse. This time-constant is measured at the collector of TR4. Also measured at this point is the minimum pulse amplitude required to trigger the transmitter, which is 0.6 V peak.

At the collector of TR5, C7 is used to decouple the remainder of the r.f. on the pulse and it is then coupled via C8 to the base of TR6. C8 and R10 in the base of TR6 form the time-constant required to give the 3 ms transmission pulse. TR2 to 7 and TR11 are all encapsulated in the 'µ min' style, TR11 being strapped as a diode because it is smaller than any conventional diodes. TR7 and TR8 form a Darlington pair to switch the push-pull oscillator, TR9, TR10 to the 'on' state. TR8, 9 and 10 are of the L1D type configuration, having high $h_{FE(min)}$ at high current levels ($h_{FE(min)}$ for $I_C = 150$ mA is 100). The 300 kHz signal produced by the oscillator is then coupled to the transducer by T1, a ferroxcube-cored transformer.

A capacitor C10 (68 µF) provides necessary decoupling for the receiver and in addition stores energy sufficient to supply the heavy current drawn in the first 200 µs of the transmit state. The transducer voltage is 100 V pk-pk for this period, decaying to approximately 60 V pk-pk at the end of the pulse. A higher value capacitor would be an advantage but physical size rules this out. All capacitors other than C10 are of the chip or non-encapsulated monobloc type.

6. Construction and Assembly

The individual components which go to make up the acoustic tag are shown in Fig. 4. The uncased battery, electronics and transducer are 4.7 cm long x 0.8 cm diameter; they weigh 5.5 g in air. For experiments carried up to the present time it has been found

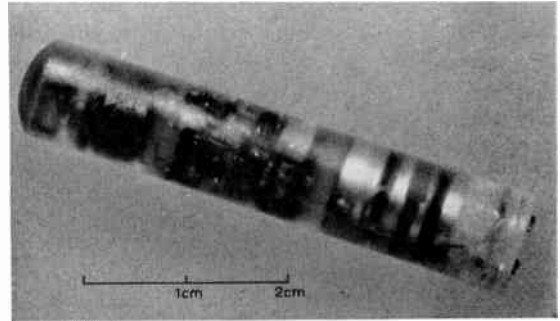


Fig. 5. Complete unit.

convenient to place the assembly inside the modified body of a disposable syringe; this is made of polythene with a 1 mm wall and has an internal diameter suitable for the tag assembly. Coupling from the transducer to the sea water is achieved by filling the whole syringe tube with castor oil before sealing it. The only disadvantage is that the weight then becomes 8.26 g in air, 4.0 g in sea water. Figure 5 shows the complete tag. A small disk seals the case and has two terminals projecting; when these are connected together the tag is switched on. The nylon cord used for attaching the tag to the fish is also fastened to these terminals. Weights of the individual components are listed in Table 1. The shape, size and weight were all adjusted so as to reduce drag and cause minimum damage to the fish.

There are three assemblies that go to make up the complete tag, these being the battery, the electronics and the transducer (Fig. 6). The cells of the battery are joined either by sticking them together with a silver-impregnated epoxy resin or preferably by welding small strips of metal to the appropriate surfaces. All the other joints in the system are soldered.

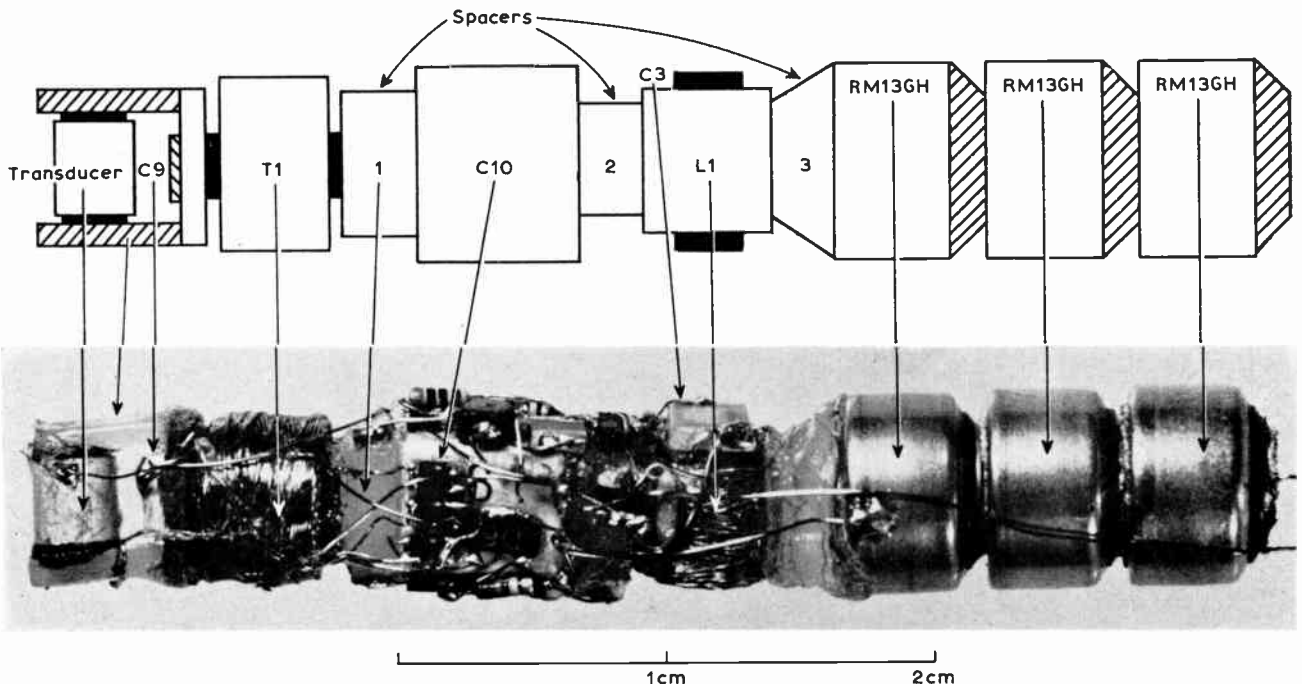


Fig. 6. Photograph of the unit with key to component parts.

Table 1. Weights of the individual components of the transponding acoustic fish tag

Component	Weight (g)	Quantity	Total weight (g)
Transducer	0.0961	1	0.0961
Rx coil L1	0.4856	1	0.4856
Tx coil T1	0.5945	1	0.5945
Transistors BCW33R	0.0078	7	0.0546
'Lid' transistors LDA-405	0.0050	3	0.0150
FET MMT 3823	0.0122	1	0.0122
RKL2 resistors	0.0049	11	0.0539
68 μ F capacitor	0.4336	1	0.4336
3300 pF "	0.0217	1	0.0217
10 000 pF "	0.0252	2	0.0504
2200 pF "	0.0148	1	0.0148
1000 pF "	0.0190	1	0.0190
680 pF "	0.0900	1	0.0900
560 pF "	0.0750	1	0.0750
82 pF "	0.0170	1	0.0170
22 pF "	0.0090	1	0.0090
Battery RM13 GH	1.0276	3	3.0828
Transducer holder	0.0533	1	0.0533
Battery spacer (polythene)	0.0590	1	0.0590
Coil spacers (polythene)	0.0300	2	0.0600
Tag case	1.5215	1	1.5215
Castor oil	1.4000	1	1.4000
Connecting wire, Durofix, etc.			0.0446
Total weight of tag in air (g)			8.2636

Although a high density of component assembly is achieved, layout is important but not critical. Chip capacitors are used where possible and these have helped to reduce the size of the electronic assembly, but it is the resistors which are of particular note. These are of a high-stability carbon film type, 2.590 mm long \times 0.889 mm diameter, used here in values from 10 k Ω to 4.7 M Ω .

Most components for the tag are mounted round the capacitor C10, which is a plastic-encapsulated tantalum of 68 μ F, rectangular in shape. Components are first glued to this capacitor with cyanoacrylate adhesive and then wired into circuit, connexion being made with the component leads or with 38 s.w.g. self-fluxing wire. Layout of components around C10 is important in order to prevent instability. Polythene blocks (1) and (2) are used to prevent capacitor C10 having a damping effect on T1 and L1, which would reduce receiver sensitivity and cause loss of power from the transmitter. The same applies for block (3), but in this case the receiver only is being spaced from the mercury cells. Block (3) is fixed to the cells by Araldite and blocks (1) and (2) are fixed to C10 with Araldite or Bostik.

6.1. Coils

Both L1 and T1 are wave wound with 42 s.w.g. en. cu. wire on ferroxcube beads FX 1242, then impregnated with silicone resin. L1 consists of one winding, but T1 is a multi-winding transformer acting as an input coil

for the receiver and an oscillator transformer for the transmitter.

Tuning capacitors for L1 and T1 are C3 and C9 respectively and these are mounted as shown in Fig. 6, C3 being mounted on the end of L1 ferroxcube and C9 being mounted below the transducer in the nylon mounting holder. L1 is fixed into place between blocks (2) and (3) by Durofix; T1 is also attached with Durofix between block (1) and the nylon transducer mounting holder.

6.2. Transducer and Mounting Holder

A fine wire is first connected to the inside of the cylindrical transducer; a piece of closed air cell neoprene, slightly larger than the outside diameter of the transducer, is then pulled through the transducer and cut off to project about 1 mm on either side of the transducer cylinder. This forms the support for the transducer element. The transducer is then mounted as shown, between the two nylon pillars, allowing enough room for C9 to be fixed to the nylon disk which forms the bottom of the assembly.

7. Electrical Performance

Detailed information on fish movements is required, so the interrogation rate is high (1, 2 or 4 times per second). This means that demand on the battery is relatively high and has two components, the current needed to maintain receiver sensitivity and the transmitter current during the pulse. Three mercury cells are used, each having a nominal voltage of 1.4 and an 85 mAh capacity at a 1 mA rate. At the *maximum* interrogation rate of 4 times per second the battery has a life of 32 hours, which is adequate for the work being carried out at present. An increase in battery size would extend the life of the tag but would limit its use to rather large fish. The present three-cell battery weighs 3.1 g in air; it measures 1.6 cm in length by 0.77 cm diameter; thus making up one-third of the total volume of the tag. Figure 7 shows duration of battery life against interrogation rate.

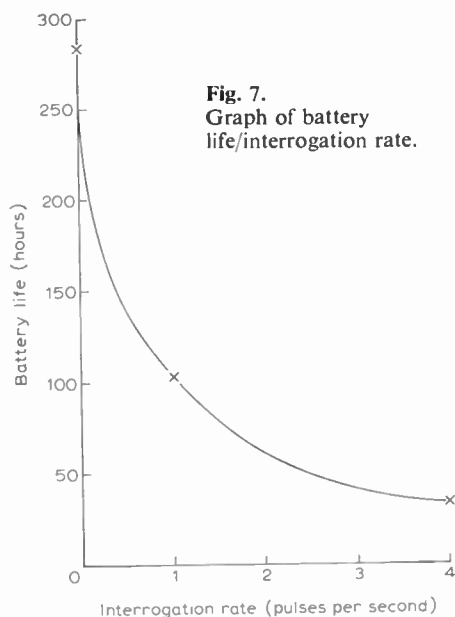


Fig. 7. Graph of battery life/interrogation rate.

A continuous drain of 300 μA is due to the receiver, this section having an input sensitivity of 20 μV for positive triggering of the transmitter. It is tuned to 305 kHz and has a bandwidth of about 5 kHz at the -6 dB points, with an overall gain of 85 dB. The transmitter has a quiescent current of 12 μA ; during the 3 ms pulse period it draws heavy current, initially, from a 68 μF capacitor across the battery supply.

8. Trials

The first trials with a transponding acoustic tag attached to a fish took place in July 1970. A 43 cm plaice (*Pleuronectes platessa* L.) had a normal Petersen tag fitted to it (Fig. 8); the acoustic tag was then tied to this by means of a short length of nylon cord. The fish was released in the Shipwash-Inner Gabbard area of the North Sea and observations of its movements were continued over a period of 15 hours. In this area the depth of water is about 27 m and the seabed is largely sand and gravel. Preliminary results of this tracking exercise have been reported in a letter to *Nature*.¹⁵

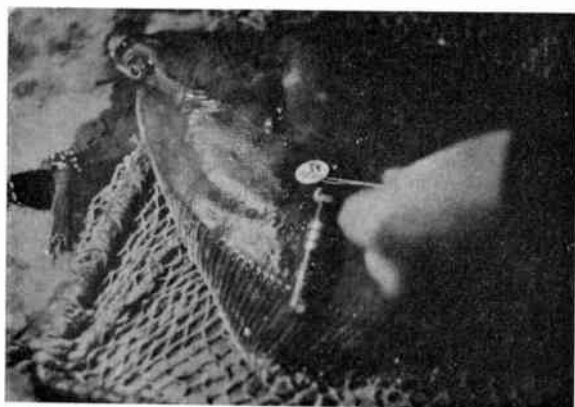


Fig. 8. Acoustic tag attached to a fish.

The method used was to record the range and bearing of the fish signal relative to the ship; then, by logging the bearing of the ship's head and fixing its position by Decca Navigator, the fish's track was plotted.

Subsequent trials have been carried out, also using plaice. Two of the recent trackings lasted for more than 26 hours each. The first of these was in the English Channel in February 1971, during bad weather when, surprisingly, the fish spent several hours very close to the surface. If the tag signal had not been such a large rectangle on the display it would have been impossible to have tracked the fish under the very turbulent sea conditions. Tracking was abandoned in wind force 9 when the ship sought shelter near the south coast. During the 26-hour observation period the depth of water was fairly constant at about 38 m. The interrogation rate was 4 per second for about 75% of the time but some additional triggering occurred due to multipath conditions. This was easily recognized because the signals appeared on the same bearing, the one at the shortest range giving the correct position of the fish. In practice double or multiple triggering was found to be

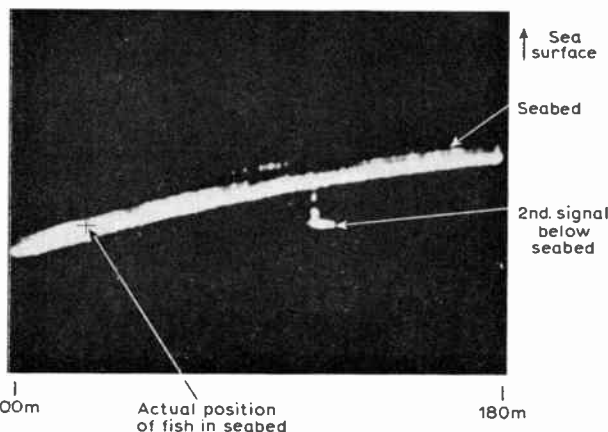


Fig. 9. Location of buried fish by means of the second signal (elevation scanning).

useful where the fish buried itself in a high-reverberation seabed, for, by switching to the elevation scanning mode, the second signal appeared below the seabed signal; however, as Fig. 9 shows, it was impossible to detect visually the pulse giving the actual position of the fish. This had to be found by holding a straight edge on the display and lining it up from the second signal back to the seabed, this point marking the true position. Under conditions where the fish was buried but where the seabed was sand, it was possible to use manual gain control of the sonar and reduce the seabed signal to such an extent that the tag pulse showed clearly. Figure 10 shows an example of this technique.

In areas where the seabed is featureless the fish can be tracked easily but very detailed movements are lost because ship positioning and plotting accuracy are limited. Such features as ridges or sand waves are particularly useful where, for instance, the fish's speed of movement over the ground is required. Because the pulse length of the tag signal is known it enables a fairly accurate measurement to be made of the distance between the crest of sand waves such as are shown in Fig. 11, and movements relative to these can be clearly seen in film sequences.

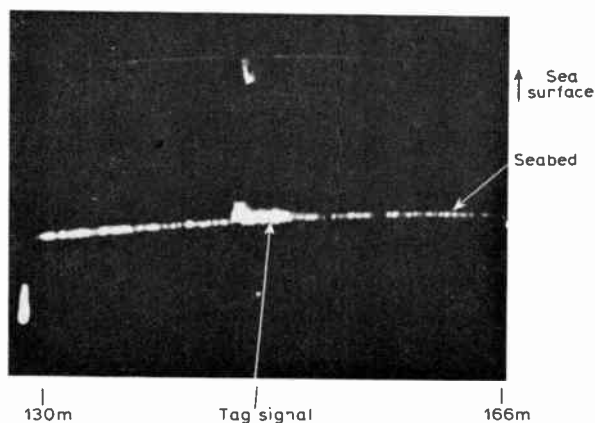


Fig. 10. Use of manual gain to accentuate the signal from a fish on the seabed (elevation scanning).

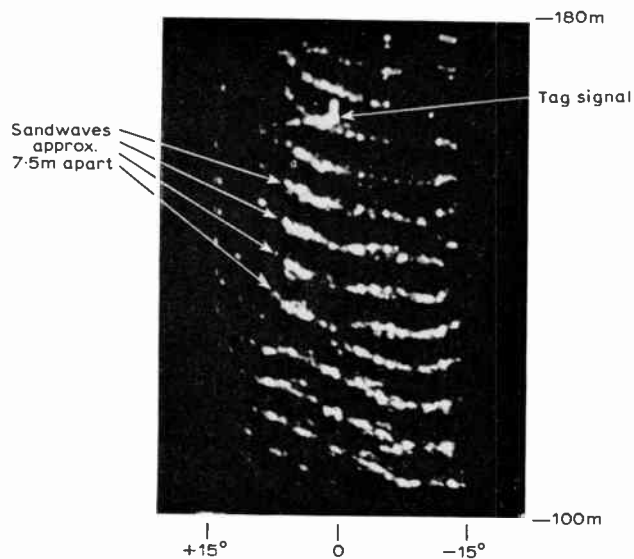


Fig. 11. Fish signal on sandwave background (azimuth scanning).

Further work to study fish behaviour and migration using these tags took place in June 1971. During the cruise 5 plaice and 1 cod were separately tracked and observed. The longest continuous track lasted for 54 hours. At the end of this period the tag was still functioning normally when it was decided to terminate the work. Other trackings during this cruise lasted for 51, 43, 38, 34 and 6 hours, bringing the total time for fish tracking with this design of tag to 301 hours, i.e. at least 2 million interrogations. Because the tidal streams are important in relation to the movements and behaviour of the fish in midwater and on the bottom, a midwater parachute drogue was tracked in the working area of the cruise. For studying bottom currents an acoustic tag fitted to a Woodhead seabed drifter was tracked for 25 hours.

9. Conclusions

It has been shown that the combination of a transponding acoustic tag and a high-resolution scanning sonar is a powerful and proven tool for fisheries research. Although this particular combination gives very detailed information for the situations likely to be encountered in the sea there is no reason why the transponding tag should not be used successfully with simpler shipboard equipment. For example, range and bearing are the measurements of interest when tracking fish in most rivers and in this case a small manually-operated transducer with suitable transmitter, receiver and display or recording units would be adequate.

10. Acknowledgments

The authors wish to thank: Dr H. A. Cole, Director of Fishery Research, for permission to publish this paper; Dr M. Greer Walker, for assistance and encouragement all through the development and trials; colleagues in the Electronics Section of the Fisheries Laboratory, and the captain and crew of R.V. *Clione*.

The reference to proprietary products in this report should not be construed as an official endorsement of those products, nor is any criticism implied of similar products which have not been mentioned.

11. References

1. Bass, G. A. and Rascovich, M., 'A device for sonic tracking of large fishes', *Zoologica, N.Y.*, **50**, No. 2, pp. 75-82, 1965.
2. Dizon, A. E., *et al.*, 'Migration orientation of Skeena River sockeye: ultrasonic telemetry study in open ocean and estuary', *J. Fish. Res. Bd Canada*, in press.
3. Hasler, A. D., Gardella, E. S., Horrall, R. M. and Henderson, H. F., 'Open-water orientation of white Bass, *Roccus chrysops*, as determined by ultrasonic tracking methods', *J. Fish. Res. Bd Canada*, **26**, No. 8, pp. 2173-92, 1969.
4. Henderson, H. F., Hasler, A. D. and Chipman, G. G., 'An ultrasonic transmitter for use in studies of movements of fishes', *Trans. Amer. Fish. Soc.*, **95**, pp. 350-56, 1966.
5. Johnson, J. H., 'Sonic tracking of adult salmon at Bonneville Dam, 1957', *Fishery Bull. Fish Wildl. Serv. U.S.*, **60**, No. 176, pp. 471-85, 1960.
6. Johnson, J. H., 'Ultrasonic fish tags: development and use as a behavior research tool', p. 24, In: Proc. B.C.F. Acoustical Workshop, November 25th-27th 1968 (Ed. by W. T. Pereyra), Seattle, Washington (Bureau of Commercial Fisheries, Exploratory Fishing and Gear Research Base), 40 pp., 1969.
7. Novotny, A. J. and Esterberg, G. F., 'A 132-kilocycle sonic fish tag', *Progve Fish Cult.*, **24**, No. 3, pp. 139-41, 1962. (In Russian.)
8. Poddubny, A. G., 'Sonic tags and floats as a means of studying fish response to natural environmental changes and to fishing gear', F.A.O. Conference on Fish Behaviour in Relation to Fishing Techniques and Tactics, Bergen, Norway, 19th-27th October 1967, FR:FB/67/E/46, 9 pp.
9. Poddubny, A. G., Spektor, Yu. I. and Kidun, S. M., 'Results of early experiments of following *Acipenseridae* bearing electronic tags', *Vop. Ikhtiol.*, **6**, 4, No. 41, pp. 725-34, 1966. (In Russian.)
10. Trefethen, P. S., 'Sonic equipment for tracking individual fish', Special Scientific Reports U.S. Fish Wildlife Service No. 179, 11 pp., 1956.
11. Trefethen, P. S., Dudley, J. W. and Smith, M. R., 'Ultrasonic tracer follows tagged fish', *Electronics*, **30**, No. 4, pp. 156-60, April 1957.
12. Yuen, H. S. H., 'Behavior of skipjack tuna, *Katsuwonus pelamis*, as determined by tracking with ultrasonic devices', *J. Fish. Res. Bd Canada*, **27**, No. 11, pp. 2071-79, 1970.
13. Voglis, G. M. and Cook, J. C., 'Underwater applications of an advanced acoustic scanning equipment', *Ultrasonics*, **4**, pp. 1-9, 1966.
14. Mitson, R. B. and Cook, J. C., 'Shipboard installation and trials of an electronic sector scanning sonar', In: Proc. Conf. on Electronic Engineering in Ocean Technology, Swansea, South Wales, 1970, pp. 187-210 (I.E.R.E. Conference Proceedings No. 19). Also in: *The Radio and Electronic Engineer*, **41**, No. 8, pp. 339-50, August 1971.
15. Greer Walker, M., Mitson, R. B. and Storeton-West, T., 'Trials with a transponding acoustic fish tag tracked with an electronic sector scanning sonar', *Nature, Lond.*, **229**, No. 5281, pp. 196-8, 15th January 1971.

Manuscript first received by the Institution on 10th May 1971 and in final form on 19th July 1971. (Paper No. 1416/AMMS42.)

Bidirectional Action in Pipe Flow Simulators

By

R. W. WILLIAMS,

Ph.D., M.Inst.P. †

The automatic reversibility of 'pipe cells' which simulate the flow of fluid in pipes is reviewed. The design and performance of a reversible cell, based on the use of an integrated circuit operational amplifier to provide unity gain, are described. The possibility is examined of replacing the resistor-diode law-forming networks customarily employed in pipe cells by space-charge-limited silicon resistors.

1. Introduction

The direct analogue technique of studying fluid distribution network problems requires the simulation of the steady state conditions of flow in a pipe section by a two-terminal electronic circuit which for brevity is termed a 'pipe cell'. In hydraulic practice, there are widely-used laws of the form $\Delta P = RQ^n$, applicable to incompressible flow, which give ΔP , the pressure loss in the pipe section, as a function of its hydraulic resistance R and the flow rate Q . Typically, the exponent n has the value 1.85. The pipe cell reproduces this behaviour in electrical terms and its law is $E = kI^n$, where E is the potential difference across the cell and I is the current flowing through it.

There is no great difficulty in applying the known techniques of function generation, using for example a network of resistors and biased diodes, to the realization of the law $E \propto I^n$ but the adjustment of the value of the parameter k over the wide range that is encountered in distribution network practice presents an interesting problem. Another requirement in pipe cell design is the provision of automatic reversibility. When the direction of flow in a pipe reverses, the sense of the pressure loss also reverses and the ability of a pipe cell to function in the same way, without demanding the intervention of the operator of the analogue, is an important practical feature.

McKay¹ has reviewed some existing designs of pipe cell and described an elegant new circuit in which he uses a current sink stage to achieve wide-range control of the k -value. The present paper considers the realization of automatic reversibility, a topic not discussed by McKay. A new cell design is described and a possible alternative to resistor-diode law-forming networks is examined.

2. Automatic Reversibility

2.1 Use of the Diode Bridge

Pipe cells embodying the current sink principle, as developed by McKay and by others,^{2,3} are unidirectional in action and they cease to function when the polarity of the cell voltage is reversed. Bidirectional operation may be achieved quite simply by connecting a cell of this type within a diode bridge; if the external current flow reverses the direction of flow through the cell itself remains unchanged. The accuracy of realization of the flow law by the cell suffers somewhat since the volt drop in the two conducting diodes is a source of error. Even

if germanium diodes are used in the bridge, this can be appreciable under the condition of low hydraulic resistance settings (i.e. high currents through the cell) combined with small values of the cell voltage.

In the case of the cell² currently used in the B.A.C. Fluid Network Analyser, a compromise is effected by designing the law-forming network for best accuracy in the centre of the hydraulic resistance range. The cell errors at low voltage for low resistance settings are then of one sign and those for high settings are of the opposite sign. The cell performance is generally satisfactory but the desirability of reducing the variation of cell behaviour with hydraulic resistance setting has been recognized for some time. As a result, a design of cell which is inherently reversible has been evolved and this is now described.

2.2. An Inherently Reversible Cell

B.A.C. cells⁴ manufactured prior to 1966 operated on the principle shown in Fig. 1. Here a unity gain amplifier is furnished with an input signal from the law-forming network. If E is the cell voltage, the current i through the law-forming network is given by $E = ai^n$, where a is a constant, and the amplifier input is $E - iR_1$. The amplifier action maintains a potential difference of $E - (E - iR_1) = iR_1$ across the bypass resistor R_L . The current through the latter is therefore iR_1/R_L and the total current I through the cell is $i(1 + R_1/R_L)$. Making the substitution $i = (E/a)^{1/n}$, it follows that the cell characteristic is:

$$E = aI^n / (1 + R_1/R_L)^n.$$

The resistance parameter of the cell is $a/(1 + R_1/R_L)^n$ and is adjustable over a wide range by variation of R_L .

A linear integrated circuit operational amplifier used in the voltage follower mode is an accurate realization of a unity gain amplifier. Furthermore its output voltage is free to change sign; a cell based on the arrangement of Fig. 1 and employing an amplifier of this type is therefore

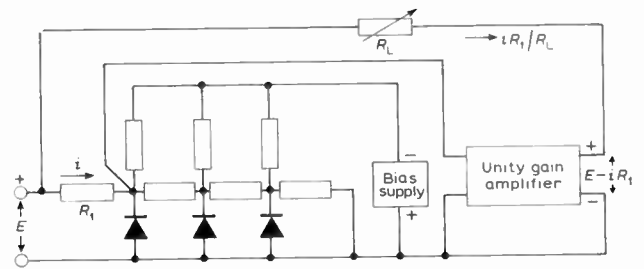


Fig. 1. Principle of pipe cell using unity gain amplifier.

† British Aircraft Corporation, Stevenage, Hertfordshire.

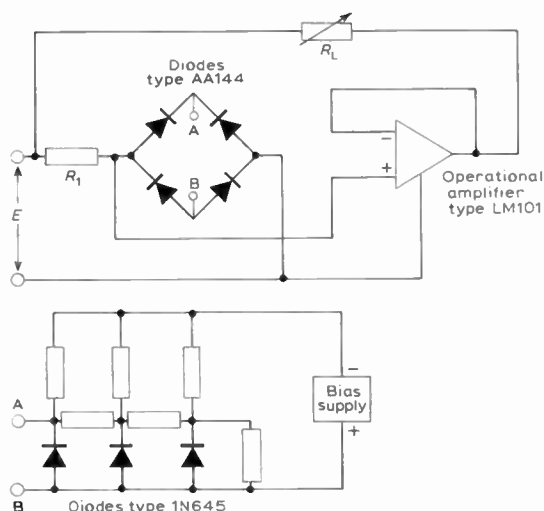


Fig. 2. Circuit diagram of new cell based on Fig. 1.

inherently reversible provided the action of the law-forming network is also reversible (which is not the case for the network of Fig. 1). Revival of the principle of Fig. 1 in terms of an integrated circuit appeared to be worthwhile and such a cell has been tested with satisfactory results. Referring to its circuit diagram (Fig. 2), the law-forming network (except for its first element, R_1) is connected within a diode bridge to secure reversibility. Since only the network current flows through the bridge diodes and not the total cell current, the effect of the volt drop in the diodes is independent of the cell resistance setting and may be taken into account, without compromise, in the design of the network.

Trials were first conducted using a type 709 amplifier but the cell performance was restricted by the fact that the common mode input voltage of the type 709 is limited to a maximum of ± 10 V. This means that in the voltage follower mode the full excursion of the output voltage (± 13 V) cannot be used. It was also found that the cell action was not completely symmetrical; reversal of the cell voltage resulted in a difference in the cell current of about 5%. Substitution of a type LM101 amplifier (similar to the type 741) removed this difficulty and also eliminated the tendency to latch-up which is a feature of the 709.

The hydraulic resistance coverage of the cell is determined at the low resistance end by the output current-handling capacity of the amplifier and at the high end by the current through the law-forming network. The range of values of the individual resistors in the network of the experimental cell extends from 75 k Ω to 2.4 M Ω ; there ought not to be any difficulty in doubling these values, in which case the hydraulic resistance coverage would be increased to about three times the figure quoted below. At the low resistance end, it would be possible to extend the coverage by using a booster stage driven from the output of the operational amplifier.

The performance of the experimental cell may be summarized thus:

Law-forming network: 1.85 power law, 4 segments, bias voltage 24 V.

Accuracy: for a given setting of R_L , the voltage across the cell for a given value of the current through it follows the 1.85 law within the extremes of error of ± 0.20 V and -0.19 V over the working range of the cell, which is 0–17 V.†

Variation of accuracy with resistance setting: negligible.

Reversibility: the change in the cell current when the voltage is reversed is less than 0.5%.

Hydraulic resistance range: ratio of maximum and minimum settings is 5830 : 1.

Behaviour at the origin: the cell current is substantially zero for zero applied voltage.

3. An Alternative to the Resistor-diode Law-forming Network

The circuit of Fig. 2 represents a useful simplification of pipe cell design. Further simplification is possible if a single device having non-ohmic characteristics can be found with which to replace the law-forming network. The square-law silicon resistor developed by Wright,⁵ in which the current flow is space-charge-limited, is worthy of consideration in this connexion. Resistors of this type follow the law $i = P(E - E_0)^2$ where P and E_0 are constants, the latter being small.

The square law is followed quite accurately; the best results are obtained if an ohmic resistor is connected in parallel with the silicon resistor of such a value as to cancel the negative conductance term $-2PE_0$. Further adjustment of the resistor value below this point is effective in producing a close approximation to the 1.85 law. In a trial on a silicon resistor shunted as described the author found that the current followed the 1.85 law to within $\pm 0.3\%$ of full scale over the range of 0–8 V of E . Unfortunately, silicon resistors are characterized by a change of about 10% in the value of the permeance P when the current flow is reversed. The use of silicon resistors for reversible cells cannot therefore be recommended; where reversibility is not a requirement, their performance would be very suitable. There is no difficulty in driving them from linear integrated circuits; the fact that voltage and current are transposed in its law, as compared with the desired cell law, means that the silicon resistor has to be used in the feed-back path. The current at $E = 8$ V is of the order of 5 mA.

4. Conclusions

With the object of improving the performance of reversible pipe cells, an existing cell principle, embodying a unity gain amplifier, has been re-examined and found to give satisfactory results. The use of an integrated circuit operational amplifier simplifies the cell construction and it is noteworthy that the maximum current through the cell is respectively one order and nearly two orders less than the maximum currents of its predecessors in the family of B.A.C. cells.

† The cell may be protected against voltages in excess of 17 V by connecting a pair of silicon diodes back-to-back across the input terminals of the amplifier and a pair of 12 V Zener diodes, also back-to-back, across its output.

Further simplification of the cell rests on the possibility of replacing the resistor-diode type of law-forming network by a single component. The space-charge-limited silicon resistor has been found to give very good law accuracy but does not meet the reversibility requirement.

5. References

1. McKay, E. M., 'Simulation of steady state fluid flow in pipes', *The Radio and Electronic Engineer*, 38, No. 5, p. 297, November 1969.

2. Williams, R. W., 'Aspects of the direct analogue technique for solving fluid distribution network problems', *Instrument Practice*, 22, p. 54, January 1968; British Aircraft Corporation Limited and Boxall, E. R., British Patent 1,161,086.
 3. Charbonnages de France, French Patent 1,457,304.
 4. British Aircraft Corporation (Operating) Limited and Woodley, F. J., British Patent 1,068,824.
 5. Büget, V. and Wright, G. T., 'Space-charge-limited current in silicon', *Solid State Electronics*, 10, p. 199, March 1967.

Manuscript first received by the Institution on 17th December 1970 and in final form on 2nd April 1971. Short Contribution No. 146/1C52.

© The Institution of Electronic and Radio Engineers, 1971

Changes to the U.K. Standard Frequency and Time Services on 1st January 1972

Communication from the National Physical Laboratory.

Following international agreement the standard frequency and time signal broadcasts in the United Kingdom will be adjusted to conform with the International Atomic Time (IAT) reference in both time indication and rate on 1st January 1972. This will involve a time step applied to the time signal emissions and also the elimination of the frequency offset where it still exists.

In accordance with the agreed procedures the Director, Bureau International de l'Heure (BIH) has announced the amount and incidence of the time step as follows:

'A negative time step of $-0.107\ 757\ 7\text{ s}$ will be applied to UTC when the date will be:

- 1971, December 31, 23 h 59 m 60.107 757 7 s, (old) UTC so that at this instant the date will become
- 1972, January 1, 0 h 0 m 0 s, exactly, (new) UTC.'

In practice this adjustment will be closely approximated in the time standard at Rugby Radio Station by delaying the emission of the minute pulse following 23 h 59 m 59 s on 31st December 1971 by 0.107 760 s. In consequence the final 'second' of 1971 will have a duration of 1.107 760 s.

The new UTC system commencing 1st January 1972, 0 h 0 m 0 s will then differ from the IAT scale by precisely 10 s. Simultaneously with this change the offset will be removed in both time signal and carrier frequency generators.

MSF 60 kHz, 2.5, 5 and 10 MHz: The time step as described above will be applied to the MSF time signal emissions. All the carrier frequencies are radiated at present without offset and no change will be necessary.

GBR 16 kHz: The present offset of -300 parts in 10^{10} will be eliminated from the GBR signal frequency coincident with the time step as already indicated. The effect of the time step will be first apparent in the time signal transmission at 0255-0300 GMT on 1st January 1972.

Droitwich 200 kHz: The carrier frequency is already adjusted to zero offset and no change will be necessary.

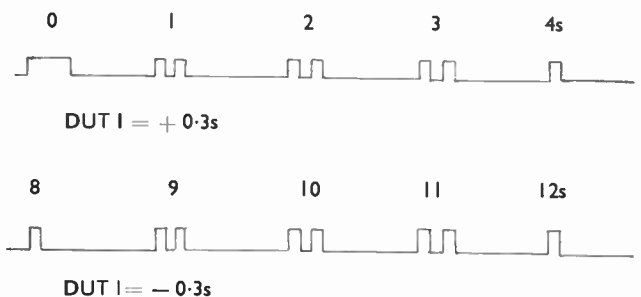
Future Time Steps

The present offset corresponds to an accumulated time difference of about 1 s in the course of a year. With the elimination of the offset the time difference between the radiated UTC signal and the astronomical reference UT 1 will be maintained within the limits $\pm 0.7\text{ s}$ by step changes of exactly 1 s made, when necessary on 30th June and/or

31st December. If the present trend in the Earth's rate of rotation continues it is likely that the first such step will be applied on 30th June 1972 when the emitted time scale will be retarded by the insertion of an additional second in the last minute of the month. Provision has been made for such a 'leap second' to be either positive, as in this case when it is an additional second, or negative, when a second is eliminated and in consequence the time indication is advanced. This possibility may arise should the Earth significantly increase its rate of rotation.

Information on the introduction of leap seconds will be provided by the BIH at least two months in advance of the date of application of the change. In addition the Bureau will furnish values of the difference between UTC and UT 1 and this difference, denoted $DUT\ 1 = UTC - UT\ 1$, will be given to a unit of 0.1 s in the form of an internationally agreed coded announcement on primary time signal emissions. When the difference is positive its magnitude will be indicated by emphasizing the appropriate seconds pulses immediately following the minute marker from pulse 1 to pulse 7, inclusive; a negative value for $DUT\ 1$ will make use of pulses beginning with pulse 9 and extending to pulse 15. In either case the magnitude of $DUT\ 1$ will be given by the total number of consecutive emphasized pulses. The absence of emphasized pulses will mean that $DUT\ 1$ has the value zero.

A common system of emphasis has been adopted for both MSF and GBR transmissions and takes the form of an additional pulse radiated 100 ms after the end of the normal second pulse. This produces a distinctive double pulse which should be easily heard and identified in the presence of noise and interfering signals. Examples are given below which it is hoped will make clear the interpretation of the coded information.



Thin Cylindrical Antenna: Variational Solution with Polynomial Current Approximation

By

BRANKO D. POPOVIĆ, D.Sc.†

and

ZORAN D. POPOVIĆ, M.Sc.†

All existing variational solutions to thin cylindrical antenna problems use two-term trial functions for currents, the form of which must either be based on some prior knowledge of current distribution along the antenna, or obtained by some other method. The present paper is aimed at eliminating these deficiencies in the applications of the variational method, by using as the trial function for current a polynomial of arbitrary order with complex coefficients. All the double integrals are transformed into sums of ordinary integrals to reduce computing time. The theory is applied to a number of isolated symmetrical cylindrical antennas of moderate lengths (up to approximately 2λ), starting with perfectly conducting dipoles in a vacuum, and ending with capacitively-loaded broadband cylindrical antennas. The theoretical results are in good agreement with available experimental data.

1. Introduction

The variational method of analysis for thin cylindrical antennas is due to Storer.^{1, 2} He demonstrated that if the particular expression he derived for the driving-point impedance Z_0 of an antenna is considered, the first variation of Z_0 with respect to small changes of current distribution about the true distribution is zero. He next represented current distribution along perfectly conducting antennas of moderate lengths in the form of a two-term trigonometric functional series with unknown complex coefficients, which he determined using the stationary property of Z_0 . The values of the driving-point impedances he thus obtained were very accurate. Note, however, that the success of the method depended critically upon knowing in advance that the appropriate choice of the unknown coefficients could result in an accurate current distribution.

The variational method has been since applied successfully to several other types of isolated cylindrical antennas,³⁻⁵ as well as to arrays of cylindrical dipoles.⁶⁻⁸ In all the cases, two-term trial functions for current have been adopted, the choice of which was necessarily based on certain prior knowledge about the true current distribution. The applicability of the variational method in analysing thin cylindrical dipoles was thus restricted to those cases only in which a two-term current distribution was known in advance to approximate the true distribution accurately. Perhaps the best illustration of the limitations of the variational method used with these restrictions may be found in reference 3, where current distribution along dipoles with non-reflecting resistive loading was approximated by a two-term trial function with an additional parameter. The optimum value of that parameter could only be determined by comparing the theoretical and experimental results, which obviously reduces greatly the usefulness of the theory.

The present paper is aimed at eliminating these deficiencies present in the existing applications of the variational method to cylindrical antennas. A very simple and extremely flexible functional series in the form of a polynomial with complex coefficients is

adopted as the trial function for current. The order of the polynomial approximating the current distribution is restricted mainly by the storage capacity of the computer used. It was found that solutions as high as the 7th order could be obtained with a digital computer having only 8k 16-bit words core memory. Thus, although the method is intended specifically for analysing cylindrical antennas of moderate lengths, antennas as long as two operating wavelengths can be analysed as well.

In addition to the possibility just described of using a trial function for current of order higher than two, which apparently was the highest order approximation used so far in a variational solution, the polynomial approximation has another important property. Only very rough previous knowledge of the current distribution along an antenna is required, i.e. that it can be approximated with a reasonable accuracy by a polynomial of a sufficiently high order. In this manner the important class of cylindrical antennas with continuously distributed resistive loading along their length, where any other than a rough guess as to current distribution is hardly possible, can also be analysed rigorously using the present method.

There is another important class of thin dipoles which can also be analysed using the proposed method, though approximately. These are capacitively loaded dipoles, made in the form of small conducting cylinders between which thin dielectric disks are sandwiched. In analysing such a structure it is assumed, first, that the field structure remains essentially the same as in the conducting antenna case (i.e. that no surface waves are excited). Second, in evaluating vector potential of current flowing along such an antenna a certain smoothed-out, equivalent conduction current along the antenna is assumed to be the source of the vector potential.

The paper deals only with isolated dipoles. After deriving briefly the variational expression for the driving-point impedance of a thin symmetrical cylindrical dipole with continuous impedance loading, situated in a linear homogeneous dissipative medium, the expressions for the current distribution parameters and the driving-point impedance are derived using the general, n th-order polynomial trial function for current. The theory is next verified in some cases of perfectly conducting dipoles in a vacuum and in a dissipative medium, and of

† Department of Electrical Engineering, University of Belgrade, P.O. Box 816, 11001 Belgrade, Yugoslavia.

imperfectly conducting dipoles, for which experimental data are available. Finally, broadband resistively and capacitively-loaded antennas, for which experimental results have been published, are analysed. In all the cases mentioned, the theoretical driving-point conductance is found to be in excellent agreement with measured values. The same could be said about the susceptance, with the reservation that this might partly be a coincidence, as different theoretical and experimental geometry of the excitation zone makes this agreement questionable. The theoretical current distribution along the antennas was also found to be reasonably accurate.

Finally, using a recently developed procedure, the double integrals appearing in the variational solution are shown in the Appendix to reduce to a sum of ordinary integrals. This greatly reduces the computer time necessary for the evaluations.

2. Basic Theory

Consider a thin symmetrical dipole of length $2h$ and radius a ($h \gg a$), centre-driven by a delta function generator of voltage V and angular frequency ω . Let the z -axis of the coordinate system coincide with the dipole axis, and the origin with the zone of the generator. We assume that the dipole is situated in a homogeneous medium of permittivity ϵ , permeability μ and conductivity σ , and that the internal impedance of the dipole per unit length is $Z_i(z)$. We shall restrict our attention to cases in which $Z_i(z)$ is an even function of the coordinate z , differentiable at all points except possibly at $z = 0$ and $z = \pm h$. Then the current $I(z)$ along the antenna will also be an even function of z , with continuous derivative $dI(z)/dz$ everywhere except at $z = 0$.

Owing to symmetry, the tangential component of the electric field intensity on the antenna surface has the z -component $E_z(z)$ only. From the definition of the internal impedance $Z_i(z)$ and of the delta function generator, it follows that the following equation must hold on the antenna surface:

$$E_z(z) + V \delta(z) = Z_i(z) I(z), \dots\dots(1)$$

where $\delta(z)$ is the Dirac delta function. Now, $E_z(z)$ can be expressed in terms of the magnetic vector potential as

$$E_z(z) = -j\omega \left(1 + \frac{1}{k^2} \frac{\partial^2}{\partial z^2} \right) A_z(z), \dots\dots(2)$$

where

$$k = \omega [\epsilon\mu(1 - j\sigma/\omega\epsilon)]^{1/2} \dots\dots(3)$$

is the complex propagation constant of the medium. Also, $A_z(z)$ can be expressed in terms of the current $I(z)$ along the antenna:

$$A_z(z) = \frac{\mu}{4\pi} \int_{-h}^h \frac{I(z') \exp(-jkr)}{r} dz' \dots\dots(4)$$

with

$$r = [(z - z')^2 + a^2]^{1/2} \dots\dots(5)$$

Substituting (2) and (4) into equation (1), multiplying the equation thus obtained by $I(z) dz$ and integrating from $-h$ to h , we get

$$V I(0) = \frac{j\zeta}{4\pi} \int_{-h}^h \int_{-h}^h I(z) I(z') K(z - z') dz dz' + \int_{-h}^h Z_i(z) I^2(z) dz, \dots\dots(6)$$

where $\zeta = [\epsilon(1 - j\sigma/\omega\epsilon)/\mu]^{-1/2}$ is the complex intrinsic impedance of the medium, and

$$K(z - z') = k \left(1 + \frac{1}{k^2} \frac{\partial^2}{\partial z^2} \right) \frac{\exp(-jkr)}{r}. \dots\dots(7)$$

Finally, if we introduce for convenience the relative current distribution function

$$g(z) = I(z)/I(0) \dots\dots(8)$$

and note that $V = Z_0 I(0)$, Z_0 representing the driving-point impedance of the antenna, we obtain

$$Z_0 = \frac{j\zeta}{4\pi} \int_{-h}^h \int_{-h}^h g(z) g(z') K(z - z') dz dz' + \int_{-h}^h Z_i(z) g^2(z) dz. \dots\dots(9)$$

It can be shown in a similar manner to that described in references 1 and 2 that the first variation of Z_0 given by (9) with respect to small changes of $g(z)$ about the true distribution is zero, i.e. that

$$\delta Z_0 = 0. \dots\dots(10)$$

If the normalized current distribution $g(z)$ is represented as a functional series with unknown complex coefficients, these coefficients can be determined so that equation (10) is satisfied. In this manner a normalized current distribution function can be found which approximates to the true distribution along the antenna, and which is particularly accurate at $z = 0$.

Obviously, the foregoing theory could yield meaningful results only if the functional series is known in advance to approximate well to the true distribution, provided that the unknown coefficients are chosen appropriately. From the practical point of view, it is necessary that the series has the least number of terms possible. In the case of a perfectly conducting antenna of moderate length and situated in a vacuum, certain guidelines for adopting simple two-term functional series do exist. However, in the present general case, of continuously loaded antennas situated in a generally dissipative medium, no such precise criteria are available. A sufficiently flexible functional series, which can approximate to a variety of current distributions with a few terms, should therefore be used.

If the antenna considered is of moderate length (not exceeding two wavelengths measured in the surrounding medium), it seems that perhaps the optimal synthesis of great flexibility and computational simplicity is obtained if polynomial expansion of the relative current distribution function is used.⁹⁻¹¹ The most convenient form of this expansion is

$$g(z) \approx \sum_{i=1}^n b_i (1 - |z|/h)^i \dots\dots(11)$$

as it takes care automatically of the condition $g(\pm h) = 0$. According to (8), however, not all of the coefficients b_i are independent, as (11) must satisfy the relation $g(0) = 1$, whence

$$\sum_{i=1}^n b_i = 1. \quad \dots\dots(12)$$

This relation can be used to express one of the b coefficients, for example b_n , in terms of the other $(n-1)$ coefficients:

$$b_n = 1 - \sum_{i=1}^{n-1} b_i. \quad \dots\dots(13)$$

Let us now substitute (11) into (9), and we obtain

$$Z_0 \simeq \sum_{i=1}^n \sum_{j=1}^n b_i b_j w_{ij}, \quad \dots\dots(14)$$

where

$$w_{ij} = u_{ij} + v_{ij}, \quad \dots\dots(15)$$

with

$$u_{ij} = \frac{j\zeta}{4\pi} \int_{-h}^h \int_{-h}^h (1 - |z|/h)^i (1 - |z'|/h)^j \times K(z - z') dz dz' \quad \dots(16)$$

and

$$v_{ij} = \int_{-h}^h Z_i(z) (1 - |z|/h)^{i+j} dz. \quad \dots\dots(17)$$

Noting that $Z_i(-z) = Z_i(z)$, by assumption, after some simple transformations (17) can be reduced to

$$v_{ij} = 2h \int_0^1 Z_i[(1-x)h] x^{i+j} dx. \quad \dots\dots(18)$$

The double integrals u_{ij} , given by (16), can be expressed as a sum of ordinary integrals using the formulae given in the Appendix. Thus all the integrals u_{ij} and v_{ij} can easily be integrated numerically by means of a high-speed electronic digital computer, and the w_{ij} parameters in (14) obtained from (15).

To take care of the condition (13), we first rewrite equation (14) in the form

$$Z_0 \simeq \sum_{i=1}^{n-1} \sum_{j=1}^{n-1} b_i b_j w_{ij} + 2b_n \sum_{i=1}^{n-1} b_i w_{in} + b_n^2 w_{nn}. \quad \dots(19)$$

Substituting b_n given by (13) into (19) and noting that $w_{ji} = w_{ij}$, after some rearrangements we obtain

$$Z_0 \simeq w_{nn} + 2 \sum_{i=1}^{n-1} b_i (w_{in} - w_{nn}) + \sum_{i=1}^{n-1} \sum_{j=1}^{n-1} b_i b_j (w_{ij} - 2w_{in} + w_{nn}) \quad \dots\dots(20)$$

To determine the coefficients b , and thus $g(z)$ and Z_0 , we make use of the condition (10):

$$\delta Z_0 \simeq \sum_{i=1}^{n-1} \frac{\partial Z_0}{\partial b_i} \delta b_i = 0, \quad \dots\dots(21)$$

from which, as δb_i are independent, $\partial Z_0 / \partial b_i = 0$, $i = 1, 2, \dots (n-1)$. The following set of linear equations in complex unknowns b_i , $i = 1, 2, \dots (n-1)$, is thus obtained:

$$\sum_{i=1}^{n-1} b_i (w_{ij} - w_{in} - w_{jn} + w_{nn}) = w_{nn} - w_{jn}, \quad j = 1, 2, \dots (n-1). \quad \dots(22)$$

Once the b_i coefficients are determined, Z_0 is evaluated from (20), and $g(z)$ from (11) and (13). If current distribution $I(z)$ corresponding to the voltage V is required

instead of $g(z)$, it can be obtained from

$$I(z) = I(0) g(z) = \frac{V}{Z_0} g(z). \quad \dots\dots(23)$$

Using the foregoing procedure and the expressions for the u_{ij} integrals in terms of ordinary integrals presented in the Appendix, a general program for determining solution of any desired order n of the trial function for current (eqn. (11)) can be constructed. As to the order n of the solution, two approaches could be adopted. The programmer can either program n as one of the input data, or the computer can be instructed to start with $n = 2$ and proceed until the difference of a convenient parameter in two successive solutions is less than the prescribed error. (In the latter case it is wise to prescribe the upper limit of n as well.)

In the following sections the general theory outlined above will be applied to diverse special cases for which experimental data are available.

3. Numerical Results

3.1. Perfectly-conducting Dipole in a Vacuum

The case of a perfectly-conducting dipole in a vacuum is interesting for us for two reasons: (1) excellent experimental data for such cases are available,^{1,2} and (2) Storer's original solution^{1,2} was done for this case only, using a trigonometric two-term function for current. It will be hence possible to compare the results obtained by the original trigonometric solution and the polynomial solution between themselves, and with experimental results. This can give an idea of the relative accuracy of the polynomial and the trigonometric trial functions.

We shall restrict our attention to cases for which experimental data are available. Consider a perfectly-conducting dipole (i.e., $Z_i(z) = 0$) of a radius $a = 0.007022 \lambda$ (λ stands for the wavelength, as usual), and lengths 0.25λ , 0.375λ and 0.5λ , situated in a vacuum. It was found that in all three cases the lowest, second-order polynomial expansion is an excellent approximation. As an illustration, the second-order values of driving-point admittances are compared in Table 1 with those obtained with Storer's trigonometric current approximation and with experimental results. It may be noted that the results obtained by the present approach are in somewhat better agreement with experimental values than those obtained by the two-term trigonometric trial function for current. As mentioned earlier, the success of the variational method

Table 1. Comparison of driving-point admittances obtained by the present theory with trigonometric solution and experimental results

h/λ	Variational		Experimental ^{1,2}
	2nd-order polynomial	2nd-order trig. function	
0.250	8.934 - j 3.445	9.061 - j 3.238	8.95 - j 3.47
0.375	1.575 - j 0.228	1.535 - j 0.314	1.59 - j 0.16
0.500	1.013 + j 1.701	0.972 + j 1.424	1.02 + j 1.68

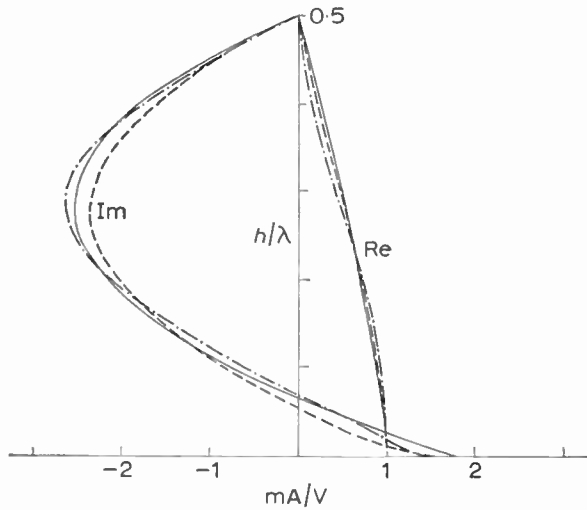
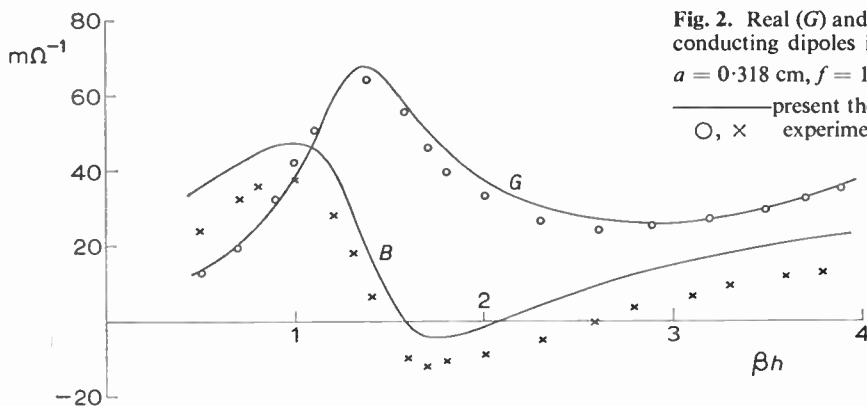


Fig. 1. Real (Re) and imaginary (Im) parts of current distribution along a full-wave perfectly-conducting dipole, with $a/\lambda = 0.007022$.
 ——— variational/polynomial, $n = 2$
 - · - · - variational/trigonometric, $n = 2$
 - - - - - measured (Mack¹²)

depends critically on the accuracy by which the trial function for current can approximate the true distribution. It might therefore be said that, for $h < 0.5 \lambda$, the simple second-order polynomial current distribution is at least as good an approximation to the true distribution as the conventional trigonometric two-term representation. To illustrate this conclusion, Fig. 1 shows these two distributions as compared with the experimental distribution¹² for $a = 0.007022 \lambda$ and $h = 0.5 \lambda$. The difference between the two theoretical distributions is small, and both are in a satisfactory agreement with the measured distribution.

3.2. Perfectly-conducting Dipole in a Dissipative Medium

As the next case, consider a perfectly-conducting dipole (i.e. $Z_i(z) = 0$) of radius a and length $2h$, situated in a dissipative medium of conductivity σ , permeability μ and permittivity ϵ . Both experimental and theoretical results for certain cases of such dipoles are available.^{11,13,14} It was found that the present method yields values of admittances close to those obtained by other theories,^{11,14} and in satisfactory agreement with



experimental values.¹³ As an illustration, Fig. 2 shows real and imaginary parts of admittances of dipoles immersed in a medium having $\sigma/\omega\epsilon = 0.35$ and $\epsilon = 78\epsilon_0$, versus the electric half-length βh of the dipole (measured in the surrounding medium), β representing the real part of k . Shown in the figure also are the experimental values of Iizuka and King.¹³ Agreement of the conductance with experimental values is very satisfactory. The difference in the susceptance is seen to be approximately $10 \text{ m}\Omega^{-1}$ for all the antenna lengths. This is a typical effect of different driving mechanisms in the theoretical model and the real system, present also in the results obtained by other theories using the slice generator excitation.^{11,14}

3.3. Dipole with Constant Resistive Loading

The two preceding examples refer to perfectly-conducting dipoles, i.e. to dipoles for which $Z_i(z) = 0$. In this and the following sections we shall consider some cases of impedance-loaded dipoles situated in a vacuum. Assume first that $Z_i(z) = R_i$ is constant along the dipole. Experimental results for dipoles with constant resistive loading were obtained by Shen,¹⁵ and theoretical methods of analysing such dipoles are due to King and Wu¹⁶ and to the present authors.^{5,10} The results obtained by the present method were found to agree satisfactorily with available experimental results. As an illustration, Fig. 3 shows real and imaginary parts of the admittance of dipoles with $a = 0.32 \text{ cm}$, $\Omega = 2 \ln(2h/a) = 9.92$ and $Z_i(z) = R_i = 700 \text{ ohm/m}$, versus the electrical half-length βh of the dipole. Agreement with Shen's experimental results is seen to be very satisfactory.

3.4. Broadband Resistive Dipole

As $\beta = \omega(\epsilon_0\mu_0)^{1/2}$, Fig. 3 can also be interpreted as a diagram showing real and imaginary parts of the resistive dipole admittance versus frequency. With this in mind, it is clear that dipoles with constant resistive loading are resonant structures just as perfectly-conducting dipoles are, though to a lesser extent.

If the resistive loading along the dipole is variable, however, with a certain distribution of this loading dipoles having admittance constant in a wide frequency range can be obtained. This conclusion was arrived at theoretically by Wu and King¹⁷ by considering a

Fig. 2. Real (G) and imaginary (B) parts of admittance of perfectly conducting dipoles immersed in a dissipative medium versus βh .
 $a = 0.318 \text{ cm}$, $f = 114 \text{ MHz}$, $\epsilon_r = 78$, $\sigma/\omega\epsilon = 0.35$
 ——— present theory, $n = 2$ for $h < 2$, $n = 3$ for $h > 2$
 O, x experimental¹³

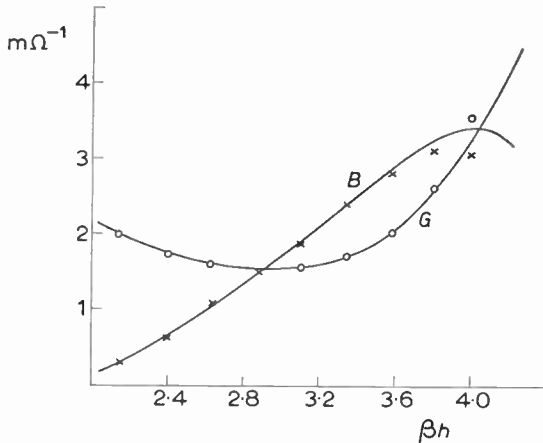


Fig. 3. Real (*G*) and imaginary (*B*) parts of admittance of resistive dipoles versus βh .
 $a = 0.32$ cm, $2 \ln(2h/a) = 9.92$, $Z_1 = R_1 = 700$ ohm/m
 — present theory, $n = 3$ experimental¹⁵
 ○, ×

differential equation approximating the integral equation for current. The loading required by the Wu-King theory is of the form

$$Z_i(z) = R_i(z) = \frac{\zeta_0}{2\pi h} \frac{|\psi|}{1 - |z|/h}, \dots\dots(24)$$

where ψ is a parameter defined in reference 17. Shen³ verified their conclusions experimentally, and explained the results also by using a two-term variational solution with exponential trial function for current containing an undefined parameter, the attenuation factor. That parameter could be determined only by comparing a set of theoretical results with experiments, which makes his approach difficult to use in new cases. One of the present authors demonstrated that the point-matching method with polynomial approximation of current gives quite accurate values of both the admittance and of the current distribution.¹⁸ We shall consider the same cases using the present variational solution.

In Shen's paper³ results for vertical monopoles above

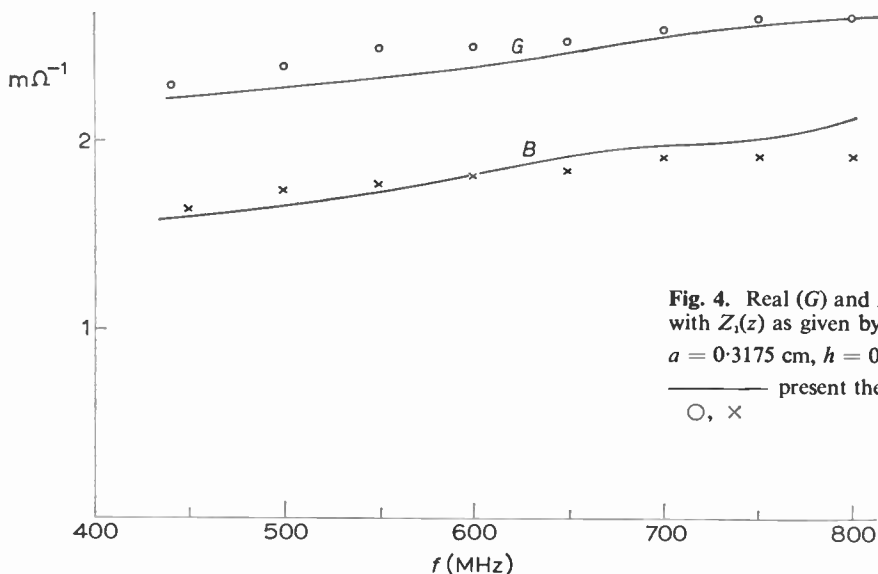


Fig. 4. Real (*G*) and imaginary (*B*) parts of admittance of dipoles with $Z_i(z)$ as given by equation (24), versus frequency.
 $a = 0.3175$ cm, $h = 0.5$ m, $|\psi| = 6.0$
 — present theory, $n = 5$ experimental³
 ○, ×

perfectly conducting ground plane, of radius $a = 0.3175$ cm, length $h = 0.5$ m, and loaded with a step-like approximation of the required resistive loading given by equation (24), are presented for several values of the parameter $|\psi|$. It was found that the results obtained by the present method are in good agreement with experimental results in all cases. As an example, consider a dipole with $|\psi| = 6.0$ (monopole number 4 in reference 3). Figure 4 shows real and imaginary parts of the dipole admittance versus frequency, and Fig. 5 current distribution for two frequencies, as compared with experimental values. Agreement may be said to be satisfactory, in spite of a relatively low order ($n = 5$) of the polynomial approximation used. In reference 18 it was found that approximation of at least one order higher is needed for the point-matching method to yield the values of admittances of the same order of accuracy.

3.5. Broadband Capacitively-loaded Dipole

The broadband resistive dipole analysed in the preceding section has very interesting properties, but has relatively low efficiency (about 50%¹⁷). To increase efficiency, it is natural to analyse the possibility of obtaining a broadband cylindrical dipole with appropriately distributed reactive loading. We shall restrict our attention to dipoles with distributed capacitive loading, and shall assume that equations (1) to (4), and thus the whole procedure of determining current distribution and Z_0 , are valid approximately in this case also.

It appears to be Hallén¹⁹ who first described such an antenna and its properties. The monopole antenna he described had a radius $a = 1.25$ cm and a length of about $h = 0.565$ m. The monopole was made in the form of a row of small conducting cylinders with dielectric disks inserted between them. To obtain a variable capacitive loading, the thickness of dielectric disks increased towards the monopole end. In reference 19 the experimentally determined $|Z_i(z)|$ at $f = 400$ MHz is presented in the form of a diagram. According to

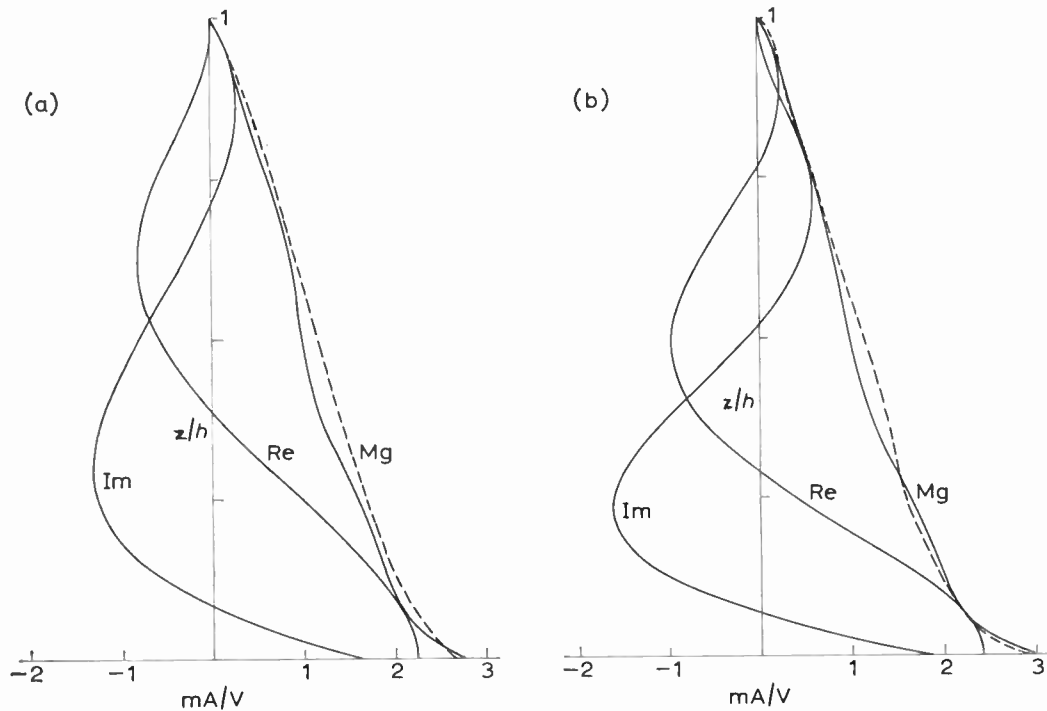


Fig. 5. Real (Re) and imaginary (Im) parts, and magnitude (Mg) of current along dipole with loading given by equation (24).
 $a = 0.3175$ cm, $h = 0.5$ m, $|\psi| = 6.0$
 (a) $f = 450$ MHz (b) $f = 600$ MHz
 ——— present theory, $n = 5$
 - - - - - experimental³ (magnitude available only)

Hallén, such a monopole had an admittance of approximately $7.85 + j5.55$ m Ω^{-1} in the wide frequency range from 340 to 550 MHz.

Lacking an analytical expression for $|Z_i(z)|$, instead of approximating $|Z_i(z)|$ from the Hallén's diagram by a polynomial in z/h , as was done in reference 18, we shall approximate $|Z_i(z)|$ by the expression

$$|Z_i(z)|_{400 \text{ MHz}} = 830[1 + 15(z/h)^4]. \quad \dots(25)$$

This expression was found to approximate fairly accurately to the diagram of $|Z_i(z)|$ given by Hallén. It should

be noted that the broadband properties of capacitively-loaded antennas should be expected not to depend critically on the amount and the distribution of the loading.

Figure 6 shows the real and imaginary parts of the admittance of the dipole corresponding to the Hallén's monopole antenna and its image, with $|Z_i(z)|$ as given by equation (25), versus frequency. Indicated in the figure are also the G and B curves (dashed) computed for the Hallén's antenna by approximating $|Z_i(z)|$ given by Hallén closely, by a polynomial of the seventh order

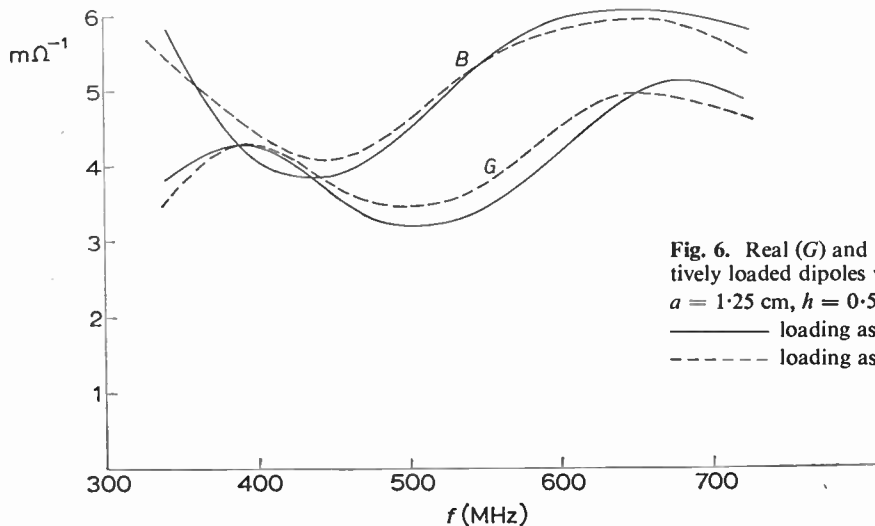


Fig. 6. Real (G) and imaginary (B) parts of admittances of capacitively loaded dipoles versus frequency.
 $a = 1.25$ cm, $h = 0.565$ m
 ——— loading as in equation (25)
 - - - - - loading as in reference 19

in z/h . It is seen that the difference between the G and B curves for the two cases is relatively small, and that in both cases the antenna exhibits broadband properties in the input admittance. It should be noted that for obtaining values of admittances of the same order of accuracy by the point-matching method,¹⁸ polynomials of one order higher were found to be necessary.

4. Conclusions

In the existing applications of the variational method for solving isolated cylindrical antenna problems, two-term trial functions for current only have been used so far, mainly in the form of combinations of trigonometric functions. In the cases of dipoles of moderate lengths (not exceeding greatly the operating wavelength), and with no distributed loading along them, the trial function of this form was found to be a satisfactory approximation. But such trial functions fail for longer dipoles, or for impedance-loaded dipoles. In addition, for impedance-loaded dipoles only a rough guess as to current distribution appears to be possible in the general case. Therefore, the variational solution with a two-term trial function for current cannot be used as a means for obtaining significant results in these cases.

The present paper eliminates this difficulty by introducing in the variational method a novel trial function for current, in the form of a polynomial of arbitrary order with complex coefficients. Explicit expressions for determining impedance and current distribution with polynomial trial function are given for symmetrical dipoles with arbitrary continuous-impedance loading and situated in an arbitrary homogeneous linear medium. Using the method, several types of symmetrical cylindrical dipoles are considered: perfectly-conducting dipoles in a vacuum and in a dissipative medium, dipoles with constant resistive loading, dipoles with non-reflecting resistive loading and broadband capacitively-loaded dipoles (the theory for the last case being valid only approximately). The values of dipole impedances (or admittances) and current distribution obtained by the present method are in a remarkable agreement with experimental results, in the cases where the latter are available.

A brief comparison between the present method and the point-matching polynomial approach^{9-11, 18} may be worthwhile at this point. Both methods use the polynomial approximation for current, but otherwise are completely independent, and each has certain relative advantages. The present method requires a lower order approximation of current than the point-matching method for obtaining dipole admittances of the same order of accuracy. From the other side, the point-matching method results in generally more accurate overall current distribution along an antenna. The two approaches could thus be regarded as in a sense complementary, and can advantageously be used independently for theoretical analysis of new types of cylindrical antennas.

The present method can be extended to coupled dipoles as well, with all the aforementioned advantages. For example, the recent variational methods of analysing

arrays of perfectly conducting non-staggered^{6, 7} or staggered⁸ dipoles in a vacuum can be generalized in the case of arrays of dipoles with continuous impedance loading and situated in an arbitrary linear medium. However, these and similar extensions of the present method are outside the scope of this paper.

5. References

1. Storer, J. E., 'Solution to Thin Wire Antenna Problems by Variational Methods', Doctoral dissertation, Harvard University, June 1951.
2. King, R. W. P., 'The Theory of Linear Antennas', pp. 237-258 (Harvard University Press, Cambridge, Mass., 1956).
3. Shen, L. C., 'An experimental study of the antenna with non-reflecting resistive loading', *I.E.E.E. Trans. on Antennas and Propagation*, AP-15, p. 606, September 1967.
4. Popović, B. D. and Surutka, J. V., 'A variational solution to the problem of asymmetrical cylindrical dipole', *I.E.E.E. Trans. on Antennas and Propagation*, AP-19, p. 17, January 1971.
5. Popović, B. D. and Popović, Z. D., 'Imperfectly conducting cylindrical antenna: the variational approach', *I.E.E.E. Trans. on Antennas and Propagation*, AP-19, p. 435, May 1971.
6. Inagaki, N., 'An improved circuit theory of a multielement antenna', *I.E.E.E. Trans. on Antennas and Propagation*, AP-17, p. 120, March 1969.
7. Popović, B. D., 'A simple method of analysing arrays of thin cylindrical dipoles', *Proc. Instn Elect. Engrs*, 117, No. 6, p. 1084, June 1970.
8. Surutka, J. V., 'Self and mutual impedances of two parallel staggered dipoles by variational method', *The Radio and Electronic Engineer*, 41, No. 6, p. 257, June 1971.
9. Popović, B. D., 'Polynomial approximation of current along thin symmetrical cylindrical dipoles', *Proc. Instn Elect. Engrs*, 117, No. 5, p. 873, May 1970.
10. Popović, B. D., 'Theory of imperfectly conducting thin cylindrical dipoles', *Proc. Instn Elect. Engrs*, 117, No. 12, p. 2205, December 1970.
11. Popović, B. D., 'Theory of cylindrical antennas in conducting media', *Proc. Instn Elect. Engrs*, 118, No. 3/4, p. 507, March/April 1971.
12. Mack, R. B., 'A Study of Circular Arrays', Cruft Laboratory, Harvard University, Cambridge, Mass., Techn. Rept. 383, 1963.
13. Iizuka, K. and King, R. W. P., 'The dipole antenna immersed in a homogeneous conducting medium', *I.R.E. Trans. on Antennas and Propagation*, AP-10, p. 384, June 1962.
14. Shen, L. C., 'Theory of dipole antennas in dissipative media', *Proc. Instn Elect. Engrs*, 117, No. 1, p. 27, January 1970.
15. Shen, L. C., 'An experimental study of imperfectly conducting dipoles', *I.E.E.E. Trans. on Antennas and Propagation*, AP-15, p. 782, November 1967.
16. King, R. W. P. and Wu, T. T., 'The imperfectly conducting cylindrical transmitting antenna', *I.E.E.E. Trans. on Antennas and Propagation*, AP-14, p. 524, September 1966.
17. Wu, T. T. and King, R. W. P., 'The cylindrical antenna with non-reflecting resistive loading', *I.E.E.E. Trans. on Antennas and Propagation*, AP-13, p. 369, May 1965.
18. Popović, B. D., 'Theory of cylindrical antennas with arbitrary impedance loading', *Proc. Instn Elect. Engrs*, 118, No. 10, p. 1327, October 1971.
19. Hallén, E., 'Electromagnetic Theory', pp. 501-504 (Chapman & Hall, London, 1962).
20. Popović, Z. D. and Popović, B. D., 'Transformation of double integrals appearing in the variational formulation of cylindrical antenna problems', Publ. of Elect. Engng Dept., Univ. of Belgrade, Electronic Series, to be published.

6. Appendix

The u_{ij} integrals given by equation (16) can be transformed into a sum of ordinary integrals as follows. Consider the integral

$$U_{ij} = \frac{4\pi}{j\zeta} u_{ij} = \int_{-H}^H \int_{-H}^H f_i(Z) f_j(Z') K(Z-Z') dZ dZ', \quad (26)$$

with

$$f_i(Z) = (1-|Z|/H)^i, \quad f_j(Z') = (1-|Z'|/H)^j \quad (27)$$

where $H = \beta h$, $Z = \beta z$, $Z' = \beta z'$ and $\beta = \text{Re}(k)$. In a recent paper by the authors²⁰ a method has been described for transforming double integrals of the type (26) for a wide class of functions $f_i(Z)$ and $f_j(Z')$ into a sum of ordinary integrals. In particular, if $f_i(Z)$ and $f_j(Z')$ are given by equation (27), the method yields the following expression for the U_{ij} integrals:

$$U_{ij} = 2\gamma H \{ (-1)^{j-1} J_{ij}^I + \frac{ij}{\gamma^2 H^2} [(-1)^{j-1} J_{i-1, j-1}^I + J_{i-1, j-1}^{II}] \}. \quad (28)$$

In this expression $\gamma = k/\beta$, and

$$J_{ij}^I = 2H \int_0^{0.5} [F_{ij}(-t, t) - F_{ij}(-t, 1-t) + F_{ij}(t, t) - F_{ij}(t, 1-t)] K_1(2Ht) dt \quad (29)$$

$$J_{ij}^{II} = 2H \int_0^{0.5} [F_{ij}(1-t, t) - F_{ij}(1-t, -t)] K_1(2Ht) dt + 2H \int_{0.5}^1 [F_{ij}(1-t, 1-t) - F_{ij}(1-t, t-1)] K_1(2Ht) dt, \quad \dots\dots(30)$$

with

$$F_{ij}(x, y) = \sum_{m=0}^i \sum_{n=0}^j \binom{i}{m} \binom{j}{n} \frac{(-1)^m}{1+m+n} x^{i+j-m-n} y^{m+n+1}, \quad \dots\dots(31)$$

and

$$K_1(x) = \exp(-j\gamma R)/R, \quad R = (x^2 + A^2)^{1/2}, \quad (32)$$

where $A = \beta a$.

Manuscript first received by the Institution on 13th April 1971 and in final form on 12th July 1971. (Paper No. 1417/Com 51.)

© The Institution of Electronic and Radio Engineers, 1971

STANDARD FREQUENCY TRANSMISSIONS—October 1971

(Communication from the National Physical Laboratory)

October 1971	Deviation from nominal frequency in parts in 10 ¹⁰ (24-hour mean centred on 0300 UT)			Relative phase readings in microseconds N.P.L.—Station (Readings at 1500 UT)		October 1971	Deviation from nominal frequency in parts in 10 ¹⁰ (24-hour mean centred on 0300 UT)			Relative phase readings in microseconds N.P.L.—Station (Readings at 1500 UT)	
	GBR 16 kHz	MSF 60 kHz	Droitwich 200 kHz	*GBR 16 kHz	†MSF 60kHz		GBR 16 kHz	MSF 60 kHz	Droitwich 200 kHz	*GBR 16 kHz	†MSF 60 kHz
2	-300.0	-0.1	+0.2	514	547.2	18	-300.0	0	-0.2	521	551.8
3	-300.0	-0.1	+0.2	514	547.7	19	-300.1	0	-0.2	522	552.3
4	-300.1	0	+0.2	515	547.4	20	-300.1	-0.1	-0.2	523	553.0
5	-300.0	-0.1	+0.2	515	548.7	21	-300.0	-0.1	-0.1	524	553.6
6	-300.1	-0.1	+0.2	516	549.4	22	-300.1	0	-0.1	525	553.9
7	-300.1	-0.1	+0.2	517	550.3	23	-299.9	0	-0.1	524	553.8
8	-300.1	-0.1	+0.2	518	550.9	24	-300.1	0	-0.1	525	554.0
9	-299.9	0	+0.2	517	550.5	25	-300.0	0	-0.1	525	553.8
10	-300.1	0	+0.2	518	550.6	26	-300.2	-0.1	-0.1	527	554.5
11	-300.0	0	+0.2	518	550.2	27	-299.9	0	-0.1	526	554.8
12	-299.9	0	+0.2	517	549.7	28	-300.1	-0.1	-0.2	527	555.3
13	-300.2	+0.1	-0.1	519	549.1	29	-300.0	-0.1	-0.2	527	561.6
14	-300.1	-0.1	-0.1	520	550.6	30	-300.1	-0.1	-0.2	528	562.5
15	-300.0	-0.1	-0.1	520	551.4	31	-300.0	0	-0.2	528	562.8
16	-300.1	0	-0.1	521	551.2						

All measurements in terms of H.P. Caesium Standard No. 334, which agrees with the N.P.L. Caesium Standard to 1 part in 10¹¹.

* Relative to UTC Scale; (UTC_{NPL} - Station) = + 500 at 1500 UT 31st December 1968.

† Relative to AT Scale; (AT_{NPL} - Station) = + 468.6 at 1500 UT 31st December 1968.

Mean monthly values: GBR: -300.04 MSF: -0.04.

State Variable Methods in Antenna Servo Analysis

By

D. R. WILSON, M.Sc.(Tech.),
Ph.D., C.Eng., M.I.E.E.†

The state space method is applied to the analysis of a servomechanism to demonstrate how the method can be used to find the response of a proposed system to any type of deterministic input or disturbance. It is shown that linear input signals can be simply incorporated in the A matrix as input state variables. The A matrix for two realistic models of an antenna control system are then developed inclusive of the system inputs. The state transition matrixes of the servos discussed are evaluated. The variation of all the variables in the servomechanism is defined by the transition matrix, without any further manipulation of system functions and leads to a method of solution which is simpler than the conventional manipulation of transfer functions.

List of Symbols

- \mathbf{A} = $n \times n$ matrix
 $[\mathbf{x}(t)]^T$ = transpose of $[\mathbf{x}(t)]$
 $[\mathbf{x}(0)]$ = initial condition matrix of $[\mathbf{x}(t)]$
 $[\Phi(t)]$ = state transition $n \times n$ matrix
 J_L = load inertia kg m²
 J_m = motor inertia kg m²
 $J = J_m + J_L/N^2$
 N = gear box ratio
 K_t = tachogenerator constant Vs/rad
 K_1 = electronic gain associated with the tachogenerator feedback signal
 K_T = motor torque constant in Nm/A
 K_A = electronic transconductance A/V
 T_1, T_2 = stabilizing time-constants
 α, K_2 = stabilizing gains
 G_R = tracking receiver gain V/deg offset
 T_R = tracking receiver cut-off frequency
 K_v = motor back e.m.f. constant Vs/rad
 $G_v(s)$ = velocity loop compensation

1. Introduction

At the present time power servomechanisms, such as are found in large antennas, missile launchers, rolling mills etc., are primarily designed by the linear frequency response technique in one of its various guises¹, while the usual servo non-linearities such as backlash, stiction, saturation effects etc. can be incorporated in the design by the describing function technique.² The basic servo configuration of a high performance servo drive³ will usually incorporate both torque (armature current) and tachogenerator feedback loops. This together with the load defines the 'plant', which is to be controlled by the position loop. The definition of the plant is then used with an appropriate error transducer to design the compensating function to meet both the steady and dynamic conditions. The complexity of the compensating networks obviously depends on the complexity of the plant model and particularly on the definition of the mechanics, which are absorbed in the plant. The resulting transfer function of the servo will normally be of fifth- or sixth-order at its simplest, consequently the manipula-

tion of the servo transfer function into a desired form, i.e. output to input, error to input, output to torque disturbance etc., necessitates a considerable amount of tedious manipulation even allowing for digital computer evaluation of the transfer function for a given input.

The state space technique removes the necessity for tedious transfer function manipulation in that the system A matrix can be defined from the servo block diagram and the designed values of system variables directly inserted. Calculation of the output state vector allows the response of any system state to be observed once and for all without any further manipulation. It is the purpose therefore of this paper to illustrate the application of the State Space method in power servo analysis and in the first instance the state equations are summarized.

2. The State Equations

Engineers are familiar with manipulating system variables in a feedback system such as position, velocity, torque etc., by the transfer function technique. The State Equations simply provide an alternative method of defining a system and by the use of computing techniques a general solution can be evaluated which completely predicts the control system performance. The definition of a control system in the state variable notation simply means that the system is described by a set of first-order differential equations. Each equation describes one of the variables in the control system, i.e. one of the chosen states.

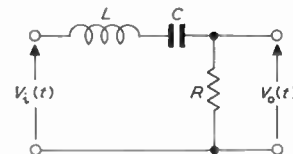


Fig. 1. LCR circuit.

As an example consider the LCR circuit shown in Fig. 1. The equations of the network can be written

$$V_i = L \frac{di}{dt} + \frac{1}{C} \int i dt + iR \quad \dots\dots(1)$$

where i is the circuit current

$$\text{and} \quad V_o = iR \quad \dots\dots(2)$$

Writing

$$x_2 = \dot{x}_1 = i \quad \dots\dots(3)$$

†Radar Engineering Laboratories, Plessey Radar Limited, Cowes, Isle of Wight.

Hence

$$\dot{x}_2 = \frac{di}{dt}$$

The variables x_1 and x_2 are a conveniently selected pair of *state variables*.

It follows that (1) and (3) can be written in terms of the state variables

$$\begin{aligned} \dot{x}_1 &= 0 + x_2 \\ \dot{x}_2 &= -\frac{x_1}{LC} - \frac{R}{L}x_2 + \frac{V_i}{L} \end{aligned}$$

and hence the state equation for the network can be written in matrix form as:

$$\begin{bmatrix} \dot{x}_1 \\ \dot{x}_2 \end{bmatrix} = \begin{bmatrix} 0 & 1 \\ -\frac{1}{LC} & -\frac{R}{L} \end{bmatrix} \begin{bmatrix} x_1 \\ x_2 \end{bmatrix} + \begin{bmatrix} 0 \\ 1/L \end{bmatrix} [V_i]$$

Similarly the output equation can be written

$$V_o = [0 \quad R] \begin{bmatrix} x_1 \\ x_2 \end{bmatrix}$$

from which it can be seen that the state equation corresponds to the general form

$$\dot{\mathbf{x}}(t) = \mathbf{A}\mathbf{x}(t) + \mathbf{D}\mathbf{m}(t)$$

In the general case $\mathbf{x}(t)$ is a column matrix representing the n state variables of the system, \mathbf{A} is a $n \times n$ matrix of system coefficients, \mathbf{D} is an $n \times 1$ matrix and $\mathbf{m}(t)$ describes the input state variables.

When a linear system is defined by the state equation

$$\dot{\mathbf{x}}(t) = \mathbf{A}\mathbf{x}(t) + \mathbf{D}\mathbf{m}(t) \quad \dots\dots(4)$$

the solution can be written

$$\mathbf{x}(t) = \phi(t)\mathbf{x}(0) + \int_0^t \phi(t-\tau) \cdot \mathbf{D} \cdot \mathbf{m}(\tau) d\tau \quad \dots\dots(5)$$

where the state transition matrix is defined by the identity

$$\phi(t) \equiv e^{\mathbf{A}t} \quad \dots\dots(6)$$

and τ is a dummy variable having the dimensions of time.

It follows that if the inputs to the system defined by $\mathbf{m}(t)$ are incorporated as additional states of the system, such that they are assumed to be input state variables⁴, then the equation of the system is defined by

$$\dot{\mathbf{x}}(t) = \mathbf{A}\mathbf{x}(t) \quad \dots\dots(7)$$

and a complete solution to the problem is defined by

$$\mathbf{x}(t) = \phi(t)\mathbf{x}(0) \quad \dots\dots(8)$$

whereby the actual system inputs are defined by the initial conditions on the input state variables.

Now let

$$t = nT \quad \dots\dots(9)$$

which implies that the continuous time variable t is represented at discrete intervals defined by nT , where $0 \leq n \leq \infty$ and nT is the time at which the continuous output is computed. In order that a stable computation

of the transition matrix can be guaranteed, it is necessary to select T to be an order lower than the smallest time-constant of the system.

It follows from equation (6) that

$$\phi(nT) = (e^{\mathbf{A}T})^n \quad \dots\dots(10)$$

Thus by choosing a sufficiently small interval of time the state transition matrix can be evaluated for the first interval and the state transition matrix at the following intervals calculated by repeated multiplication. Liou⁵ has developed a method for evaluating $e^{\mathbf{A}T}$ by writing it in the form

$$e^{\mathbf{A}T} = \sum_{k=0}^{\infty} \frac{\mathbf{A}^k T^k}{k!}$$

where

$$\mathbf{A}^0 = \mathbf{I} = \text{unity matrix}$$

and by letting

$$e^{\mathbf{A}T} = \mathbf{M} + \mathbf{R}$$

where

$$\begin{aligned} \mathbf{M} &= \sum_{k=0}^K \frac{\mathbf{A}^k T^k}{k!} \\ \mathbf{R} &= \sum_{k=K+1}^{\infty} \frac{\mathbf{A}^k T^k}{k!} \end{aligned}$$

If each element in the matrix $e^{\mathbf{A}T}$ is required to within an accuracy of d significant digits then

$$[r_{ij}] \leq 10^{-d}[m_{ij}] \text{ for all } i, j$$

where r_{ij} and m_{ij} are the elements of matrices \mathbf{R} and \mathbf{M} respectively. It follows that \mathbf{M} can be evaluated to whatever accuracy is required. The results of the computation can be printed out for each small interval of time or an appropriate multiple of the basic computing period, e.g. if $T = 0.005$ seconds the results could be printed out for every fifty iterations to give results at 0.25s intervals.

It follows the method only requires the \mathbf{A} matrix to be defined and that once this has been done there are effectively no lengthy manual manipulations to obtain the desired results. As examples, the \mathbf{A} matrix for two antenna servos will be developed with sample computations, but first the method of representing system inputs as input state variables will be discussed.

2.1. Input State Variables

The conventional test signals that are applied to a control system are steps, ramps, parabolas and simple harmonic motion. Figure 2 represents three state variables ($r_1(t)$, $r_2(t)$, $r_3(t)$), which in terms of the time variable, t , and the initial condition on $r_1(t)$ can be expressed:

$$r_1(t) = R = \text{step input}$$

$$r_2(t) = Rt = \text{ramp input} = \text{step of velocity}$$

$$r_3(t) = \frac{R}{2}t^2 = \text{parabola input} = \text{step of acceleration}$$

from which it follows that any particular input or combination of input can be simulated by addition of the

appropriate states into the control system. A simple harmonic input can be incorporated by application of the variable $r_4(t)$ and $r_5(t)$ which can be generated by the circuit shown in Fig. 3.

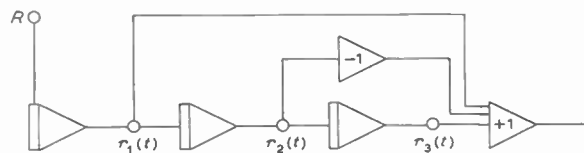


Fig. 2. State representation of an input sequence $R + Rt + \frac{R}{2}t^2$. Integrators are assumed to have sign reversal.

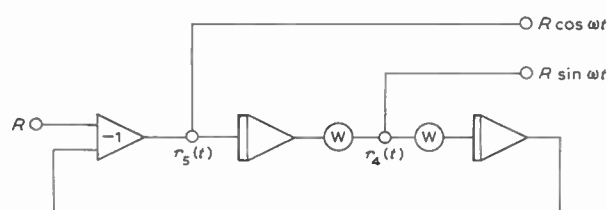


Fig. 3. State representation of simple harmonic motion. Integrators are assumed to have sign reversal.

3. Antenna Servo Models

The design of antenna servos has been reviewed³ and detailed design examples given^{6,7}, consequently it is sufficient to note that when the coefficients of the velocity loop have been chosen the position loop design should produce a single pair of predominant closed loop complex poles, which effectively define the natural frequency of the position loop and hence the servo bandwidth.

It has been inferred above that the complexity of the servo plant is largely a function of the load structure. The linear model of an electric or hydraulic drive is relatively easy to define, but the problem of defining the mechanics, albeit only a linear model, is extremely difficult with any complex structure, such as a large antenna. Canfield⁸ treats a simple two-inertia system coupled with a resilience and three damping terms, viscous friction to ground at the motor and load and viscous friction across the resilience. This simple definition allows six variants depending on which combination of viscous damping is taken. Further, no matter what structural model is assumed, the assessment of the mechanical structural damping in a numerical sense is a wellnigh impossible task and at best can only be quantitatively assessed by assuming a certain damping factor to be associated with the resonance. It follows therefore that although the inertias and stiffnesses in a mechanical structure can be reasonably accurately calculated and hence the likely natural frequency calculated, the effect on the servo loop is virtually impossible to predict, without reasonable data as to magnitude and nature of the damping. Typically mechanical resonances are lightly damped with damping

factors of the order of 0.1. Further when it is considered that a large structure such as a 28m (90ft) antenna can be reasonably sub-divided into 6 or 7 significant inertias coupled by resilienties the complexity of the resulting model can be self-defeating. Fortunately realistic results can be obtained in many cases for much simplified mechanical structural models.

In practice therefore if a mechanical resonance occurs within the bandwidth of a servo loop it presents severe stability problems, and the mechanical engineer is normally asked to produce a structure with a minimum natural frequency, which is a factor, say 10, higher than the desirable servo bandwidth. With large antennas the predominant mechanical resonance can be kept to the order of 2Hz, while optimum servo bandwidths, with respect to noise and disturbance inputs, are of the order of 0.1 Hz. Consequently a linear model of motor inertia coupled to a load inertia through a stiff gear box is quite reasonable. However in the case of a wide bandwidth tracking antenna with, say, a 3Hz bandwidth requirement, it follows that an extremely stiff structure is required with the lowest mechanical resonance about 30Hz. Unless the mechanical resonant frequency (locked rotor frequency) is high then a design based on the linear model would almost certainly have to be tuned on site with anti-resonant elements before the desired bandwidth could be achieved. For reasons discussed above it is not practical to set out to design anti-resonant elements for an assumed mechanical resonance within or near the servo bandwidth. In the servo designs used to illustrate this paper no attempt will be made to do so, because the assumption is made that a satisfactory ratio of mechanical frequency to servo frequency can be achieved and under these conditions a stiff motor-gearbox-load model is acceptable.

3.1. A 20-foot (6.1 m) Diameter Antenna

The 20ft antenna servo model discussed in an earlier paper² is shown in Fig. 4 and the block diagram in Fig. 5. The state space diagram which is, in effect, an analogue computer diagram for the control system is shown in Fig. 6, where input state variables representing a torque disturbance, a velocity demand and the input signal, are included. The states are:

- $x_1(t) = \theta_L(t)$, output shaft position
- $x_2(t) = \dot{\theta}_m(t)$, motor shaft velocity
- $x_3(t) =$ output of the velocity loop compensating circuit
- $x_4(t) =$ output of the position loop electronic integrator
- $x_5(t) =$ output of the tracking receiver
- $x_6(t) =$ input state variable. An initial condition on $x_6(t)$ represents a demand of position
- $x_7(t) =$ input state variable representing a disturbance torque
- $x_8(t) =$ input state variable at the input to the velocity loop

i.e. $[x(t)] = [x_1 \ x_2 \ x_3 \ x_4 \ x_5 \ x_6 \ x_7 \ x_8]^T$

and the A matrix can be written down from inspection of Fig. 6 as follows:

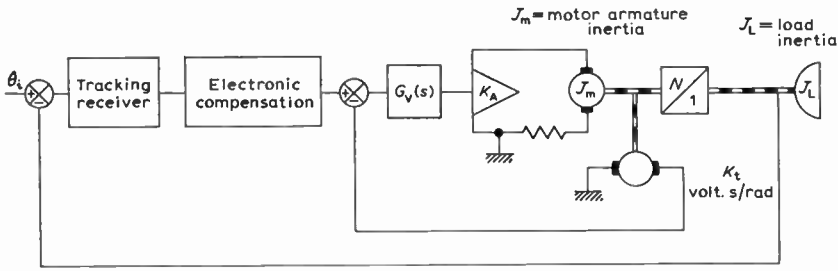


Fig. 4. Servo control system for a satellite tracking antenna.

Fig. 5. Servo block diagram.

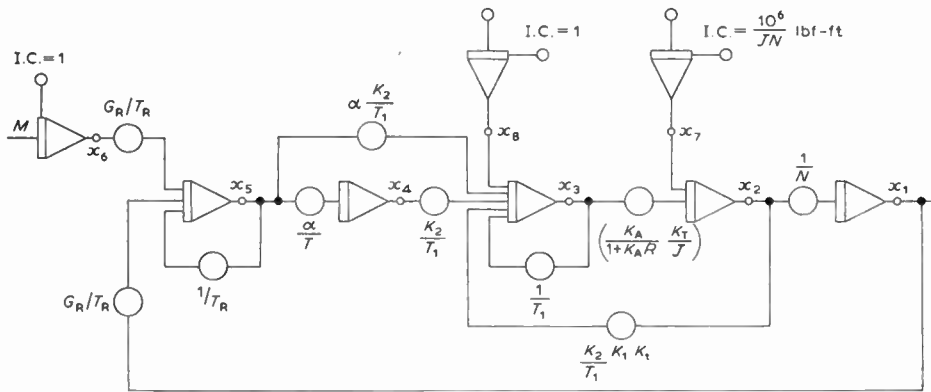
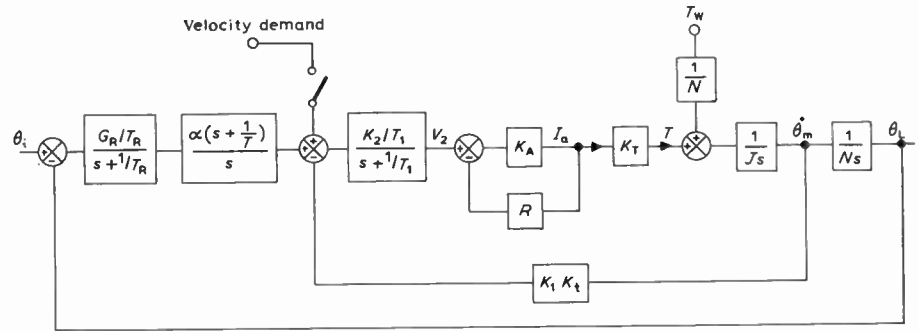


Fig. 6. State variable diagram of the servo control system.

Table 1

Numerical data from which the A matrix of the 20ft diameter antenna is calculated

Antenna load inertia	$J_L = 2720 \text{ kgm}^2$ (2000 slugft ²)
Motor armature inertia	$J_M = 7.1 \times 10^{-3} \text{ kgm}^2$ (5.23×10^{-3} slugft ²)
Motor torque constant	$K_T = 0.49 \text{ Nm/A}$ (0.36 lbf-ft/A)
Tachogenerator constant	$K_t = 0.172 \text{ Vs/rad}$
Gear box ratio	$N = 12000 : 1$
Tracking receiver cut-off frequency	$= 20 \text{ Hz}$ ($T_R = 1/40\pi$)
Tracking receiver sensitivity	$G_R = 5 \text{ Vs/deg}$
Electronic position loop gain	$\alpha = 10$
Electronic position loop time-constant	$T = (1/2.2) \text{ s}$
Electronic gain of the velocity loop	$K_2 = 6.05$
Armature current feedback resistance	$K_1 K_t = (1/26.2) \text{ Vs/rad}$
	$1/T_1 = 20\pi \text{ s}^{-1}$
	$R = 1 \Omega$

	1	2	3	4	5	6	7	8
1		$\frac{1}{N}$						
2			$\frac{K_T}{J} \frac{K_A}{(1+K_A R)}$					1
3		$-\frac{K_2}{T_1} K_1 K_t$	$-\frac{1}{T_1}$	$\frac{K_2}{T_1}$	$\frac{\alpha K_2}{T_1}$			1
4					$\frac{\alpha}{T}$			
5		$-\frac{G_R}{T_R}$			$-\frac{1}{T_R}$	$\frac{G_R}{T_R}$		
6								
7								
8								

A plot of $\phi_{1,6}(t)$ is given in Fig. 7.

The disturbance response of the output $x_1(t)$ to a step of wind torque is represented by an initial condition on the input state variable $x_1(t)$, i.e.

$$x(0) = [0 \ 0 \ 0 \ 0 \ 0 \ 1 \ 0]^T$$

and hence the output shaft response to a step of wind torque is predicted by $\phi_{1,7}(t)$ and plotted in Fig. 8. It follows that if the response of any other variable is required for either these or any other input, it can be identified from the state transitions matrix, e.g. motor shaft velocity $x_2(t)$ is predicted by $\phi_{2,7}(t)$, following a step of wind torque.

and, using the numerical data defined in Table 1, it follows:

$$A =$$

	1	2	3	4	5	6	7	8
1	0	83.3×10^{-6}	0	0	0	0	0	0
2	0	0	68.7	0	0	0	1	0
3	0	-14.55	-62.84	381	3810	0	0	1
4	0	0	0	0	22	0	0	0
5	-36×10^3	0	0	0	-125.68	36×10^3	0	0
6	0	0	0	0	0	0	0	0
7	0	0	0	0	0	0	0	0
8	0	0	0	0	0	0	0	0

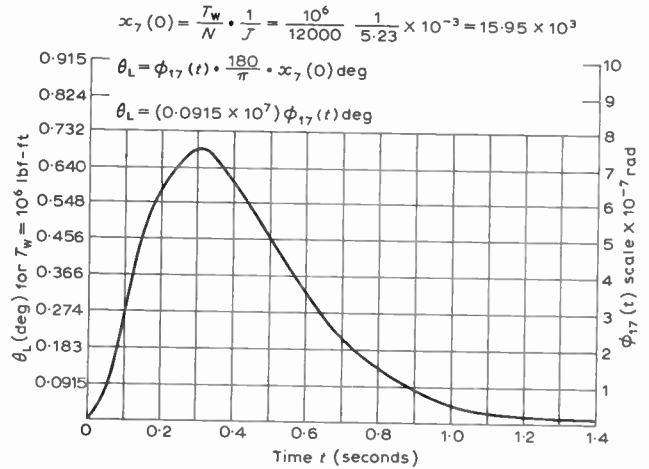


Fig. 8. Response $x_1(t) (= \theta_L(t))$ to a step input of wind torque (initial conditions on $x_7(t)$)

Using the method of Liou⁵ the state transition matrix can be computed. Table 2 gives a sample print-out. It follows that a step input is represented by an initial condition on $x_6(t)$, hence the initial condition vector can be written

$$x(0) = [0 \ 0 \ 0 \ 0 \ 1 \ 0 \ 0]^T$$

and, therefore, the coefficient of the transition matrix representing the step response is represented by $\phi_{1,6}(t)$ where

$$x_1(t) = \phi_{1,6}(t)x_6(0)$$

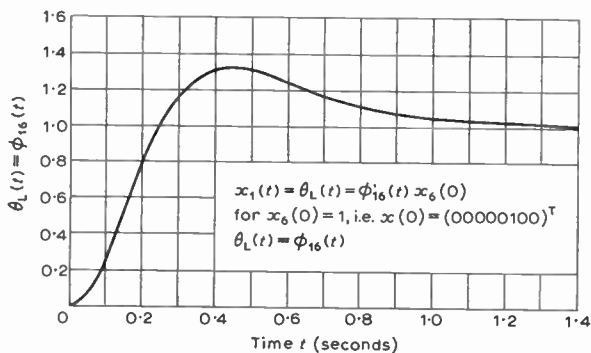


Fig. 7. Output step response (initial conditions on $x_6(t)$)

An interesting observation can be made on the nature of the response to a velocity demand, which is shown in Fig. 5 to be applied at the tachogenerator feedback summing junction. In practice, facilities are often provided for such an input so that the load responds directly to a velocity demand. Such a demand point is incorporated in the state space formulation as the input state variable $x_8(t)$ and, therefore, motor velocity is defined by

$$x_2(t) = \phi_{2,8}(t)x_8(0)$$

where

$$x_8(0) = [0 \ 0 \ 0 \ 0 \ 0 \ 0 \ 1]^T$$

i.e.

$$x_8(0) = 1$$

Observation of the print-out illustrates that $x_2(t) \rightarrow 0$ as $t \rightarrow \infty$, which implies that the velocity tends to zero and not to a set speed, which would appear to be an undesirable result. This is because the position loop is still in circuit in this analysis and hence the system is brought to rest. In reality, of course, the input step demand is scaled to be such that it saturates the velocity demand amplifier, thereby effectively breaking the position loop. The equivalent response in state space form must therefore be evaluated with the position loop broken at, say, $x_5(t)$.

3.2. A 90-foot (25.4 m) Diameter Antenna with opposed Motor Drive

The principle of the opposed motor drive⁹ to eliminate backlash is shown in Fig. 9. The linearized system block diagram, assuming the motor is coupled to the load with an infinitely stiff shaft, is shown in Fig. 10. The servo model includes the effect of motor armature back e.m.f.

as opposed to the current drive assumption made in the 20ft diameter antenna analysis. The state space model is shown in Fig. 11 with the torque bias incorporated as an input state variable, however for the purpose of a linear analysis it can be ignored. From observation of the state space diagram the A matrix can be defined:

Table 2

Computer print-out of the state transition matrix at selected time intervals for the 20-ft diameter antenna example. Basic computing period $T = 0.005$ s.

TIME INTERVAL = .2

0.214695	2.34288E-06	2.99462E-06	2.45561E-04	1.23992E-04
.795395	6.33128E-07	6.44514E-07		
-55747.	-318375	-326848	13.6969	7.28348
55747.	2.81258E-02	3.59498E-02		
-3774.76	1.67698E-03	-1.94967E-02	-1.81265	-26.9184
3774.76	-1.91983E-02	-4.75761E-03		
-898.761	-3.84754E-03	-3.91675E-03	.883005	-0.42211
898.761	-3.37892E-04	-3.07072E-04		
69.0724	-8.12637E-04	-8.27151E-04	-6.78311E-02	.445834
-69.0728	-1.74888E-04	-1.78934E-04		
0	0	0	0	0
1	0	0	0	0
0	0	0	0	0
0	1	0	0	0
0	0	0	0	0
0	0	1	0	0

TIME INTERVAL = .4

-1.311822	-1.311101E-16	-1.97939E-04	2.65108E-04	2.81426E-06
1.31118	6.65721E-07	7.48052E-07		
-4241.56	-8.83312E-02	-116164	-5.85171	1.94729
4241.54	-1.67292E-02	-1.53588E-02		
-1223.41	1.94551E-02	1.79855E-02	-6.44115	-11.8774
1223.44	-1.58418E-02	-1.69059E-03		
-751.224	-4.25029E-03	-4.78148E-03	.516283	-9.43877E-02
751.225	-1.23995E-03	-1.26965E-03		
154.322	3.17885E-04	3.85412E-04	-8.28065E-02	.226953
-154.323	-1.23191E-04	-2.17340E-04		
0	0	0	0	0
1	0	0	0	0
0	0	0	0	0
0	1	0	0	0
0	0	0	0	0
0	0	1	0	0

TIME INTERVAL = .6

-1.241382	-1.41973E-06	-1.60489E-06	1.58793E-04	-2.28892E-05
1.24138	3.57869E-07	4.16779E-07		
9888.18	3.89281E-02	.039732	-7.34907	3.05815
-9888.2	-1.70436E-02	-1.92653E-02		
-1602.52	3.57474E-03	2.58516E-03	.220347	-5.74164
1602.56	-1.39894E-02	5.78339E-04		
-369.298	-2.32436E-03	-2.71174E-03	.228242	-6.26461E-02
369.298	-1.89230E-03	-2.02561E-03		
102.512	3.95149E-04	4.87364E-04	-4.69623E-02	.1165
-102.513	-1.05653E-04	-1.23261E-04		
0	0	0	0	0
1	0	0	0	0
0	0	0	0	0
0	1	0	0	0
0	0	0	0	0
0	0	1	0	0

	1	2	3	4	5	6	7	8	9	10
1	$\frac{1}{N}$									
2		$\frac{K_T}{J}$	$\frac{K_T}{J}$							$\frac{1}{J}$
3		$-\frac{K_V}{L_a}$	$-\frac{1}{T_a}$		$\frac{1}{L_a}$					
4		$-\frac{K_V}{L_a}$	$-\frac{1}{T_a}$		$\frac{1}{L_a}$					
5		$-K_1 K_2 K_A$	$-K_A R_f$				$K_2 K_A$	$\frac{G_R \alpha K_2 K_A}{T_R}$		
6		$-K_1 K_2 K_A$	$-R_f K_A$				$K_2 K_A$	$\frac{G_R \alpha L_2 K_A}{T_R}$		
7								$\frac{G_R \alpha}{T_R}$	$\alpha \frac{1}{T}$	
8	-1							$-\frac{1}{T_R}$		+1
9										
10										

TIME INTERVAL = .8

-1.188593	-7.28592E-07	-8.39692E-07	6.59563E-05	-1.59684E-05
1.1885	1.46256E-07	1.73114E-07		
6512.16	3.65938E-02	4.23364E-02	-3.79944	2.15965
-6512.18	-8.58542E-03	-9.97230E-03		
-1131.7	-1.07033E-03	-2.13136E-03	.234791	-2.81967
1131.73	-1.40234E-02	6.16249E-04		
-145.243	-9.56879E-04	-1.13572E-03	8.81825E-02	-2.89484E-02
145.243	-2.29562E-03	-2.39322E-03		
47.3795	2.01179E-04	2.55950E-04	-1.96685E-02	5.68727E-02
-47.3713	-4.34945E-05	-5.16235E-05		
0	0	0	0	0
1	0	0	0	0
0	0	0	0	0
0	1	0	0	0
0	0	0	0	0
0	0	1	0	0

TIME INTERVAL = 1.

-3.98971E-02	-2.71518E-07	-3.23103E-07	2.44194E-05	-6.24288E-06
1.0399	5.39228E-08	6.40929E-08		
2697.16	1.65391E-02	1.98143E-02	-1.47782	1.08722
-2697.18	-3.25951E-03	-3.87879E-03		
-569.721	-9.26125E-04	-1.58513E-03	.109887	-1.36333
569.759	-1.43153E-02	2.83417E-04		
-53.3548	-3.53251E-04	-4.21598E-04	3.31158E-02	-1.16848E-02
53.3553	-2.32742E-03	-2.53775E-03		
19.1219	7.68085E-05	1.01129E-04	-7.30130E-03	2.68559E-02
-19.1217	-1.69569E-05	-1.91635E-05		
0	0	0	0	0
1	0	0	0	0
0	0	0	0	0
0	1	0	0	0
0	0	0	0	0
0	0	1	0	0

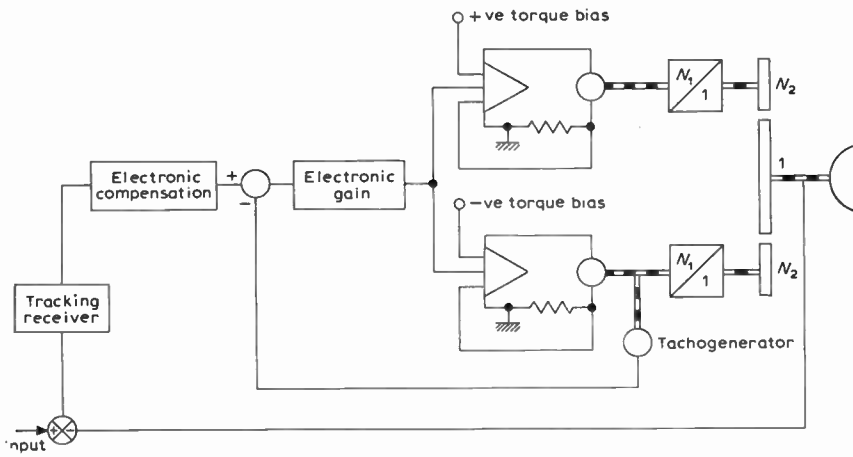


Fig. 9. Servo system with opposed motor drive taking up the backlash zone.

Fig. 10. Servo block diagram of the opposed motor drive.

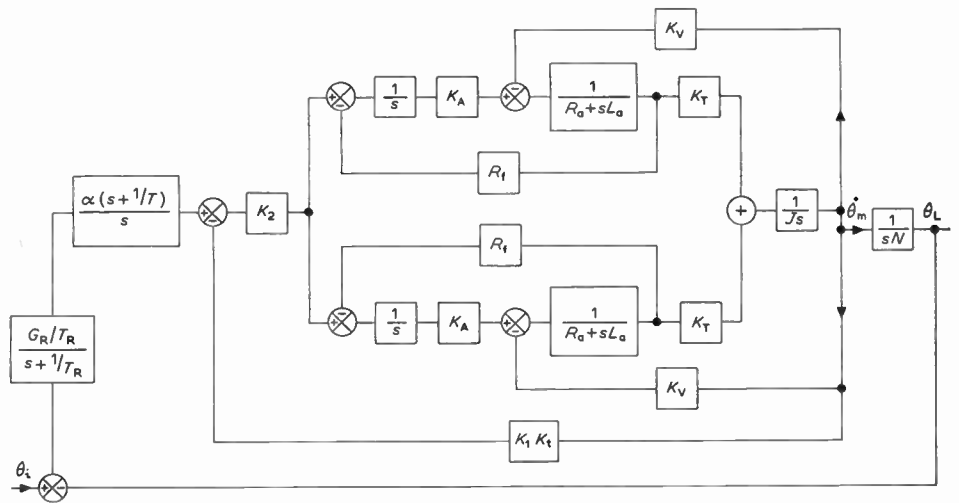


Fig. 11. State space diagram of the opposed drive servo.

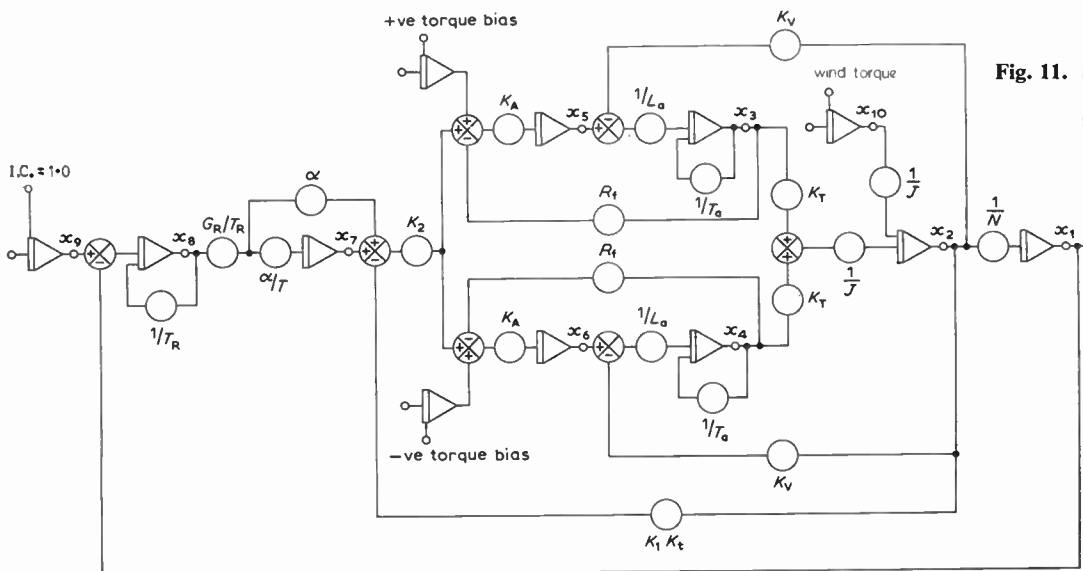


Table 3
 Computer print-out of the state transition matrix at selected time intervals for the 90-ft diameter antenna sample. Basic computing period $T = 0.005s$.

TIME INTERVAL = 1.					TIME INTERVAL = 2.				
1.349588	1.97129E-05	-2.56464E-09	-2.56464E-09	1.32193E-07	-1.22973	-8.16217E-07	-4.99435E-09	-4.99435E-09	-5.29511E-09
1.32193E-07	8.90242E-04	.919895	.650411	4.57468E-05	-5.29511E-09	1.28799E-03	.345911	1.32287	7.34403E-05
-1.2656.6	-1.1913	-1.18352E-04	-1.18352E-04	-1.28740E-03	-5136.73	-1.298129	4.90997E-05	4.90997E-05	-1.99918E-03
-1.28740E-03	14.4282	-2265.47	13656.6	.821579	-1.99918E-03	-1.568125	-10593.1	518.697	-3.40195E-02
735.543	-1.179688	7.19944E-04	4.97419E-04	-1.33558E-03	3419.98	6.48124E-02	2.21613E-05	2.21582E-05	4.32540E-04
-1.22369E-03	-3.0264	-7914.17	-735.544	-1.07526	4.32694E-04	-4.72533	842.932	-3410.39	-1.17169
735.543	-1.179688	4.97419E-04	7.19944E-04	-1.22369E-03	3419.98	6.48124E-02	2.21582E-05	2.21613E-05	4.32694E-04
-1.33558E-03	-3.0264	-7914.17	-735.544	-1.07526	4.32694E-04	-4.72533	842.932	-3410.39	-1.17169
-10999.8	-2.33977	8.15295E-04	4.18786E-05	-9.82341E-04	-2788.46	-1.217082	4.34566E-05	4.39137E-05	-1.45620E-03
-1.24241E-03	10.4343	-4255.09	14909.8	-1.72939	-1.45618E-03	-2.5968	-8294.93	2788.46	-5.72093
-10999.8	-2.33977	4.18786E-05	8.15295E-04	-1.24241E-03	-2788.46	-1.217082	4.39137E-05	4.34566E-05	-1.45618E-03
-1.24241E-03	10.4343	-4255.09	14909.8	-1.72939	-1.45618E-03	-2.5968	-8294.93	2788.46	-5.72093
-212.102	-4.61708E-03	-1.13445E-06	-1.13445E-06	-3.95415E-05	-283.787	-7.58429E-03	3.29451E-08	3.29455E-08	-5.02533E-05
-3.98495E-05	.989929	101.974	212.102	-5.16505E-03	-5.02533E-05	.59918	-90.6937	283.787	-2.34154E-02
-3.58711E-03	-1.98358E-07	2.47995E-11	2.47995E-11	-1.33319E-09	3.19344E-03	6.16953E-09	4.03058E-11	4.03058E-11	3.6290E-11
-1.33319E-09	-7.90559E-06	-9.12244E-03	3.58711E-03	-4.51954E-07	3.86293E-11	-1.28818E-05	-3.52934E-03	-3.19344E-03	-7.34575E-07
0	0	0	0	0	0	0	0	0	0
0	0	0	1	0	0	0	0	1	0
0	0	0	0	0	0	0	0	0	0
0	0	0	0	1	0	0	0	0	1
TIME INTERVAL = 3.					TIME INTERVAL = 4.				
-376025	-1.22194E-05	-5.36839E-10	-5.36839E-10	-8.17942E-08	-1.152871	-9.15404E-06	1.31599E-09	1.31599E-09	-6.13839E-08
-8.17942E-08	8.98927E-04	-1.164999	1.37692	5.11977E-05	-6.13839E-08	3.40337E-04	-2.21958	1.15287	1.93608E-05
2460.25	-3.95695E-02	4.73991E-05	4.73991E-05	-2.68002E-04	3314.22	9.81854E-02	8.22572E-06	8.22571E-06	6.57907E-04
-2.68002E-04	-8.92748	-3994.26	-2460.26	-5.92225	6.57197E-04	-6.69979	1459.16	-3314.23	-381533
1296.84	7.62695E-02	-1.96399E-05	-1.96399E-05	5.11394E-04	-473.752	1.31747E-02	-1.11454E-05	-1.11454E-05	8.89341E-05
5.11394E-04	-633466	2466.29	-1296.84	-9.38312	8.89341E-05	1.55292	917.391	473.746	-813976
1296.84	7.62695E-02	-1.96399E-05	-1.96399E-05	5.11394E-04	-473.752	1.31747E-02	-1.11454E-05	-1.11454E-05	8.89341E-05
5.11394E-04	-633466	2466.29	-1296.84	-9.38312	8.89341E-05	1.55292	917.391	473.746	-813976
2602.14	8.62495E-04	3.43844E-05	3.43843E-05	3.58583E-06	2537.25	8.79693E-02	1.93671E-06	1.93671E-06	5.82955E-04
3.58583E-06	-7.69155	-2225.37	-2602.15	-8.61439	5.82955E-04	-4.88652	1604.48	-2537.25	-791931
2602.14	8.62497E-04	3.43843E-05	3.43844E-05	3.58587E-06	2537.25	8.79693E-02	1.93671E-06	1.93671E-06	5.82955E-04
3.58581E-06	-7.69155	-2225.37	-2602.15	-8.61439	5.82955E-04	-4.88652	1604.48	-2537.25	-791931
-92.5158	-5.26497E-03	6.95971E-07	6.95971E-07	-3.52998E-05	-15.565	-2.00404E-03	5.27236E-07	5.27236E-07	-1.34525E-05
-3.52998E-05	.265337	-107.25	92.5157	-0.41928	-1.34525E-05	9.15466E-02	-44.0461	15.5649	-5.18215E-02
3.77639E-03	1.21914E-07	5.68575E-12	5.68574E-12	8.16949E-10	1.55992E-03	9.21925E-08	-1.31927E-11	-1.31927E-11	6.18202E-10
8.16949E-10	-9.04879E-06	1.61383E-03	-3.77640E-03	-5.15367E-07	6.18203E-10	-3.44840E-06	-2.22912E-03	-1.55993E-03	-1.96171E-07
0	0	0	0	0	0	0	0	0	0
0	0	0	1	0	0	0	0	1	0
0	0	0	0	0	0	0	0	0	0
0	0	0	0	1	0	0	0	0	1
TIME INTERVAL = 5.					TIME INTERVAL = 6.				
1.51795E-03	-2.76159E-06	1.93975E-09	1.93975E-09	-1.85566E-08	1.219.22	7.68896E-02	-1.19110E-05	-1.19110E-05	5.15671E-04
-1.85566E-08	5.57306E-05	-8.13221E-02	-999481	3.16470E-06	5.15671E-04	-2.02539	2994.9	-1219.24	-1.15998
1219.22	7.68896E-02	-1.19110E-05	-1.19110E-05	5.15671E-04	-699.163	-1.92484E-02	-2.01955E-06	-2.01955E-06	-1.28778E-04
-1.28778E-04	1.21869	1.21869	-312.133	680.156	-1.28778E-04	1.21869	1.21869	-312.133	680.156
1219.22	7.68896E-02	-1.19110E-05	-1.19110E-05	5.15671E-04	-699.163	-1.92484E-02	-2.01955E-06	-2.01955E-06	-1.28778E-04
-1.28778E-04	1.21869	1.21869	-312.133	680.156	-1.28778E-04	1.21869	1.21869	-312.133	680.156
715.912	5.53277E-02	-1.07266E-05	-1.07266E-05	3.71190E-04	715.912	5.53277E-02	-1.07266E-05	-1.07266E-05	3.71190E-04
3.71190E-04	-1.16926	1596.48	-715.923	-48871.6	715.912	5.53277E-02	-1.07266E-05	-1.07266E-05	3.71190E-04
715.912	5.53277E-02	-1.07266E-05	-1.07266E-05	3.71190E-04	715.912	5.53277E-02	-1.07266E-05	-1.07266E-05	3.71190E-04
3.71190E-04	-1.16926	1596.48	-715.923	-48871.6	715.912	5.53277E-02	-1.07266E-05	-1.07266E-05	3.71190E-04
2.96186	-3.31281E-04	1.61217E-07	1.61217E-07	-2.22779E-06	2.96186	-3.31281E-04	1.61217E-07	1.61217E-07	-2.22779E-06
-2.22779E-06	4.19947E-02	-1.96157	-2.96199	5.46387E-02	-2.22779E-06	4.19947E-02	-1.96157	-2.96199	5.46387E-02
-6.99173E-06	2.81319E-08	-1.04965E-11	-1.04965E-11	1.89033E-10	-6.99173E-06	2.81319E-08	-1.04965E-11	-1.04965E-11	1.89033E-10
1.89033E-10	-5.71083E-07	8.27258E-04	8.27258E-04	6.89098E-06	1.89033E-10	-5.71083E-07	8.27258E-04	8.27258E-04	6.89098E-06
0	0	0	0	0	0	0	0	0	0
0	0	0	1	0	0	0	0	1	0
0	0	0	0	0	0	0	0	0	0
0	0	0	0	1	0	0	0	0	1

Table 4. Numerical data for 90 ft diameter antenna

Motor-load gear ratio	= $N = 1500 : 1$
Motor armature inductance	= $L_a = 0.03 \text{ H}$
Motor armature time constant	= $T_a = 0.064 \text{ s}$
Motor armature feedback resistance	= $R_f = 0.01 \Omega$
Motor torque constant	= $K_T = 0.75 \text{ Nm/A}$
Total referred inertia of load and both motor armatures at motor speed	= $J = 0.49 \text{ kgm}^2$
Motor back e.m.f. constant	= $K_v = 0.85 \text{ Vs/rad}$

Typical figures for a 90-foot diameter antenna are given in Table 4, from which the electronic gains required to achieve the desired natural frequency can be easily determined using the specified root method referred to above. For the purpose of the example a desired natural frequency of 1 Hz is specified with the predominant complex roots lying on the $\zeta = 0.8$ line so that an acceptable transient response can be guaranteed.

The electronic gains satisfying this requirement are:

- $K_1 K_t = 0.0378 \text{ Vs/rad}$
- $K_2 = 1.58 \text{ V/V}$
- $K_A = 2300 \text{ V/V}$
- $G_R = 20 \text{ V/deg}$
- $T_R = 0.01 \text{ s}$
- $\alpha = 35.4 \text{ V/V}$
- $T = 2.5 \text{ s}$

from which the numerical values of the A matrix can be computed:

	1	2	3	4	5	6	7	8	9	10
1		6.67×10^{-5}								
2			1.54	1.54						2.78
3		-28	-15.6		33.3					
4		-28		-15.6		33.3				
A-5		-137	-230				3640	25.8×10^7		
6		-137		-230			3640	25.8×10^7		
7								28.4×10^3		
8		-1						-100	1	
9										
10										

and the state transition matrix evaluated. Table 3 gives a series of typical print-outs where in this case the output response is defined by $\phi_{1,9}(t)$ for a step input, i.e.

$$x(0) = [0 \ 0 \ 0 \ 0 \ 0 \ 0 \ 0 \ 0 \ 1 \ 0]^T$$

and the response to a step of wind is defined by $\phi_{1,10}(t)$, i.e. for a step of wind:

$$x(0) = [0 \ 0 \ 0 \ 0 \ 0 \ 0 \ 0 \ 0 \ 0 \ 1]^T.$$

It follows that the response of any other variable, i.e. state, in the system can be observed and hence the limit of linear performance deduced by approximately scaling the input demand, until a particular state reaches the extremity of its linear range.

4. Conclusion

The paper has illustrated the application of the state space technique in servomechanism analysis. The system A matrix has been derived for two antenna servo models and the methods of applying inputs to the system via input state variables has been illustrated. The advantage of the method is that by using computer evaluation of the state transition matrix directly from the A matrix the response of the servo can be predicted without any manipulation of the transfer functions of the system. In the case of a realistic design employing a sixth- or seventh-order servo model the manipulation of the transfer functions is time consuming, tedious and a likely source of numerical errors. It follows that by eliminating the necessity for transfer function manipulation by application of the state transition matrix approach, an overall increase in the accuracy and efficiency of the analysis will result.

5. Acknowledgment

The Author wishes to thank the Directors of Plessey Electronics Group for permission to publish this paper and Dr. K. Milne for useful discussions. Thanks are also due to one of the Papers Committee's referees for helpful suggestions.

6. References

1. Wilson, D. R., 'Modern Servo Design Practice'. (Pergamon Press, Oxford 1970.)
2. Shinnars, S. M., 'Control System Design'. (Wiley, New York, 1964.)
3. Wilson, D. R., 'A survey of the developments in antenna servo techniques', *The Radio and Electronic Engineer*, 38, No. 3, pp. 169-77, September 1969.
4. Wilson, D. R., 'The analysis and synthesis of optimal control systems incorporating a digital computer', *Control*, 12, No. 126, pp. 1031-36, December 1968.
5. Liou, M. L., 'A novel method of evaluating transient response', *Proc. Inst. Elect. Electronics Engrs*, 54, No. 1, pp. 20-23, January 1966.
6. Prime, H. A. et al., 'Electric drive system for a steerable aerial at a satellite-communications earth station', *Proc. Instn Elect. Engrs* 111, No. 3, pp. 556-64, March 1964.
7. Wheeler, R. G., 'Design study of control system for 210 ft radio telescope', I.F.A.C., Basle 1963.
8. Canfield, E. B., 'Electromechanical Control Systems and Devices'. (Wiley, New York, 1965.)
9. Stallard, D. V., 'Servo problems and techniques in large antennas' *I.E.E.E. Trans on Applications in Industry*, No. 71, pp. 105-14, March 1964.

Manuscript first received by the Institution on 23rd September 1970, in revised form on 10th December 1970 and in final form on 7th May 1971. (Paper No. 1418/IC 53.)

Biquadratic Sections using Generalized Impedance Converters

By

Professor L. T. BRUTON,

B.Sc., M.Eng., Ph.D.†

A low-sensitivity RC-active biquadratic section is proposed which employs a generalized impedance converter embedded in a simple passive RC-structure. This may be used to realize complex high-Q pole-pairs and transmission zeros. The multi-parameter sensitivity of the transfer function is independent of Q factor. A high-quality narrow-band elliptic band-pass filter is given as a design example.

1. Introduction

The purpose of this contribution is to propose a new low-sensitivity RC-active second-order section. The essential feature of the technique is the use of a generalized impedance converter (g.i.c.)^{1,2,3} as the active part of the realization; voltage transfer functions of the form

$$T(s) = H \left[\frac{s^2 + a}{s^2 + bs + c} \right], H \text{ constant} \quad \dots\dots(1)$$

are achieved by suitably embedding the g.i.c. in a passive-RC structure. The synthesis technique is illustrated by means of an example in which a narrow-band sixth-order elliptic band-pass transfer function is realized.

2. The Basic Configuration

The method uses a g.i.c. that is completely defined by its transmission matrix *T*, where

$$T = \begin{bmatrix} 1 & 0 \\ 0 & Ks^2 \end{bmatrix} \quad \dots\dots(2)$$

This two-port g.i.c. is embedded in the passive structure containing admittances *Y*₁, *Y*₂, *Y*₃ and *Y*₄, as shown in Fig. 1(a). Direct analysis assuming *K* normalized to unity, gives

$$\frac{E_2(s)}{E_1(s)} = \frac{Y_1 + s^2 Y_3}{(Y_1 + Y_2) + s^2(Y_3 + Y_4)} \quad \dots\dots(3)$$

It is now not difficult to envisage the selection of *Y*₁...*Y*₄ that will ensure that the general form of equation (1) is always obtained. We will consider the three possibilities:

(i) *a* < *c*

We select the following parameters for *Y*₁...*Y*₄,

$$\begin{aligned} Y_4 &= 0 \\ Y_3 &= G_3 \\ Y_1 &= G_1 \\ Y_2 &= G_2 + sC_2 \end{aligned}$$

giving

$$\frac{E_2(s)}{E_1(s)} = \frac{G_1 + s^2 G_3}{(G_1 + G_2) + sC_2 + s^2 G_3}$$

or

$$\frac{E_2(s)}{E_1(s)} = \frac{s^2 + \frac{G_1}{G_3}}{s^2 + \frac{sC_2}{G_3} + \frac{G_1 + G_2}{G_3}} \quad \dots\dots(4)$$

which, for any particular *a*, *b*, *c*, has unique *G*₁, *G*₂, *C*₂ and *G*₃.

(ii) *a* > *c*

We select the following parameters for *Y*₁...*Y*₄,

$$\begin{aligned} Y_2 &= 0 \\ Y_3 &= G_3 \\ Y_1 &= G_1 + sC_1 \\ Y_4 &= G_4 \end{aligned}$$

giving

$$\frac{E_2(s)}{E_1(s)} = \frac{G_1 + s^2 G_3}{G_1 + sC_1 + s^2(G_3 + G_4)} \quad \dots\dots(5)$$

which has unique *G*₁, *C*₁, *G*₃, *G*₄ for any *a*, *b*, *c*.

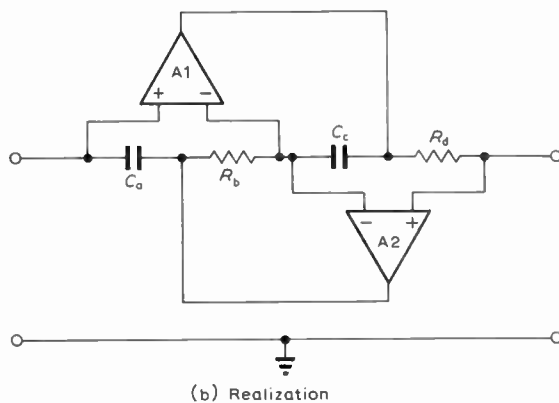
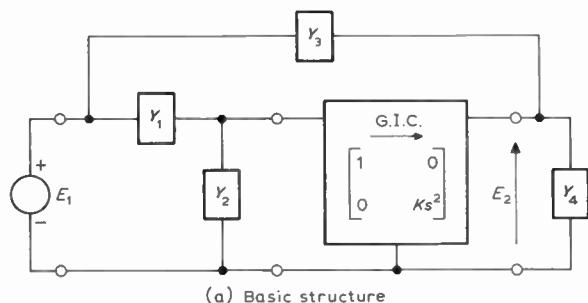


Fig. 1. Generalized impedance converter.

† Department of Electrical Engineering, The University of Calgary, Alberta, Canada.

(iii) $a = c$

In this case, select $Y_4 = 0$ and $Y_1 = G_1$, $Y_2 = sC_2$, $Y_3 = G_3$ giving

$$\frac{E_2(s)}{E_1(s)} = \frac{s^2 + \frac{G_1}{G_3}}{s^2 + \frac{sC_2 + G_1}{G_3} + \frac{G_1}{G_3}} \quad \dots\dots(6)$$

3. Operational Amplifier Realization

Generalized impedance converters of the required form have been proposed¹ and analysed^{2,3} in the literature; a Type A1 g.i.c. is given as an example in Fig. 1(b) from which it is straightforward to prove that the K parameter corresponding to equation (2) is given by

$$K = C_a R_b C_c R_d \quad \dots\dots(7)$$

It has been shown that this particular g.i.c. realization does not exhibit low-frequency unstable modes² and that extended wide-band operation is possible such that the effect of non-ideal amplifier phase shift is minimized.³ For these reasons, the realization in Fig. 1(b) will be used to synthesize the biquadratic section.

It is of interest to note that if $Y_3 = 0$ and Y_4 is resistive, then the output of Fig. 1(a) may be taken from the output of amplifier A1; this is a practical advantage because the output resistance is then zero, thereby allowing the section to be directly cascaded to a similar section.

4. Transfer Function Sensitivity

The transfer function in equation (4), for example, becomes

$$\frac{E_2}{E_1} = \frac{C_a R_b C_c R_d s^2 + \frac{G_1}{G_3}}{C_a R_b C_c R_d s^2 + s \frac{C_2}{G_3} + \frac{G_1 + G_2}{G_3}} \quad \dots\dots(8)$$

and therefore the Q of the pole-pair is given for $Q \gg 1$, by

$$Q \approx \sqrt{\frac{C_a R_b C_c R_d G_3 (G_1 + G_2)}{C_2^2}} \quad \dots\dots(9)$$

and the zero locations by

$$Z_{1,2} = \pm \sqrt{\frac{G_1}{C_a R_b C_c R_d G_3}} \quad \dots\dots(10)$$

Thus, it follows directly that the multi-parameter zero and Q sensitivities⁴ are given by

$$\sum Q = 4 \quad \text{and} \quad \sum z_{1,2} = 3 \quad \dots\dots(11)$$

These results are similar in magnitude to the multi-parameter sensitivities obtained using the two-integrator loop synthesis of a biquadratic section.^{5,6,7} However, the proposed g.i.c. structure employs two operational amplifiers whereas the two-integrator loop technique requires four operational amplifiers in order to realize transmission zeros. For both methods, the multi-parameter sensitivities are independent of the magnitude of Q .

5. Practical Considerations

To illustrate the practical implementation and problems involved with this method, we consider the realization of a sixth-order narrow-band band-pass elliptic filter with stringent requirements. The centre frequency f_0 is to be 200 Hz, the passband is 20 Hz and the stopband attenuation must be greater than 38 dB outside the frequency range 170–230 Hz.

A suitable normalized design, which is found by conventional methods, is given by

$$T(s) = \frac{s(s^2 + 1.327)(s^2 + 0.753)}{[s^2 + 0.1s + 1][s^2 + 0.0258s + (1.051)^2] \times [s^2 + 0.0233s + (0.951)^2]}$$

which may be realized by three sections as follows

$$T(s) = \left[\frac{s}{s^2 + 0.1s + 1} \right]_{\text{SECTION 1}} \times \left[\frac{s^2 + 1.327}{s^2 + 0.0258s + (1.051)^2} \right]_{\text{SECTION 2}} \times \left[\frac{s^2 + 0.753}{s^2 + 0.0233s + (0.951)^2} \right]_{\text{SECTION 3}}$$

Using the proposed method for sections 2 and 3 and a straightforward capacitively-terminated gyrator^{2,3} for section 1 gives the normalized realization in Fig. 2; equations (4) and (5) are used to determine the element values of sections 3 and 2 respectively.

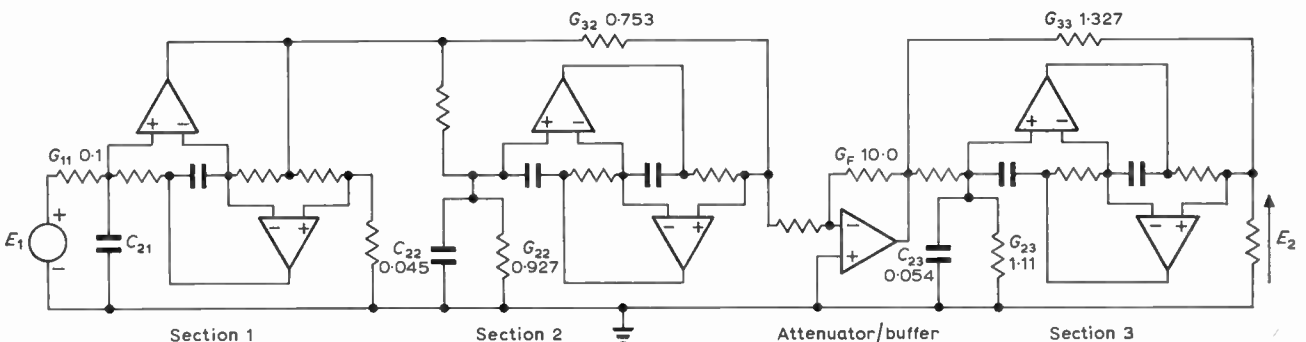


Fig. 2. Normalized band-pass elliptic filter; passband ripple = 0.8 dB; centre frequency = 1; bandwidth = 0.1; zeros of transmission = 1.15 and 0.87; stopband attenuation = 40 dB. All capacitances and conductances equal to unity unless otherwise indicated.

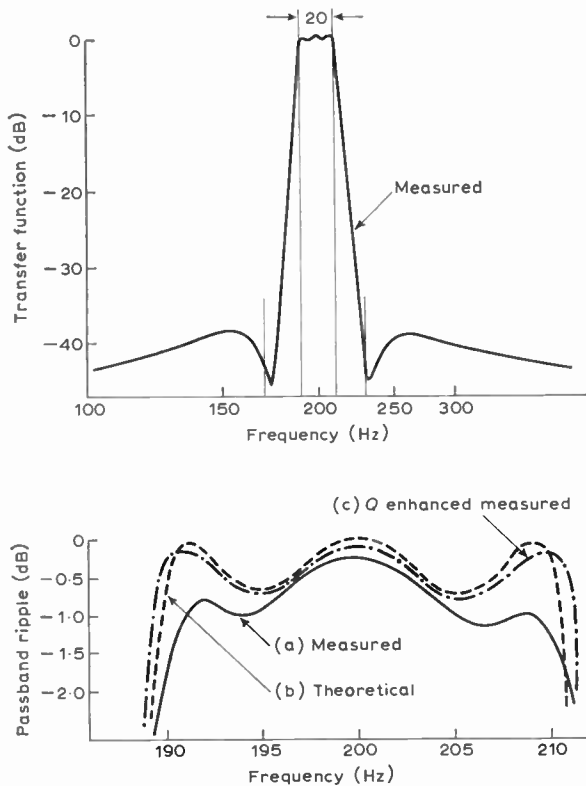


Fig. 3. Measured transfer function.

A practical denormalized circuit is given in Table 1 where the resistors are scaled from 1Ω to 15kΩ and the frequency is scaled from 2πHz to 200Hz. Note that an active attenuator is included between section 2 and 3; this is because the high *Q*s of the three sections (10, 44.6 and 40.7, respectively) cause a large centre-frequency gain; the attenuator section is employed in order to provide isolation and to reduce the overall gain so that the section 3 amplifiers do not handle excessive signal levels.

Table 1

The realization of Fig. 2 is denormalized to a centre frequency of 200Hz and impedance level of 15.0kΩ by employing the following element values:

G_{11} $\mu\Omega^{-1}$	C_{22} nF	G_{22} $\mu\Omega^{-1}$	G_F $\mu\Omega^{-1}$	C_{23} nF	G_{23} $\mu\Omega^{-1}$	G_{32} $\mu\Omega^{-1}$	G_{33} $\mu\Omega^{-1}$
6.18	2.49	61.8	667	2.88	74.0	50.2	88.5

All other capacitances = 53.1 nF
All other conductances = 66.7 $\mu\Omega^{-1}$

The measured transfer function is given in Fig. 3 from which it is observed that excellent agreement with theory is achieved. The measured passband ripple is shown on Fig. 3, curve a, for the calculated capacitance values as derived from equations (4) and (5). The theoretical ripple is given by curve b, and is seen to be 0.8dB.

6. Improvement of Passband Response

The measured passband response is about 0.7dB below the theoretical response at the edges of the passband.

This diminished response is due to the *actual Q* pole-pairs of sections 2 and 3 being slightly less than the required values of +44.6 and 40.7. This is due to the loading effects of the non-ideal unloaded g.i.c.s, which introduce an additional damping *Q* factor of approximately $A_0/4$, where A_0 is the finite gain of the amplifiers.² This effect may be adequately compensated by reducing the damping capacitors C_{22} and C_{23} so that the *Q* factors are restored to give a flat passband. In this example, reducing both C_{22} and C_{23} by 400 pF resulted in the measured passband curve c in Fig. 3. The measured curve is in excellent agreement with the theoretical curve (± 0.1 dB). This technique of reducing C_{22} and C_{23} is effectively *Q* enhancement and is a standard technique⁸ in the final adjustment of high-quality active filters.

7. Conclusion

A second-order section, employing a g.i.c. two-port network, has been suggested. This section realizes imaginary zeros and complex poles of the voltage transfer function. The method gives low sensitivities of zero and pole positions that are comparable to the two-integrator loop method. The complex zeros are achieved using only two amplifiers, whereas the two-integrator loop method requires four amplifiers. The proposed method has been used to realize a high-quality bandpass design; the concept of *Q* enhancement may be used where necessary by appropriately reducing the damping capacitors that appear in the first-order coefficient of equations (4), (5) and (6). For the majority of applications, for which the *Q* of the pole-pairs will be considerably less than the values used in the narrow-band design example, it is not necessary to employ *Q* enhancement.

8. References

- Gorski-Popiel, J., 'RC-active synthesis using positive-immittance converters', *Electronics Letters*, 3, pp. 381-2, August 1967.
- Bruton, L. T., 'Non-ideal performance of two-amplifier positive impedance converters', *I.E.E.E. Trans. on Circuit Theory*, CT-17, No. 4, pp. 541-49, November 1970.
- Antoniou, A., 'Realization of gyrators using operational amplifiers and their use in RC-active network synthesis', *Proc. Instn Elect. Engrs*, 116, pp. 1838-50, November 1969.
- Newell, W. E., 'Selectivity and sensitivity in functional blocks', *Proc. Inst. Radio Engrs*, 50, p. 2517, December 1962.
- Good, E. F., 'A two-phase low-frequency oscillator—parts 1 and 2', *Electronic Engng*, 29, pp. 164-9, April 1957; pp. 210-13, May 1957.
- Kerwin, W. J., Huelsman, L. P. and Newcomb, R. W., 'State-variable synthesis for insensitive integrated circuit transfer functions', *I.E.E.E. J. Solid-State Circuits*, SC-2, No. 3, pp. 87-92, September 1967.
- Tow, J., 'Design formulas for active RC filters using operational amplifier biquad', *Electronics Letters*, 5, No. 15, pp. 339-41, 24th July 1969.
- Orchard, H. J. and Sheahan, D. F., 'Inductorless bandpass filters', *I.E.E.E. J. Solid-State Circuits*, SC-5, No. 2, pp. 108-18, June 1970.

Manuscript received by the Institution on 18th March 1971. (Short Contribution No. 147/CC 110)

An Observed R.F. Hysteresis Characteristic of Particular Gunn Diodes

By

R. P. OWENS, M.Sc.†

Certain Gunn diodes, when mounted in half-wave resonant cavities, exhibited marked hysteresis in r.f. power when the bias voltage was increased above threshold and then reduced. Observations and measurements are described of the dependence on circuit loading of this phenomenon, and the associated $I-V$ curve of the diode. Explanations of the phenomenon are proposed, based on recent investigations into the effect of imperfect cathode boundary conditions on the behaviour of Gunn devices. Some possible practical applications of the hysteresis are suggested, assuming that controlled manufacture of such devices might eventually be possible.

1. Introduction

An r.f. hysteresis effect in waveguide cavity oscillators driven by some Gunn devices manufactured by Plessey was reported by Meade¹ in 1968. The observed characteristics of such devices are as follows. As the bias voltage is increased from zero, r.f. oscillations are inhibited until a threshold voltage V_A is reached, which is well above the expected onset of the transferred-electron effect (around 3.2 V for an X-band device). At this point r.f. power suddenly appears, and thereafter reacts normally to further increase in bias voltage. When the bias voltage is returned to zero, oscillations persist at voltages below V_A until a sustaining voltage V_B is reached, at which they abruptly cease. V_B is also well above 3.2 V. The direct current versus bias voltage curve also exhibits hysteresis, but in contrast to Meade's observations, the particular devices to be discussed in this paper showed a drop in current at V_A followed by a rise at V_B .

Any Gunn diode oscillator is likely to exhibit small amounts of r.f. hysteresis, but this usually occurs near the 3.2 kV/cm threshold field at low power levels due to the general properties of non-linear negative conductance devices. R.f. hysteresis associated with mode

switching also occurs, but this is a circuit effect influenced very little by bias voltage tuning in a high-Q circuit. The pronounced hysteresis to be discussed here is a device effect which has been observed only in a limited number of Plessey diodes issued in 1967-68. Some devices obtained from the same source at this time exhibited unusual properties including hysteresis, but these were attributed to some transitional effect at the contacts since the diodes had a limited lifetime.‡ The two devices available to the author were used extensively over a two-year period, with no observed deterioration. One of the two was recently tested for a further 40 hours in continuous 8-hour periods, driven by a sinusoidal bias voltage sweeping from 0-15 V at 70 Hz, and there was no change in the hysteresis characteristic. Meade¹ noticed a drop in r.f. output of about 2 dB and a drop of about 1 V in V_A after 20 hours operation of one of his devices, but on the whole the existing evidence suggests that this particular phenomenon is not due to some short-term transitional effect.

Interest in such an isolated batch of devices is believed to be justified in view of recent investigations into the influence of imperfect cathode boundary conditions on diode performance.³⁻⁸ These suggest a possible explana-

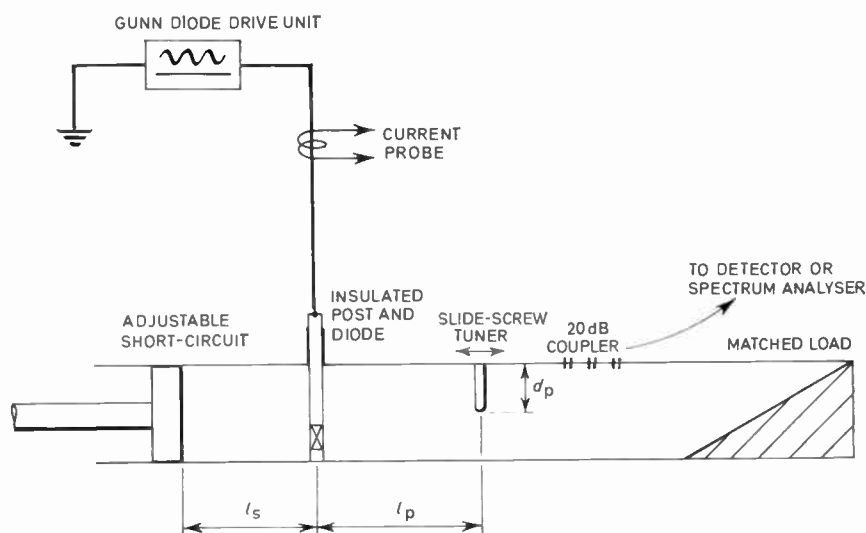


Fig. 1.
Experimental arrangement
for hysteresis measurements.

† Electronics Branch, Royal Military College of Science, Shrivenham, Swindon, Wiltshire.

‡ Referee's observations.

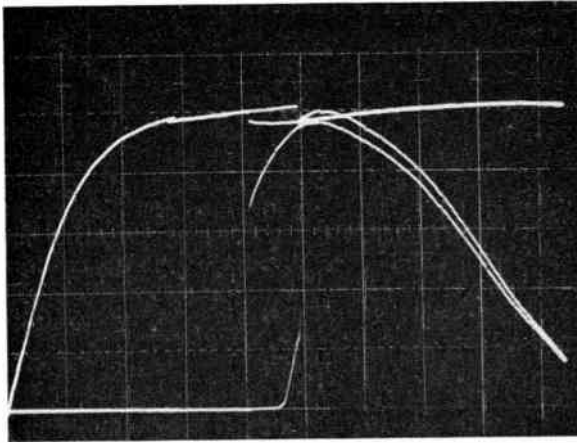


Fig. 2. B66 132 diode I - V and P - V curves. Voltage sweep rate 1 Hz. Horizontal scale 2 V/cm.

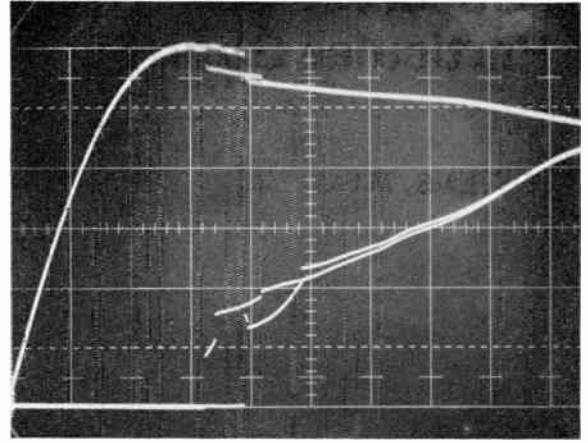


Fig. 3. B231/E diode I - V and P - V curves. Voltage sweep rate 1 Hz. Horizontal scale 1 V/cm.

tion of the effect, and some indication of how it might be reproduced in future devices. This could be a worthwhile undertaking in view of some obvious applications of such devices.

Extensive observations have been made on two devices exhibiting this hysteresis phenomenon and its dependence on circuit loading and bias voltage modulation. The effect occurred with the devices in either coaxial or waveguide cavity oscillators, but all quantitative measurements were made using a waveguide cavity, since it was easier to adjust and calculate the loading in the plane of the device using a waveguide system.

2. Experiments and Results

The experimental arrangement is shown in Fig. 1. The Gunn diode drive unit consists essentially of a wide-band, direct-coupled amplifier, which amplifies the a.c. signal from a Wavetek 114 voltage generator, and gives a constant voltage output of up to 20 V pk-pk (amplitude and frequency controlled by the Wavetek) superimposed on a d.c. voltage variable between 3 and 10 V (controlled by the drive unit itself). A rectifier is introduced across the output terminals to prevent negative bias being applied to the Gunn device. The current through the device was measured with a Tektronix P 6042 current probe. The sliding waveguide probe could be adjusted in depth and lateral position to provide a wide variation of complex admittance in the plane of the Gunn device. Using a Tektronix 547 oscilloscope with a 1A1 dual channel plug-in unit, both the current and detected r.f. power versus bias voltage characteristics of the Gunn device could be displayed simultaneously. Apart from its use in the investigation of hysteresis, this experimental set-up is extremely useful for the rapid evaluation of the effects of circuit loading, oscillator frequency and bias voltage variation on the r.f. output of Gunn devices in any cavity.

2.1. Qualitative Observations

Figures 2 and 3 are typical characteristic curves obtained using this apparatus. Most results on the

hysteresis phenomenon were obtained with Plessey diodes B66 125 and B66 132, which exhibited equally pronounced hysteresis effects. Figure 2 shows the I - V and P - V curves obtained for the latter diode. Figure 3 shows curves of the same parameters obtained for a 'normal' Plessey B 231/E42 diode. The difference in horizontal scale should be noted. The vertical scales are uncalibrated.

Some initial qualitative observations on the differences in behaviour shown by the 'abnormal' device in comparison with the normal device may be made, with reference to Figs. 2 and 3.

(a) The threshold voltage V_A is well above the threshold for onset of Gunn oscillations observed in normal devices.

(b) The hysteresis ($V_A - V_B$) is significantly larger than in normal devices, where it is typically somewhat less than 1 V (Fig. 3) if it exists at all.

(c) The r.f. power rises to its maximum almost immediately after threshold voltage V_A is reached, and continues at a high level right down to the sustaining voltage V_B . In normal devices power rises almost linearly with voltage from a very low level at threshold.

(d) Complete current saturation is never apparent in the abnormal devices, and threshold, accompanied by a current drop, occurs apparently arbitrarily at a point where current was previously still rising gradually with voltage. In normal devices, current clearly saturates just before threshold.

(e) Slight discontinuities in current are observed in the abnormal devices around $5\frac{1}{2}$ V but they are accompanied by r.f. power in the microwatt range, which dies as the bias is further increased. The first current discontinuity occurs in normal devices at about 3.2 V.

In attempting to account for the origin of the hysteresis and its associated effects, any explanation must be consistent with the fact that hysteresis of the magnitude shown in Fig. 2 is not apparent in the great majority of Gunn diodes. It is therefore justifiable to continue to refer to the two devices mentioned as 'abnormal' diodes.

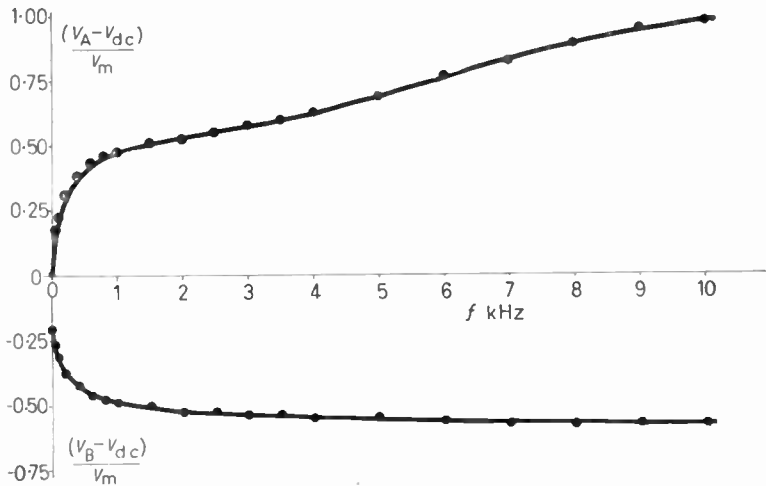


Fig. 4. Variation of V_A and V_B with modulation frequency.

2.2. Effect of Swept Bias Voltage

The bias voltage sweep frequency f_m and amplitude V_m were found to affect the magnitude of the hysteresis appreciably. Measured changes in V_A and V_B over a large range of frequencies f_m are plotted in Fig. 4. V_m was fixed at 4 V and the constant d.c. bias V_{dc} was 10 V during this experiment. Without anticipating later arguments, these results may be attributed to a dependence on temperature of the parameters controlling the threshold and sustaining voltages in these devices. As the sweep frequency is increased, the thermal time-constants of the device mount and the cavity become appreciable fractions of the period of the sweep. As a result a frequency-dependent phase lag between the oscillating temperature of the device and the bias voltage develops, accompanied by a change in the amplitude of the temperature swing.

One parameter which must affect V_A and V_B is the resistivity of the device material, and this will be a function of both voltage and temperature, $\rho(V, T)$. A possible requirement for the onset and quenching of oscillation could be that ρ must reach respective constant values ρ_A and ρ_B . Thus for each frequency f_m there would be a unique pair of voltages V_A and V_B for which the instantaneous voltage and temperature at the device resulted in the resistivities ρ_A and ρ_B . In order to derive a full theoretical explanation of the curves shown in Fig. 4 in terms of such a model, the function $\rho(V, T)$ would have to be known, together with knowledge of the relationship between V, T and f_m , and the various thermal time-constants operating in the oscillator. This is not attempted in this paper, which is restricted to reporting the experimental results obtained, and suggesting explanations for the observations listed in Section 2.1.

2.3. Loading Effect

The measurements now described were made at very low bias voltage sweep rates to eliminate the thermal delay effects discussed in the previous section. The voltages V_A and V_B were measured with a digital voltmeter to an accuracy of about ± 0.02 V. Subsidiary measurements were made to determine the susceptance

of the slide-screw tuner as a function of frequency and probe depth d_p . The admittance y_p of the matched load plus the probe could then be found in the plane of the diode by transforming through the line length l_p . Likewise the susceptance b_s of the short-circuit transformed to the plane of the diode was calculable.

In the first experiment, both l_s and d_p were kept constant, and l_p was varied over a range of 1.3 cm. Both the frequency f and the voltages V_A and V_B were affected by this adjustment, and the most significant way of presenting the results is to plot V_A and V_B , and also the normalized admittance $y_p = g_p + jb_p$, both as a function of f . This is done in Figs. 5(a) and (b), which

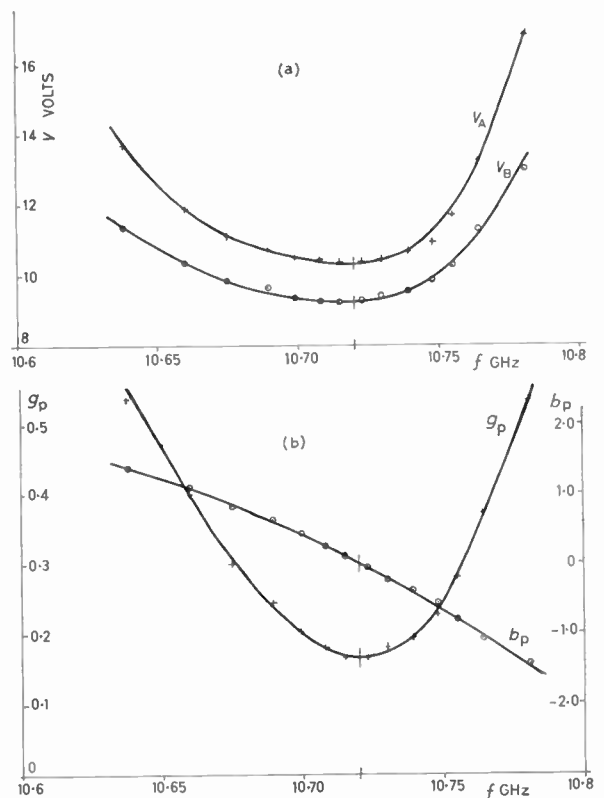


Fig. 5. (a) Variation of l_p, V_A, V_B versus frequency. (b) Variation of l_p, g_p, b_p versus frequency.

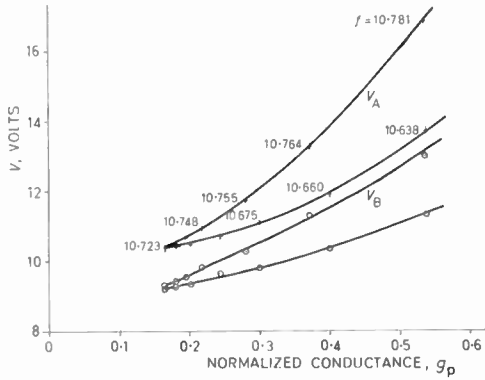


Fig. 6. Variation of I_p , V_A , V_B versus normalized conductance.

show that V_A and V_B reach minimum values when the conductive loading in the plane of the diode is also at a minimum. Moreover, the voltage difference ($V_A - V_B$) is also minimized at this frequency, $f = 10.72$ GHz. The frequency tuning is controlled by the variation of b_p shown in Fig. 5(b). Figure 6 shows how V_A and V_B change with normalized conductance and in particular shows that at a fixed absolute conductance (the characteristic impedance of the guide is virtually constant over such a small frequency range), V_A and V_B are very sensitive to frequency. To avoid the frequency effect, use is made of the fact illustrated in Fig. 5, that when the slide-screw tuner does not influence the frequency of the oscillation because its susceptance in the plane of the diode is zero, then V_A and V_B are at a minimum. A second experiment was therefore made, keeping I_s constant and varying d_p to change the conductance, but also adjusting I_p to obtain the minimum of V_A and V_B .

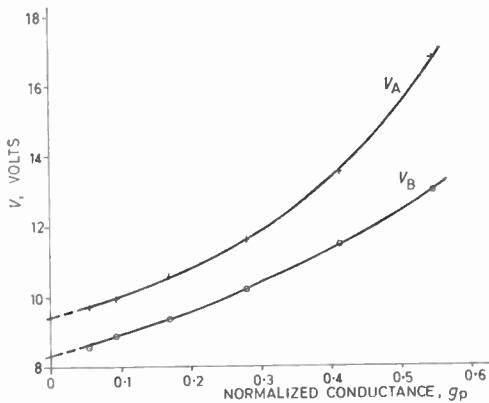
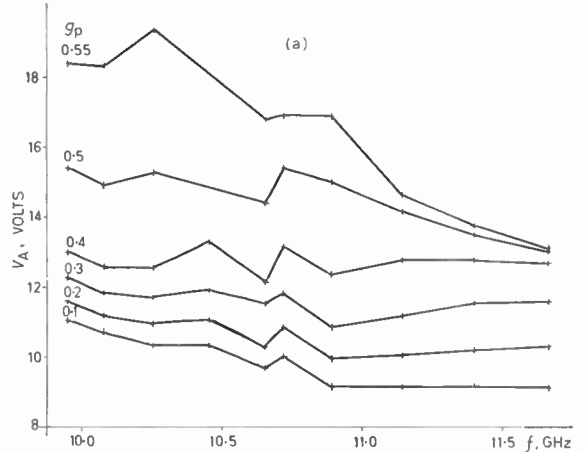
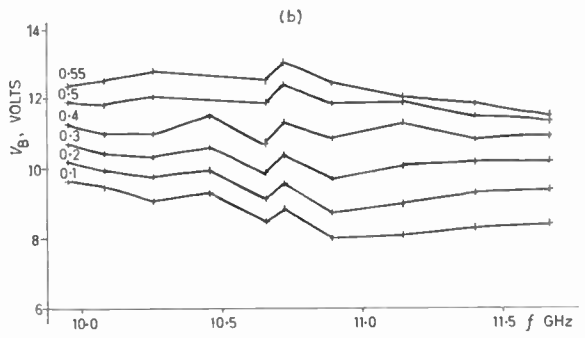


Fig. 7. Variation of I_b (I_p adjusted for minimum V_A , V_B). V_A , V_B versus normalized conductance for $f = 10.72$ GHz.

The frequency then remained substantially constant. Figure 7 shows how V_A and V_B changed with conductance for the frequency 10.72 GHz. Further measurements were made at other frequencies, controlled by varying I_s , resulting in curves similar to Fig. 7. From these, by interpolation, the curves of V_A and V_B versus f for various normalized conductance values could be derived, as shown in Figs. 8(a) and (b).



(a) Minimum V_A versus frequency.



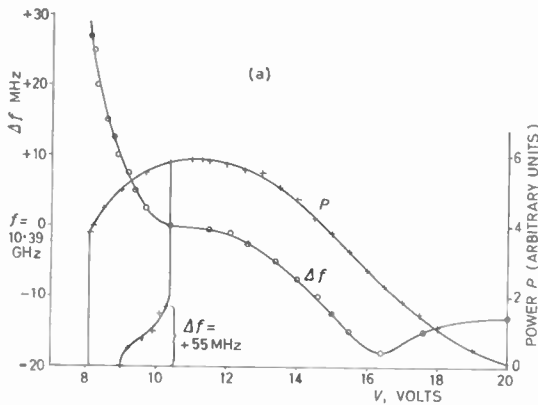
(b) Minimum V_B versus frequency.

Fig. 8.

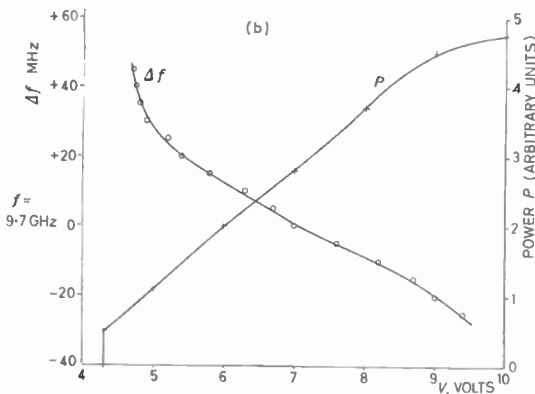
The following points of interest arise from these curves:

- (a) V_A and V_B increase as the conductance increases, with V_A rising faster than V_B .
- (b) The general trend is for V_A and V_B to decrease as the frequency increases for constant conductance. The slope increases with g_p in the V_A curves, but remains approximately constant in the V_B curves.
- (c) The rapid variation of V_A and V_B with frequency at constant conductance which is apparent in Fig. 6 is not as marked in Figs. 8(a) and (b) over the same frequency range.

A final experiment was made with the drive unit replaced by a standard constant-voltage d.c. supply which was adjusted manually slowly enough for thermal equilibrium to be reached at all voltages. At fixed voltages throughout the cycle, power and oscillator frequency were measured, and the results are plotted in Fig. 9(a). Similar results obtained for a normal ASM CXY 11B device are plotted in Fig. 9(b) for comparison. (Note the change in voltage scale.) These figures show that the frequency tuning versus bias voltage curve for the abnormal device shows the same smooth variation obtained for the normal device over the lower part of the voltage range, but has a point of inflexion and a minimum at higher voltages.



(a) Diode B66 125.



(b) Diode CXY 11B.

Fig. 9. Variation of frequency and power with bias voltage.

3. Possible Mechanisms to Explain Abnormal Device Behaviour

3.1. Static I-V Curve

For bias voltages up to the threshold of r.f. oscillations V_A , the observed static d.c. behaviour has the characteristics of elevated threshold voltage and an extended range of near-saturation in the current before and after threshold. These characteristics were noticed by Gunn² to coincide with the presence of a stationary high field domain close to the cathode just prior to threshold, and he considered that the phenomenon could be caused by a thin high resistivity region in the bulk material adjacent to the cathode contact.

Recent papers³⁻⁸ have all stressed the significance of cathode boundary conditions in the behaviour of bulk GaAs devices. They have shown that a number of observed phenomena, including Gunn's 'cathode drop', inexplicable in terms of 'perfect' bulk material parameters, can be attributed to particular combinations of electric field and carrier concentration at the cathode boundary. It has also been made clear that a wide range of different physical situations at the cathode boundary could all lead to similar electrical behaviour.^{3, 5, 8} It therefore appears that the performance of unsatisfactory devices encountered by many workers is in many cases not due to poor material or contacts, but to cathode boundary conditions unsuitable for the required application of the device.

The X-band devices now under consideration are all made from epitaxial layers of n-type GaAs grown on n⁺ GaAs substrates, with alloyed contacts to the substrate (anode) and the active layer (cathode). It is likely that the manufacturing process could produce two possible non-uniformities. These are (a) doping gradients extending through all or part of the active layer due to out-diffusion,⁹ or to auto-doping effects by substrate impurities,¹⁰ and (b) impurity diffusion occurring during the laying-down of the alloyed Ag-Sn contact and producing a thin, high resistivity layer at the cathode.^{4, 11} The consequences of such specific non-uniformities have been considered in detail by Hasty *et al.*⁴ and Suga *et al.*⁵ The following discussion, however, is based on the more general analysis of imperfect cathode boundary conditions carried out in particular by Kroemer³ and Conwell.⁸

The many possible physical situations which result in imperfect cathode conditions can be represented by a simple model consisting of a perfect cathode and the homogeneous negative mobility material, separated by a thin semi-conducting layer with an I-V characteristic quite distinct from that of the negative mobility material.³ The behaviour of the complete device is influenced greatly by the characteristics of this control section, and in particular by the conditions at the boundary between this section and the negative mobility material, referred to by Kroemer as the 'control plane'. Conwell⁸ takes this plane to be the new cathode, and discusses all possible stationary solutions of Poisson's equation

$$\frac{dE}{dx} = \frac{4\pi e}{\epsilon} (n - n_0) \quad \dots(1)$$

and the current continuity equation

$$\frac{dn}{dx} = \frac{1}{D} \left(n\mu E - \frac{j}{e} \right) \quad \dots(2)$$

given for various values of carrier concentration n_c and electric field E_c existing in this plane. The notation of Conwell has been employed in equations (1) and (2).

Kroemer considers the effects of changes in control plane characteristics with bias voltage for a few particular cases, but Conwell gives general solutions which differ in character as n_c and E_c move between different ranges of values. In following her analysis, therefore, one must be prepared for important changes in the stationary solution which might occur for specific control plane characteristics should n_c or E_c change appreciably as bias voltage is increased.

The present interest is in solutions which predict near-saturation of current at fairly low bias voltages, and give rise at higher bias voltages to unstable conditions from which large-signal cavity controlled Gunn oscillations can begin. Solutions exist which allow part of the negative mobility material to experience fields in the negative differential conductivity (n.d.c.) range. The device might then sustain oscillations in a reactive circuit, but Gunn oscillations involving moving domains could not occur.^{3, 8}

Only one set of solutions satisfies the experimental $I-V$ curve observations and gives rise to Gunn oscillations. This requires n_c to be approximately equal to n_0 , and E_c to be approximately equal to the field E_{11} , defined by Conwell to be the singular point of the two curves $n_1(E) = n_0$ and $n_2(E) = j/\epsilon\mu E$ which occurs in the n.d.c. range for a suitably high current value j . The current near-saturation and cathode drop phenomena are predicted by this solution. Provided the n_0L product of the material is high enough, a large proportion of the sample experiences fields in the n.d.c. region. Instabilities will grow, and travelling Gunn domains will eventually form; i.e. a stationary solution will no longer exist.

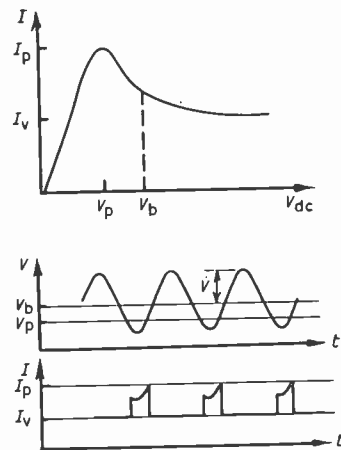
The stationary solution is described by Kroemer in terms of a crossover between the control plane current density characteristic and the neutral $j-E$ curve of the active material, occurring at some field above E_p , the field at which the neutral current is a maximum. At fields between E_p and the crossover field E_{11} , a stationary depletion layer forms in the negative mobility region adjacent to the control plane. When the field is increased above E_{11} , the depletion layer changes to an accumulation layer which eventually degenerates into a dipole domain and conventional Gunn oscillations can begin. Again, the cathode drop, the delayed onset of oscillation, and the range of near-saturation of current preceding this onset are all explained by this model.³

3.2. R.F. Hysteresis

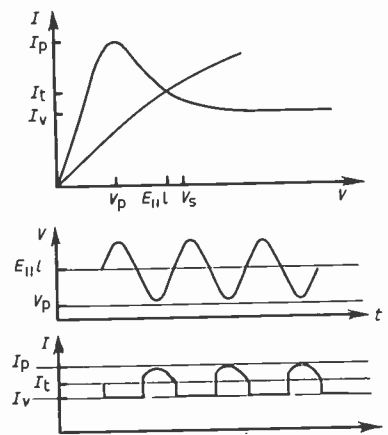
The three characteristics just mentioned have all been commonly observed since Gunn's initial observations,² but as far as is known the phenomenon of hysteresis has not previously been reported to occur with them, except by Meade.¹ The following is therefore a first attempt to explain its presence qualitatively in terms of the Kroemer model. We first outline the generally accepted description of the behaviour of a normal Gunn-effect device operating in a triggered domain mode,^{12, 13} and then consider how a device incorporating the control layer would differ in its performance.

Figure 10(a) shows the neutral characteristic of the active material, $j_n(E)$. When d.c. biased above the threshold field E_p , the current variation through the device during a complete r.f. voltage cycle will be as shown. As the voltage rises through threshold a new domain forms, and the current drops almost to valley level. It remains at this level until the domain reaches the anode, when it rises to a point on the low field portion of the $j_n(E)$ curve corresponding to the total bias field at that instant. Further voltage variation is followed in-phase by the current until threshold is exceeded once more and the current cycle repeats itself.

At the onset of oscillation, the r.f. voltage swing adjusts in amplitude until the mean (large-signal) negative conductance for the complete cycle, G_n , is equal in magnitude to the load conductance in the plane of the active device, G_L . This negative conductance is obtained from the ratio of the r.f. voltage V and the fundamental in-phase component of the current waveform, I , using Fourier analysis.^{12, 13} On reducing the bias voltage again, oscillations are able to continue, perhaps even



(a) Normal device voltage and current waveforms.



(b) Abnormal device voltage and current waveforms.

Fig. 10.

below E_p , provided that $|G_n| = G_L$. Hysteresis is therefore possible, although normally it would be expected to be of small magnitude. The magnitude would be closely linked to the amplitude of the oscillations developed at the threshold field.

The output power from the oscillator is $P = \frac{1}{2}V^2G_L$, so for a given load conductance the largest possible voltage swing is desirable. In normal devices the current component is unaffected by V while a domain exists, but during the whole of the ohmic part of the cycle the differential conductance is always positive and therefore the instantaneous current varies in such a way as to reduce I . This imposes a severe restriction on V , and hence P , as the voltage swing adjusts itself to provide the necessary negative conductance $-G_L$.

The behaviour of devices incorporating a control layer differs in several respects. Figure 10(b) shows the crossover between the hypothetical control characteristic $j_c(E)$ and the neutral characteristic of the active material $j_n(E)$. It occurs at a field E_{11} taken to be well beyond the field E_p at which j_n is a maximum. The accumulation layer which leads to dipole formation and transit across the device only appears when the bias field exceeds E_{11} .

Having formed, the dipoles will collapse unless there is sufficient domain voltage available to sustain them during transit.³ This domain voltage gets larger as the current at crossover gets closer to the neutral characteristic valley current. Once the applied voltage has exceeded $E_{11} \cdot L$, weak high frequency oscillations due to partial transit of domains are possible, but full domain transit and large amplitude oscillations will not occur until the bias voltage reaches the dipole sustaining voltage V_s associated with the particular value of E_{11} concerned. The transition between the two would be expected to coincide with gradually increasing oscillation amplitude and strong negative voltage tuning of the transit frequency as the domains are able to progress further across the sample before collapsing. This explanation could apply to the transition region between no oscillation and full scale oscillation observed in Fig. 9(a) between 9 and 10.4 V. These oscillations were at a constant frequency 55 MHz above the frequency of strong oscillations at 10.4 V. Strong voltage tuning would not be expected because the device was operating in a tuned system, and its effect on the frequency would be due more to the effective device capacitance than to the transit dynamics. If the effect of loading on the threshold is neglected for the moment, it therefore seems reasonable to identify the 9 V threshold with $E_{11} \cdot L$, and the 10.4 V threshold V_A with V_s .

Once full domain transit is achieved, conventional cavity-controlled Gunn oscillations can build up, and if the crossover is near the middle of the effective n.d.c. versus bias voltage curve for the device then the r.f. swings can reach a large amplitude very rapidly. The large switch in power observed experimentally as the voltage is increased from just below to just above threshold is an indication that this is the case.

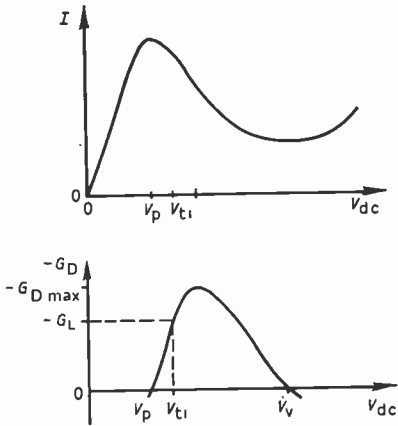
The current waveform to be expected when the d.c. bias exceeds V_s is shown in Fig. 10(b). The behaviour during domain transit is the same as for the normal device, except that the current drop is now from the crossover current level down to some value approaching the valley current. The difference occurs during the period when the domain has reached the anode but the applied field has not yet returned to E_{11} , and this part of the waveform requires further explanation. Kroemer shows that in the region for which the control field is greater than E_p but less than E_{11} , a static solution exists such that at least part of the negative mobility material experiences field in the n.d.c. region.³ Thus during this particular part of the cycle the device current will be 180° out of phase with the r.f. voltage. The current will not quite follow the neutral $j_n(E)$ characteristic for fields between E_p and E_{11} , but n.d.c. will be available in this range to some degree. The restriction on voltage swing encountered in normal devices due to the positive differential conductivity during the same part of the current waveform is therefore not present. Clearly if the current drop happened to be about the same, the r.f. voltage amplitude required to produce a given conductance I/V would be greater if the current waveform were that shown in Fig. 10(b) rather than the one of Fig. 10(a).

Having obtained large amplitude oscillations at a bias voltage just above V_s , further increase in bias voltage should lead to quite normal r.f. behaviour. When bias voltage is reduced again the power should return along the same curve until V_s is reached. Since a substantial r.f. swing is in existence at this point, a large hysteresis is to be expected. In normal devices, r.f. hysteresis is small, because at d.c. bias levels below threshold, the part of the current waveform with positive differential conductance tends to cancel out the negative conductance due to the current drop. Very small voltage swings dwindling to zero are all that can develop in order to achieve the negative conductance required to drive the load. But in abnormal devices the n.d.c. available at voltages well below V_s enhances the negative conductance due to the current drop. Even if the r.f. voltage cannot swing above V_s during any part of the cycle, the static n.d.c. is available if $E_c > E_p$, and oscillations could still be sustained. However, the evidence seems to indicate that the presence of fully formed Gunn domains is necessary for strong oscillations to exist. A good deal of negative conductance must still be available just above the measured voltage V_B because the oscillations are still so strong, although falling fairly steeply. The very sharp drop that sets in at V_B itself would therefore not be expected on this count. The fact that the drop does occur would appear to be due to the inability to generate full domains, and thereby achieve a current drop, at any time during the cycle because the voltage never swings above V_s .

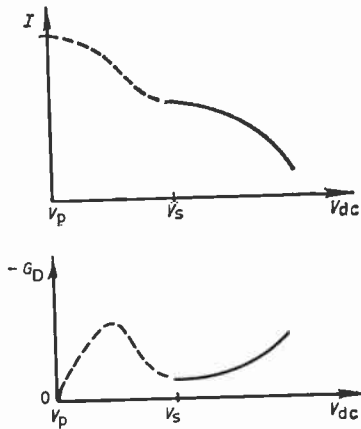
It appears, therefore that cavity-controlled oscillations do not occur if fully formed domains are not generated, although static negative conductance is still available in at least part of the device if E_c lies between E_p and E_{11} . It is therefore possible for weak negative conductance oscillations to build up anywhere in this field range, at a suitable resonance of the circuit. This could be the explanation for the presence of weak signals observed at a bias voltage of 5½ V in Fig. 2.

4. Discussion of Results

In the light of the above explanations, some comments may now be made on the experimental results concerning the effects of loading on the hysteresis. It has been shown that the effect of increasing the load conductance in the plane of the device was to raise V_A and V_B appreciably, and to increase the hysteresis voltage difference ($V_A - V_B$). Now apart from the requirement that fully formed domains must be able to traverse the active material, as described in the previous section, a second necessary condition for sustained oscillations to take place is that the device negative conductance over the r.f. cycle should match the load conductance. At a given bias voltage there is a maximum small-signal negative conductance $-G_D$ available from the device. With a tunnel diode, for example, the variation of $-G_D$ with bias voltage is as shown in Fig. 11(a). It is derived from the slope of the diode's $I-V$ curve, so the peak value $-G_{D(\max)}$ corresponds to the point of maximum slope. If the diode is presented with a load G_L , the figure shows that oscillations will occur as soon as the bias voltage exceeds V_{11} . Only operation in the part of



a) Negative resistance device. Differential conductance characteristic.



(b) Suggested differential conductance characteristic and equivalent stable $I-V$ curve for abnormal devices.

Fig. 11.

the curve between V_p and $V_{t(max)}$ would give rise to the results now under discussion. As can be seen from the figure, as G_L is increased, the threshold voltage for oscillation increases. It is suggested, therefore, that even at such high threshold voltages the abnormal devices are still operating in the region for which $-G_D$ is still rising with bias voltage, i.e. they operate in the same way as would a stable negative resistance device, uncomplicated by the presence of moving domains, having the $I-V$ characteristic of Fig. 11(b). The region below the crossover point is dotted in to indicate how the static n.d.c. region might affect the complete curve. It is clear that this arrangement would explain the large r.f. amplitude at the onset of oscillation, since large voltage swings could develop either side of the region of inflection if the negative conductance did rise again below threshold as shown. Some objections can be raised against this model, considering the high voltage levels involved, but no other mechanism has been discovered that could explain the observed results so well.

The above comments might explain why V_A increases as it does with a change in circuit loading. The extent

of the hysteresis would depend on the effects of the detailed $-G_D$ versus V_{dc} curve on the r.f. voltage swing. V_B would thus behave somewhat differently from V_A as the circuit loading was changed. It is possible also, that at such elevated voltages, thermal effects become significant. For example, the crossover point between the neutral j_n curve and the control characteristic might move to higher fields as the temperature rises, thus contributing to the rise in V_A . At lower voltages, the crossover would come down again, and $(V_A - V_B)$ would be enhanced.

Figure 8 shows that, as the oscillating frequency falls, at a given loading V_A and V_B tend to increase. This may be attributed to the change in current waveform resulting from the change in the ratio of transit time to r.f. period. The $-G_D$ versus bias voltage curve must alter such that the voltage required to sustain oscillation is increased.

5. Conclusions

Experiments have been carried out on two Gunn-effect devices which exhibited abnormal current-voltage and power-voltage behaviour involving a substantial amount of hysteresis. The influence of bias voltage sweep frequency and amplitude appears to be a thermal effect depending on some voltage and temperature dependent parameter of the active material and the thermal time constants of the oscillator. Both the threshold and sustaining voltages depend markedly on r.f. loading, and to a lesser extent on frequency.

The main aim of the paper has been to suggest an explanation for certain qualitative characteristics of the two devices which differ from those of normal Gunn devices. The four important differences are the delayed oscillation threshold, current near-saturation preceding threshold, the availability of large r.f. power immediately at threshold, and the exceptionally large hysteresis between the threshold and sustaining voltages. An explanation for all these phenomena has been developed, based on the concept of a control layer at the cathode contact having different current-voltage characteristics from the negative mobility material. The arguments used are quite general, and are valid for a wide variety of physically attainable control layer structures; a particular structure is neither assumed nor predicted, to explain the observations. Only one assumption is made; that the control plane $j-E$ characteristic cuts the neutral negative mobility characteristic in the n.d.c. region of the latter. The analysis, based particularly on the work of Kroemer,³ predicts that r.f. oscillation will only begin when the applied bias field exceeds this crossover field. It suggests that with no circuit loading, large r.f. oscillations would begin just above this field value for an applied voltage V_A at which fully formed travelling domains can be sustained. The magnitude of the hysteresis is considered to be dependent on the signal strength at threshold, which is itself governed by the detailed shape of the negative conductance versus bias voltage curve for the device. The sustaining voltage V_B is predicted to be at a level for which the total voltage, d.c. plus r.f., is unable to exceed V_A at any part of the cycle.

In the discussion of the results obtained when the circuit loading was changed, it was pointed out that a second necessary condition for sustained oscillations to occur at a given bias voltage was that the load conductance at the device should be less than the maximum value of device negative conductance. The assumption was made that once the domain sustaining voltage had been exceeded, this second condition governed the threshold voltage V_A . The resulting curve of maximum negative conductance versus bias voltage was described, with reservations about its validity. The dependence of V_A and V_B on frequency can be explained qualitatively in similar terms.

Complete understanding of this hysteresis phenomenon might lead to controlled production of Gunn devices exhibiting hysteresis. Certain properties of such devices could be of great practical interest in the fields of computer logic or digital communications.

The hysteresis itself, if controlled by bias voltage pulsing, would make such a diode attractive as a memory device. The fact that full microwave power occurs immediately after the threshold of oscillation, in contrast to the behaviour of conventional devices, suggests improved efficiency in the conversion of small amplitude pulses, superimposed on a d.c. bias just below threshold, into continuous microwave power. This property could be an advantage in p.c.m. systems such as the Gunn-effect frequency shift keyed pulse regenerators reported by Bestwick *et al.*¹⁴ There is a great deal of interest at present in methods of inhibiting domain formation in Gunn devices so that they can be used as bulk negative resistance for travelling-wave amplification. In this connexion, consideration might be given to the use of a cathode control layer in the device, which can prevent dipole formation until the crossover field is reached, whilst providing n.d.c. at the device terminals at fields between E_p and E_{11} .

6. Acknowledgments

The author is grateful to Mr. M. L. Meade of Reading University, for first drawing his attention to the hysteresis phenomenon. Mr. W. H. T. King of this department deserves credit for designing the Gunn diode drive unit used in the experiments. Professor M. H. N. Potok and Mr. D. Cawsey are thanked for their helpful comments during the course of this work.

The work was carried out under a contract from the U.K. Ministry of Technology.

7. References

1. Meade, M. L., 'Investigation of current-noise and frequency modulation noise in Gunn oscillators', Proceedings of IPPS Conference on Physical Aspects of Noise in Electronic Devices, Nottingham, September 1968, pp. 174-9.
2. Gunn, J. B., 'Properties of a free, steadily travelling electrical domain in GaAs', *IBM J. Res. Development*, **10**, pp. 300-9, July 1966.
3. Kroemer, H., 'The Gunn effect under imperfect cathode boundary conditions', *I.E.E.E. Trans. on Electron Devices*, ED-15, pp. 819-37, November 1968.
4. Hastly, T. E., Stratton, R. and Jones, E. L., 'Effect of non-uniform conductivity on the behaviour of Gunn effect samples', *J. Appl. Phys.*, **39**, No. 10, pp. 4623-32, September 1968.
5. Suga, M. and Sekido, K., 'Effects of doping profile upon electrical characteristics of Gunn diodes', *I.E.E.E. Trans. on Electron Devices*, ED-17, pp. 275-81, April 1970.
6. Shaw, M. P., Solomon, P. R. and Grubin, H. L., 'The influence of boundary conditions on current instabilities in GaAs', *IBM J. Res. Development*, **13**, pp. 587-90, September 1969.
7. Böer, K. W. and Döhler, G., 'Influence of boundary conditions on high field domains in Gunn diodes', *Phys. Rev.* **186**, pp. 793-800, October 1969.
8. Conwell, E. M., 'Boundary conditions and high field domains in GaAs', *I.E.E.E. Trans. on Electron Devices*, ED-17, pp. 262-70, April 1970.
9. Lawley, K. L., 'Vapour growth parameters and impurity profiles on N-type GaAs films grown on N⁺-GaAs by the hydrogen water vapour process', *J. Electrochem. Soc.*, **113**, pp. 240-5, March 1966.
10. Hasegawa, F. and Saito, T., 'Occurrence of a high resistance layer at vapour epitaxial GaAs film-substrate interface', *Japan. J. Appl. Phys.*, **7**, p. 1125, September 1968.
11. Bolton, R. M. G. and Jones, B. F., 'Effects of temperature on contact resistance of Gunn diodes', *Electronics Letters*, **5**, pp. 662-3, 11th December 1969.
12. Robson, P. N. and Mahrous, S. M., 'Some aspects of Gunn effect oscillators', *The Radio and Electronic Engineer*, **30**, No. 6, pp. 345-52, December 1965.
13. Warner, F. L., 'Extension of the Gunn effect theory given by Robson and Mahrous', *Electronics Letters*, **2**, pp. 260-1, July 1966.
14. Bestwick, P., Hartnagel, H. L. and Huntingdon, R., 'Frequency shift keyed pulse retiming with Gunn oscillator', *Electronics Letters*, **6**, pp. 46-7, 22nd January 1970.

Manuscript first received by the Institution on 2nd March 1971 and in final form on 19th August 1971. (Paper No. 1419/CC 111.)

© The Institution of Electronic and Radio Engineers, 1971

A Royal Intervention in Early Submarine Telegraphy

By

R. M. BARKER,
M.Sc., C.Eng., M.I.E.R.E.†

A brief note on Wheatstone's contributions to submarine telegraphy together with a suggestion made by the Prince Consort on the use of sea water as conductor.

1. Introduction

It is well known that Prince Albert, the Prince Consort, gave his general support to science; the Great Exhibition of 1851, in the organization of which he was the prime mover, was proof enough of that. A letter he wrote to Wheatstone in 1860 shows that he had much more than a general interest in the scientific problems of the day and that he was prepared to offer a suggestion which he hoped would lead to an improvement in submarine telegraphy. In order to set the Prince Consort's letter in context, a résumé will first of all be given of the progress made in submarine telegraphy up to that time.



H.R.H. Prince Albert, the Prince Consort 1819-1861.
(Radio Times Hulton Picture Library)

cable is not known but he had, no doubt, progressed beyond the 'tared rope' stage and was probably trying out a cable insulated with rubber.^{1,2} Two years later, he tried again in Portsmouth Harbour with a lead-covered cable but this was not a success.^{1,3} Several other men were experimenting at about this time but no further progress was possible until a satisfactory insulator for submarine cables could be found. There was little difficulty in insulating cables for land telegraphy, as these were normally overhead wires, which needed insulation only at the poles. Where it was necessary to run cables underground, rubber was a satisfactory insulator, but this material was unsuccessful when used to insulate submarine cables, as it was soon affected by sea water.

The turning point was the introduction into this country of gutta-percha, a substance obtained from a species of tree found in Malaya, which resembles rubber, but which withstands the action of sea water. This material proved to be the best insulator for submarine cables and continued to be used for this purpose until about thirty years ago, when it began to be superseded by polythene. Wheatstone was probably the first person to suggest using gutta-percha for submarine cable insulation, but he did not put the idea into practice, probably because he had difficulty in obtaining supplies of the material.¹

Submarine telegraphy can be said to have begun with the successful laying of a cable from Dover to Calais in 1851, the year of the Great Exhibition, by the Brett brothers, John and Jacob. (A cable laid by them the previous year worked for one day only.) Once it had been shown that submarine telegraphy was a practical possibility, many other cables were laid, with varying degrees of success. The first two attempts to lay an Atlantic cable were made in 1857 and 1858 but they were failures. The difficulties of laying cables in such depths of water were immense. If the cable were paid out too quickly, it

2. Early Submarine Telegraphy Attempts

Charles Wheatstone (1802-1875), whose name nowadays is remembered chiefly in connexion with the Wheatstone Bridge, invented the first electric telegraph to be put into commercial operation in 1837. Once his telegraph had been accepted and put into use by the Railway Companies, Wheatstone's thoughts naturally turned to the possibility of submarine telegraphy. In 1840, he appeared before a Select Committee of the House of Commons and expressed an opinion that a link between England and France was a practical possibility. His plans showed the proposed route across the Channel, details for constructing the cable and loading it on board, laying and jointing it, and under-running to find a fault.¹ However, since the cable was to be of seven wires 'each wire to form the core of a rope line well saturated with boiled tar, and all the lines to be made into a rope prepared in the same manner', it is not surprising these plans came to nothing.

Wheatstone carried out a short experiment in Swansea Bay in 1844 and succeeded in passing signals from a boat through a cable to the shore. The insulating material he used for his



Charles Wheatstone.

From the painting by Sir William Llewellyn belonging to the Institution of Electrical Engineers.

† Department of Electrical Engineering, Llanelli Technical College, Llanelli, Carmarthenshire.

was liable to develop 'kinks', which would cause breakdown in the insulation; if it were paid out too slowly, the strain on it might cause it to break; and all the time the ship was rising and falling.⁴

As a result of the failure of so many cables, the Government set up a joint committee consisting of Douglas Galton, Wheatstone, William Fairburn and George P. Bidder, for the Board of Trade, and Edwin Clark, C. F. Varley, Latimer Clark and George Saward, for the Atlantic Telegraph Co. The Committee met for the first time in December, 1859, and after hearing evidence from over forty witnesses, presented its Report in 1861. Out of a total of 11,364 miles of cable laid in various parts of the world, only about 3000 miles were actually working. Blame for the failure of the Atlantic cable was attributed to 'the original design of the cable having been faulty owing to the absence of experimental data, to the manufacture having been conducted without proper supervision, and to the cable not having been handled, after manufacture, with sufficient care. We have before us samples of the bad joints which existed in the cable before it was laid; and we cannot but observe that practical men ought to have known that the cable was defective, and to have been aware of the locality of these defects before it was laid'.⁵

3. The Prince Consort's Letter

It was while the Committee was acquiring evidence for its Report that the Prince Consort wrote his letter to Wheatstone, whom he had known at least since 1843. In that year, Queen Victoria presented the collection of scientific instruments of George III to King's College, where Wheatstone was Professor



Wheatstone's ABC telegraph recorder, an instrument typical of the period described in this paper.
(Science Museum photograph)

of Experimental Philosophy. History has dealt unkindly with 'Farmer George', who is remembered chiefly for his mental instability and for the loss of the American colonies, but he at least deserves credit for being interested in science. A museum displaying this equipment at King's College was opened by the Prince Consort, who also saw demonstrations by several of the professors, including Wheatstone. It had been planned to demonstrate the electric telegraph across the Thames to the shot tower on the South Bank, but the wire was broken, so His Royal Highness saw only the apparatus.⁶

This is the Prince Consort's letter:

Windsor Castle

Dec. 17 1860

Sir,

I am commanded by His Royal Highness the Prince Consort to draw your attention to the following matter.

The Prince, in common with everyone to whom the progress of our telegraphic communications as one of the great civilising agents of the day is of great importance, has often reflected upon the unsatisfactory results obtained by our submarine cables, which have from their construction hitherto baffled all exertions to establish long deep-sea communications. The bulk weight of the cables, the want of elasticity, the difficulty of transporting them and spinning them out, and perhaps above all the difficulty of their manufacture on account of the incongruity of the many different substances of which they are composed, together with the great pressure exercised by the water upon them,—may be looked upon as some of the most essential causes of failure.

In reflecting upon how some of these might be overcome, the idea suggested itself to His Royal Highness, whether Water itself could not be used as the conducting medium? A simple tube of caoutchouc* such as our flexible gas-tubes, might enclose and isolate a column of water, through which the spark might be sent. It would be cheap of manufacture, homogeneous in material, flexible, light, and the outward pressure would be neutralised as the fluid inside would be the same as that outside.

There may occur to you a thousand reasons, why this idea cannot be carried out; but His Royal Highness thought you would forgive the trouble if he asked you, who stand in such a parental position to our telegraph system, to let His Royal Highness have your opinion on it.

I am, Sir,

Your obedient Servant,

C. Ruland

Librarian

4. Wheatstone's Reply

In the Library of King's College is a collection of rough notes written by Wheatstone, and among them is one which he almost certainly wrote when considering his reply to the royal letter. It reads:

India Rubber tubing:

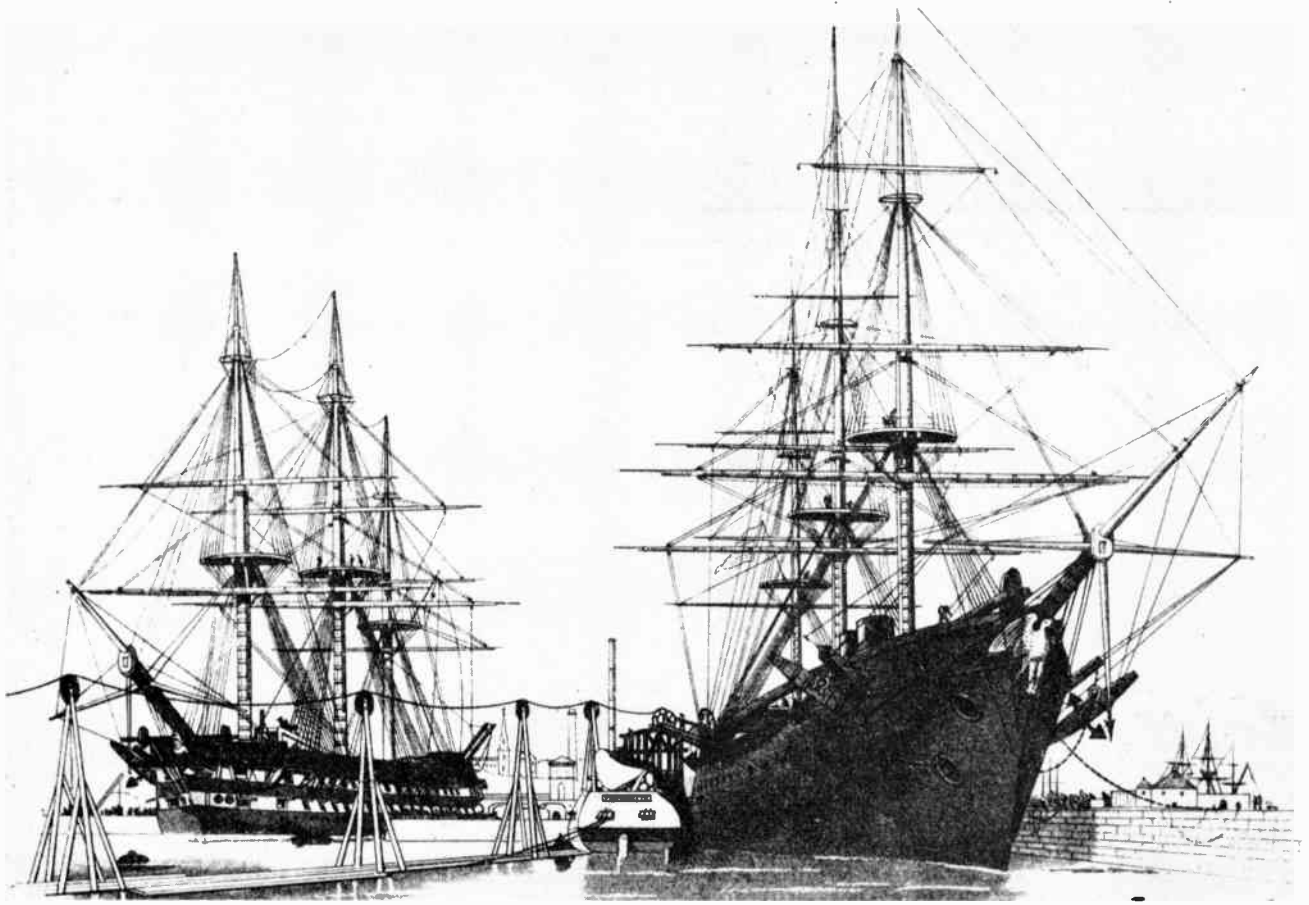
$\frac{1}{4}$ inch diameter £88 per mile

$\frac{1}{2}$ inch diameter £176 per mile

1 inch diameter £484 per mile

It would require a tube 9 feet in internal diameter for the salt water it contains to be equal in conductivity to a copper wire one sixteenth of an inch in diameter. The conductivity of silver being 100,000,000 that of water saturated with chloride of lime . . .

* i.e. rubber



Re-shipment of the Atlantic telegraph cable on board the *Agamemnon* and *Niagara* in Keyham Basin, Plymouth, May 1858. (Print from *The Illustrated London News*, loaned by Mr. K. R. Haigh)

From this rough note, it is apparent that Wheatstone rejected the Prince Consort's suggestion on economic grounds; there were other possible reasons. There is considerable advantage in the fact that the pressure outside the cable would be neutralized by the sea water inside it, but a light cable would tend to drift about on the sea bed and probably suffer damage, particularly at the two shore ends, where submarine cables are provided with extra armouring because of the action of rocks and waves.

The Prince Consort's proposal thus came to nothing, but it throws interesting light on his character and proves that he had a genuine desire to further the progress of submarine telegraphy. It is also significant that, wanting an opinion upon his proposal, the man to whom he wrote was Wheatstone, whom he must have regarded as the doyen of telegraphic experimenters.

5. Conclusion

A year after writing his letter to Wheatstone, the Prince Consort was dead. At the time of the Great Exhibition of 1851, British science and technology led the world, but other countries were soon to challenge our position. It is at least arguable that, had he lived, the Prince Consort, by his interest in science and encouragement of scientists, might have made a significant contribution to the maintenance of Britain's position of supremacy.

6. Acknowledgments

The Prince Consort's letter is published by gracious permission of Her Majesty the Queen.

The author is grateful for assistance received from the Secretary and Librarian of King's College, from Mr. B. Bowers of the Science Museum, South Kensington, from Professor W. Gosling of Swansea University College, and from Mr. K. R. Haigh.

7. References

1. Sabine, R., Letter to the Secretary of the Society of Telegraph Engineers. *Journal of the Society of Telegraph Engineers*, pp. 86-91, 23rd February 1876.
2. Dillwyn, L. W., Diary, August 1844. National Library of Wales, Aberystwyth.
3. Varley, C. F., *Journal of the Society of Telegraph Engineers*, February, 1876.
4. Garratt, G. R. M., 'One Hundred Years of Submarine Cables,' pp. 9-12. (H.M.S.O. 1950).
5. Report of the Privy Council Committee with Minutes of Evidence on the Construction of Submarine Telegraph Cables, 1861.
6. *The Illustrated London News*, 1st July 1843.

Manuscript first received by the Institution on 7th April 1971 and in final form on 2nd June 1971 (Short Contribution No. 148/Com. 52).

© The Institution of Electronic and Radio Engineers, 1971